
Contributions to the damping of interarea modes in extended power systems

A turbine governor approach with the help of the Unrestricted Horizon Predictive Controller

Von der Fakultät für Elektrotechnik und Informatik
der Gottfried Wilhelm Leibniz Universität Hannover
zur Erlangung des Grades
Doktor-Ingenieur (Dr.-Ing.)
genehmigte Dissertation

von

M.Sc. Rodrigo Trentini Preuss

geboren am 03.04.1985
in Joinville, Brasilien

2017

Vorsitzender: Prof. Dr.-Ing. Richard Hanke-Rauschenbach
Referent: Prof. Dr.-Ing. habil. Lutz Hofmann
Korreferent: Prof. Dr.-Ing. Rüdiger Kutzner

Tag der Promotion: 04.04.2017

To my beloved wife and son, Carina and Felipe.

Acknowledgements

First of all, to God.

Besides, I must acknowledge the Brazilian Research Agency (CNPq) for the financial support.

A very special thanks goes to Prof. Dr-Ing. Rüdiger Kutzner for all help and kindness spent towards me. Without his support this thesis would not become true, and I will never find words to express all my gratitude. I also would like to thank Prof. Dr.-Ing. habil. Lutz Hofmann, who gave me the invaluable chance to perform my PhD studies at his institute.

Further, the guidance and friendship of Prof. Dr. Antonio da Silva Silveira have played a major role in this research, which I must thank deeply.

Many thanks to the colleagues at Hochschule Hannover (HsH): Christopher Tebbe, Thiemo Schunder, Daniel Počuč, Oliver Schmerling, Markus Lindhorst, Andreas Würger, Marvin Bartsch, Hanqing Zhou, Robert Dzido, Christian Böttcher and Mathias Poets. Thanks for making the room 2512 the funniest workplace of the university!

Still within the HsH borders, I thank Prof. Dr.-Ing. Blath, Prof. Dr.-Ing. Freund, Prof. Dr.-Ing. Wenzel, Manfred Hermeling and Timo Möhle. Besides, a special thanks goes to Prof. Dr.-Ing. Jörg Wehmeier, who opened to me the opportunity of working at this amazing place.

My father Ademar (*in memoriam*) and specially my mother Doralice I must thank a lot, since they gave the necessary support for me to perform my studies and to become who I am. *Obrigado, mãe.*

Also to the Schroeder's family and to Valli Gehrman, all my gratitude. Your support and friendship always make me feel so warmly welcome that I can barely find words to thank.

Finally, my deepest thanks and love I send to Carina and Felipe. Thanks for being so understanding, thanks for sharing the joy and difficulties during this time abroad, thanks for forgiving me for being away, thanks for existing, thanks for everything. *Einfach vielen Dank!*

*A little science estranges men from God, but much science
leads them back to Him.*

— Louis Pasteur

Abstract

This thesis presents a novel approach for the damping of low frequency oscillations in extended power systems, which, in contrast to the current Power System Stabilizer (PSS) solution, is fully based on the turbine governor. The structure responsible for this additional damping is here called PSS_t, which stands for *Power System Stabilizer at the turbine side*. The main justification for this new governor approach lies on the fact that low frequency oscillations are very prejudicial to power systems and can be better damped from the turbine.

Besides the PSS_t, the next pages show that a new governor may be obtained with the help of a special case of Model-based Predictive Controller (MPC) that was specially designed aiming at its implementation in power systems. The *Unrestricted Horizon Predictive Controller*, short UHPC, is a state feedback controller that is also shown to be stochastic, long range and light computing, bringing unprecedented contributions to both Power Systems and Linear Control fields. Further, the UHPC and the PSS_t may be combined, becoming therefore an interesting novel governor structure with an intrinsic ability to damp out low frequency oscillations.

However, being a state-space controller, the UHPC requires the model of the system to be known. Since power grids models are usually very complex and large, a new control-based model is also developed. This modelling is here called *Electromechanical Energy Approach* since it is entirely based on a mechanical representation of the power system, which enables one to use the Lagrangian Energy Method to obtain its differential equations. The method here established is fairly reduced and accurate in comparison to actual systems.

Further, as an alternative for the selection of some of model's parameters that do not have physical meanings, a parameter identification method specially turned to power systems is also presented. This method inherently concerns system's uncertainties (noise and parameter mismatches) through the use of the Extended Kalman Filter (EKF).

At last, the simulation of three benchmark systems are performed in order to evaluate the presented UHPC-based governor structure. The

results have shown that the proposed governor architecture is able to contribute positively to the damping of the most problematic modes of the systems without harming their ability of tracking voltage and power references.

Keywords: Power Systems, Predictive Control, Electromechanical Systems, Power System Stabilizer, Turbine Governor.

Kurzfassung

In dieser Arbeit wird ein neuartiger Ansatz zur Dämpfung von niederfrequenten Schwingungen in ausgedehnten Energieversorgungssystemen präsentiert, der im Gegensatz zu den aktuellen Pendeldämpfungsgeräten (*Power System Stabilizer*, kurz PSS) über den Turbineregler eingreift. Die Struktur, die diese zusätzliche Dämpfung erreicht, wird hier als PSSst bezeichnet, da das Pendeldämpfungsgerät auf die Turbine wirkt. Die wichtigste Begründung für diesen neuen Regleransatz liegt darin, dass niederfrequente Schwingungen die Stabilität ausgedehnter Netze gefährden können und über die Turbine besser gedämpft werden können.

Außerdem wird gezeigt, wie ein neuartiger Turbinenregler auf Basis der Modellprädiktiven Regelung (*Model-based Predictive Controller*, kurz MPC) entworfen werden kann. Der *Unrestricted Horizon Predictive Controller*, kurz UHPC, ist ein Zustandsregler, der ebenfalls stochastische Einflüsse berücksichtigt und vorausschauend ist, aber nur geringe Rechenressourcen benötigt. Dies ermöglicht neue Beiträge sowohl in der Energietechnik als auch in der linearen Regelungstheorie. UHPC und PSSst stellen zusammen einen neuartigen, vielversprechenden Regleransatz dar, um niederfrequente Pendelungen zu dämpfen.

Für den UHPC wird ein Modell des zu regelnden Systems in Zustandsdarstellung benötigt. Da Energieversorgungssysteme im Allgemeinen sehr komplex und ausgedehnt sind, wird ein neuer Ansatz zur Modellierung von Energieversorgungsnetzen für den Reglerentwurf vorgestellt. Diese Modellierung wird *Electromechanical Energy Approach* genannt, da sie vollständig auf einer mechanischen Analogie des Energiesystems basiert. Dies ermöglicht die Anwendung der Lagrange-Gleichungen zur Bestimmung der Differenzialgleichungen. Das resultierende Modell ist im Vergleich zu dem tatsächlichen System deutlich reduziert, aber für die Regelung ausreichend genau.

Weiterhin wird als Alternative zur Vorgabe von einigen Modellparametern, die keine physikalischen Bedeutungen haben, ein Parameteridentifikationsverfahren vorgestellt, das speziell für Energieversorgungssysteme entwickelt wurde. Diese Methode berücksichtigt alle Unsicherheiten des Systems (Rausch- und Parameterfehlanspassungen) durch den Einsatz eines *Extended Kalman Filters* (EKF).

Zum Schluss wird die UHPC-basierte Reglerstruktur in drei Benchmarksysteme untersucht und bewertet. Die Ergebnisse zeigen, dass die vorgeschlagene Turbinenreglerarchitektur einen positiven Beitrag zur Dämpfung der besonders kritischen Modi der Systeme leisten kann, ohne das Führungsverhalten der Turbinenregelung und Spannungsregelung zu beeinträchtigen.

Schlüsselwörter: Energieversorgungssysteme, Prädiktive Regelung, Elektromechanische Systeme, Pendeldämpfungsgerät, Turbinenregler.

Resumo

Esta tese apresenta uma nova abordagem para o amortecimento de oscilações de baixa frequência em sistemas elétricos de energia, no qual, em contraste com a atual solução através do Estabilizador de Sistemas de Potência (*Power System Stabilizer*, ou PSS), é baseado no regulador da turbina. A estrutura responsável por este amortecimento adicional é aqui denominada PSS_t, que significa Estabilizador de Sistemas de Potência aplicado no lado da turbina. A principal justificativa para esta nova abordagem de regulador reside no fato de que as oscilações de baixa frequência são muito prejudiciais aos sistemas de energia e podem ser melhor amortecidas a partir deste equipamento.

Além do PSS_t, as próximas páginas mostram que um novo regulador pode ser obtido com a ajuda de um caso especial de Controlador Preditivo baseado em Modelo (*Model-based Predictive Controller*, ou MPC) que foi especialmente projetado visando sua implementação em sistemas elétricos de energia. O *Unrestricted Horizon Predictive Controller*, ou UHPC, é um controlador de estados que é ao mesmo tempo estocástico, de longo alcance e leve computacionalmente, trazendo contribuições sem precedentes para os campos de Sistemas Elétricos de Energia e de Teoria de Controle Linear. Além disso, o UHPC pode ser combinado com o PSS_t no seu projeto, tornando-se assim uma interessante nova estrutura de regulador com uma capacidade intrínseca de atenuar as oscilações de baixa frequência.

No entanto, sendo um controlador de estados, o UHPC requer que o modelo do sistema seja conhecido. Uma vez que os modelos de redes elétricas são geralmente muito complexos e extensos, um novo modelo baseado em controle também é desenvolvido. Esta modelagem é aqui chamada de *Electromechanical Energy Approach*, uma vez que é inteiramente baseada em uma representação mecânica do sistema elétrico, que permite usar o Método de Lagrange para obter suas equações diferenciais. O método aqui estabelecido é bastante reduzido e preciso em comparação com sistemas reais.

Além disso, como uma alternativa para a seleção de alguns dos parâmetros do modelo que não têm significados físicos, um método de identificação de parâmetros especialmente voltado para sistemas elétricos de energia também é apresentado. Este método considera intrin-

camente as incertezas do sistema (ruído e incertezas nos parâmetros) através da utilização do Filtro de Kalman Estendido (*Extended Kalman Filter*, ou EKF).

Por fim, simulações de três diferentes sistemas são realizadas para avaliar a nova estrutura de controle baseada no UHPC. Os resultados mostram que a arquitetura proposta para o regulador é capaz de contribuir positivamente para o amortecimento dos modos mais problemáticos dos sistemas sem prejudicar sua capacidade de rastreamento de referências de tensão e potência.

Palavras-chave: Sistemas Elétricos de Potência, Controle Preditivo, Sistemas Eletromecânicos, Estabilizador de Sistemas de Potência, Regulador da Turbina.

Contents

List of Abbreviations	xvii
List of Symbols	xix
1 Introduction	1
1.1 Motivation of the thesis	1
1.2 Aims of the thesis	7
1.3 Contributions of the thesis	10
1.4 Organization of the thesis	13
2 Power Systems modeling	15
2.1 Prime mover	17
2.2 Governor	18
2.3 Synchronous machine	19
2.4 Excitation system	21
2.5 Multi-machine systems	23
3 The Electromechanical Energy Approach	27
3.1 Basis for the method	28
3.2 The modeling	30
3.2.1 Simplification of the load and passive buses . . .	37
3.2.2 Regulated system	39
3.3 Modal analysis: 2M/1L system	42
4 Uncertainties and parameter identification in Power Systems	51
4.1 Uncertainties	52
4.1.1 Parameter mismatch	53
4.1.2 Stochasticity	54
4.2 Parameter identification	55
4.3 Identification results: 2M/1L system	57

5	The Power System Stabilizer at the turbine side	65
5.1	The PSSSt	66
5.2	2M/1L system: Evaluation of the PSSSt	68
5.2.1	Singular values behavior	69
5.2.2	Modal analysis	70
5.2.3	Dynamic simulation	71
6	The Unrestricted Horizon Predictive Controller	77
6.1	Related researches	78
6.2	UHPC in power systems	80
6.3	UHPC's equating	82
6.4	2M/1L system with the UHPC	89
6.4.1	UHPC evaluation	89
6.4.2	UHPC-based governor	92
7	Benchmark test systems	99
7.1	SMIB system	99
7.2	Two-Area system	107
8	Conclusions and outlook	117
8.1	Conclusions	117
8.2	Outlook	121
	Bibliography	123
	Appendix A	
	Matrices of the regulated system	131
	Appendix B	
	Simulation data	133
	Appendix C	
	The N_y -steps ahead Kalman Predictor	137
	Appendix D	
	The intrinsic solution of the Diophantine Equations	139
	Curriculum Vitae	143

List of Abbreviations

AVR	Automatic Voltage Regulator
EKF	Extended Kalman Filter
FACTS	Flexibel AC-Transmission System
GMVC	Generalized Minimum Variance Controller
GPC	Generalized Predictive Controller
KF	Kalman Filter
LQG	Linear Quadratic Gaussian
LQR	Linear Quadratic Regulator
MPC	Model-based Predictive Control
MV(R)	Minimum Variance (Regulator)
NRMSE	Normalized Root-Mean-Square Error
PFC	Predictive Functional Controller
PSS	Power System Stabilizer
SIMO	Single-Input Multiple-Outputs
SISO	Single-Input Single-Output
SMIB	Single-Machine Infinite-Bus
UHPC	Unrestricted Horizon Predictive Controller

List of Symbols

A	State matrix
B	Input matrix
C	Output matrix
D	Damping matrix / Feedforward matrix
d	Discrete delay
e	Internal voltage
F	Noise's Diophantine solution
f	Terminal frequency
H	Control signal's Diophantine solution
H	Inertia constant
I	Identity matrix
I	RMS current
i_r	Reactive current
J	Moment of inertia
\mathcal{J}	Cost function
\mathbb{J}_h	Output Jacobian matrix
\mathbb{J}_f	State Jacobian matrix
K	EKF gain
K_p	Proportional gain
K_ω	Compensation for the speed deviation
k	Current discrete sample
L	Observer gain
\mathcal{L}	Lagrangian
N	Number of nodes
N_G	Number of generator nodes
N_y	Prediction horizon
P	Covariance matrix (EKF)
P	Active power
Q	State / output error weighting matrix
Q	Reactive power
q^{-n}	Discrete backward shift operator (n samples)
R	Control signal weighting matrix
S_b	Apparent power base
T_n	Reset time

\mathcal{T}	Kinetic energy
\mathbf{u}	Input vector
\mathcal{U}	Potential energy
V	RMS voltage
\mathbf{v}_c	Output random variable
\mathbf{w}_c	State random variable
X	Reactance
\mathbf{x}	State vector
Y	Admittance
\mathbf{y}	Output vector
z	Order of a generic system

Greek symbols

β	Turbine Droop (governor)
χ	Flag (PSS)
Δ	Linearized variable / Discrete difference
δ	Deviation
ϵ	Additional state
$\mathbf{\Gamma}$	State disturbance matrix / Kalman gain
γ	Feedforward gain (governor)
$\mathbf{\Lambda}$	Weighting matrix for the confidence on the parameters (EKF)
λ	Voltage angle
ω	Shaft's speed
ω_0	Synchronous frequency
τ	Torque
τ_i	Lead-lag time constants (PSS) ($i = 1, 2, 3, 4$)
τ_{i0}	Open-loop time constant ($i = d, q$)
τ_{tf}	Torsional filter time constant (PSS)
τ_w	Washout filter time constant (PSS)
$\boldsymbol{\theta}$	Vector of unknown parameters
$\boldsymbol{\xi}$	Noise vector

Super-indexes

ω	Speed
e	Electric variable
m	Mechanic variable
p	Power

r	Reference
T	Transpose
t	Turbine
\dagger	Power/torque and field voltage inputs
$'$	Transient
$''$	Sub-transient

Sub-indexes

d	d-axis
q	q-axis
G	Generator node
L	Load node

Accents

$-$	p.u. value
$\hat{}$	Estimate
\sim	Equilibrium
\cdot	First derivative
$\ddot{}$	Second derivative

1

Introduction

This chapter presents the motivation and the aims of the thesis, introducing the stability issues that arise in Power Systems and how they may be tackled. At last, the contributions of the work are also highlighted, followed by a summary on the organization of the thesis.

1.1 Motivation of the thesis

Power systems are by far the most complex electrical structure ever developed by man [1]. The connection of several busbars to generating units, transmission lines, compensators, loads, etc., led, in the course of time, to very sophisticated and intricate power grids, such as the North American, the Chinese, the Brazilian and the European ones, among many others.

However, such complexity takes its toll: the larger the power grid, the less stable it will be if no counteraction is taken in order to improve its stability [2]. This is the main reason why power engineers are often working on ways of improving grid's safety. As an illustrative example, Phil Harris, the former president and CEO of PJM Interconnection, one of the largest US electrical distribution company, once declared:

Voltage collapse is still the biggest single threat to the transmission system. It is what keeps me awake at night.

Phil Harris, March 2004.

In his speech Mr. Harris was talking specifically about voltage collapse, which might occur due to several different reasons [1]. Among these reasons, perhaps one of the most fundamental and threatening ones are the so-called *interarea modes* [1–4], which are under the classification of the *rotor angle small signal stability*. For a clearer overview on the stability issue in power systems consider the diagram shown in Figure 1.1.

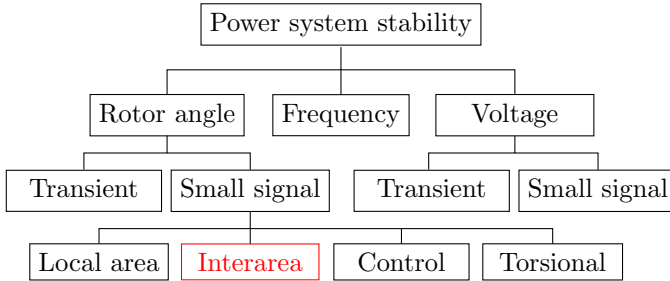


Figure 1.1: Classification of power system stability - based on [5] ©2007 CIGRÉ.

The analyses to be performed in this thesis are focused on the cited interarea modes, which are mainly connected to electromechanical phenomena [4]. These modes are represented by low frequency oscillations on the power exchange between two or more generating areas, typically in the range of 0.1-0.7 Hz. The active power exchange causes the generators of one area to oscillate against the generators in other areas, *i.e.*, during transients the generators of different areas rotate with contrasting phases, resulting in frequency deviations.

Generally speaking, the larger the power system is, the lower the frequencies of its interarea modes will be. The reason for that can be easily understood whenever one thinks on a simple mechanical *multi-mass-spring* system. For instance, in the system of Figure 1.2, if further masses are attached through springs, more oscillatory modes will arise. At the same time, the frequency of the slowest mode will be further decreased due to the increased inertia of the overall system.

The difference for an actual power system lies on the fact that the masses are rotating, and therefore the addition of new rotating masses increases the kinetic energy of the system. Hence, more energy is also required to damp out the inevitable oscillations that arise following a change in system's equilibrium point.



Figure 1.2: Multi-mass-spring mechanical system.

This fundamental example gives a rough idea on the relation between the size of the power system and its low frequency oscillations, which are hard to damp due to their mechanical characteristics [4]. Rogers [6] has observed that when the oscillations of the interarea modes diminish too much, these oscillatory phenomena interact with the dynamics of the speed governor.

A clear example of problems caused by the interarea oscillations are the cases occurred on 19 and 24 February 2011 in Europe, where 0.18 and 0.25 Hz oscillations appeared in the power grid without any apparent cause [7]. Figure 1.3 shows a short part of the measured data on 19 February 2011, where it is evident the counter-oscillations between Italy, Portugal and Turkey with the rest of Europe.

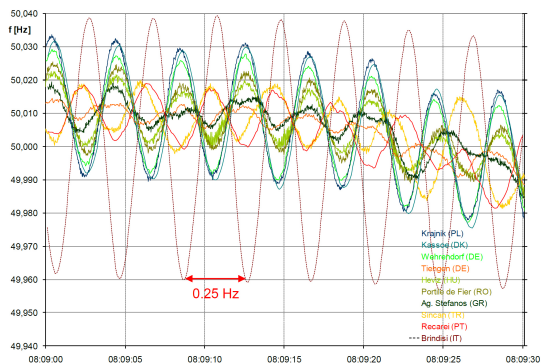


Figure 1.3: Interarea oscillations detected in Europe on 19 February 2011 - Reproduced from [7] ©2011 ENTSO-E

Fortunately the oscillations disappeared after about 15 minutes, however they occurred again on 24 February 2011. Since the active power exchange between some areas in these periods increased to critical limits, the Swiss operator Swissgrid has acted protective devices in order to reduce the effect of the oscillations. However, if on one hand these protective devices help on reducing the generators swings, on the other it changes the operating point of the system, what might

also deteriorate grid's performance in terms of the stability margins at some level.

Moreover, in their seminal paper, Kamwa *et al.* [8] exemplify how dangerous the interarea modes can be. According to the authors, major outages that occurred in the USA (1996), Brazil (1999), Italy (2003), USA-Canada (2003) and Sweden (2003) are known to, at some point, be influenced by low frequency oscillations with increasing amplitude. Interesting to notice is that most of these outages occurred not so long ago, what confirms the expectation of some power engineers in the last century when they affirmed that the expansion of the power grid and the sharp increase in the electric energy consumption would lead the whole systems to a dangerous state near to their stability limits [2, 9–11].

In fact and as an illustration, the literature is full of examples (see, *e.g.*, [12–15]) stating that the connection of the continental Europe to Turkey on 18 September 2010 is responsible for a never experimented interarea mode of frequency about 0.15 Hz between its own generating units and the west towards Spain and Portugal.

Within Europe, other low frequency modes are also known. For instance:

- Scandinavia: East-West (0.48 Hz) and North-South (0.33 Hz);
- Great Britain: North-South (0.5 Hz);
- Ireland and Northern Ireland: North-South (0.7 Hz);
- Iceland: around the island (0.8 Hz);
- Continental Europe: North-South (0.26 Hz), Balkans-West (0.22 Hz) and Turkey-West (0.15 Hz).

The main interarea modes presented in North America are:

- West Coast: North-South (0.25 Hz);
- East Coast: North-South (0.4 Hz);
- Across USA: East-West (0.45 Hz);
- British Columbia: 0.6 Hz;

In Brazil an interarea mode of about 0.2 Hz has been identified after the connection of a very long AC transmission line with 1276 km which connects the Northern and the Southern parts of the country [16].

In Southern China, interarea oscillations in the range of 0.4-0.7 Hz were also identified [17].

Several other examples of these low frequency oscillations may be easily found in literature, however the aim of this section so far is to exemplify how common and dangerous the interarea modes can be when not well damped, rather than giving examples of real problems occurred due to these modes. Besides, this introduction also wants to show that the increase in consumption and the extension of the power grid might create new oscillations with lower frequencies and considerably high amplitudes in the future. This is particularly important whenever one remarks that day-by-day the power systems are being extended, resulting in more power exchange in order to adapt the power delivery to the current consumption of industries and end customers, as Anderson and Foad [3] have correctly pointed out in their book.

For this reason, the control of the interarea oscillations in order to avoid systems outages is of vital importance within the Power Systems research field, and the number of publications states it. A quick look at the IEEE web-based library shows 537 published works on the topic “interarea”, being 284 published from 2010*. In other words, about 53% of all available literature in the IEEE library is less than 6 years-old, proving the relevance of the theme.

With this said, it is also important to regard that the origin of most of the cited interarea modes are known, and therefore counteractions were already been taken in order to avoid or at least to mitigate them.

Despite researches that cope with damping of these oscillations through Flexible AC-Transmission Systems (FACTS) (see, *e.g.*, [18, 19]), the most used device for tackling the interarea modes is still the *Power System Stabilizer*, short PSS [2], which is a device connected to the input of the Automatic Voltage Regulator (AVR) and serves to damp out undesired oscillations (more details in Chapter 2). The PSS was first developed to damp local modes out (0.7-2 Hz). However, when the interarea modes were finally identified as an important problem in power system stability, it was also implemented for the damping of these modes, obtaining well-accepted results over the years through several different approaches (see, *e.g.*, [9, 20–22]).

The main issue of the PSSs is that, since historically they were tuned to damp out only the local-area modes, the appearance of the interarea ones made the power engineers to re-tune them. Nonetheless, as the PSS is nothing but a high-pass passive filter, its re-tuning changes the bandwidth of the system, resulting in a sub-optimum filtering charac-

* Access on 11 June 2016 at 22:55h.

teristics. Or putting in other words, the mere re-tuning of the PSS might lead the device to not filter well neither the local- nor the inter-area modes. For example, after the West Coast Blackouts of 1996 it was found that key's PSSs were either out of service or poorly tuned, however it is still not possible to ensure that the re-tuning of these PSSs was enough to assure that such huge outages will not happen again in the future [23].

Although several attempts were made with the aim at providing acceptable system's filtered bandwidth both for local- and interarea modes (see, *e.g.*, [24–27]), undoubtedly the most successful one is the implementation of the so-called *Dual-Input PSS* (or also PSS2B) along with its evolution, the *Multi-band PSS* (or also PSS4B), which are brilliantly presented in [8]. Both regard a PSS with two inputs (frequency and power), where the former utilizes one filter per input and the latter implements three different filtering characteristics, each having one specific cutoff frequency. For the PSS4B, the clear benefit is to win by “brute force” the desired filtered trait. On the other hand, the price to be paid is relatively high, since 26 parameters must be set to each PSS4B, hampering the natural selection of the parameters based on known information from the system. In other words, despite giving acceptable results in practice, its tuning is not intuitive since the designer hardly ever knows which parameter is having more or less influence on the obtained filtered characteristics, or even worst, which parameter is *really* impacting on the output and which can be set to zero. For this reason and despite its advantages, the PSS2B is still the most used PSS in industry [8].

As a matter of fact, the PSS is usually implemented at generator's side, *i.e.*, in spite of the interarea modes being basically *mechanical* oscillations, the PSS acts on an *electromechanical* device. The reason for such selection is historic, as already cited in this introduction. However, one must notice that, about 50 years after its first implementation in the mid-1960s, the justification for utilizing the PSS along with generator's excitation system no longer holds.

Two interesting examples of this unusual paradigm shift are the works of Wang *et al.* [28] and Milanovic [29]. Using simulation results, both have shown that the damping of local- and interarea modes can be obtained through the utilization of governor-based PSSs, *i.e.*, the PSS is applied specifically at the turbine instead of using it at the generator side. As observed by Machowski *et al.* [4], although these PSSs were never implemented in practice, such solutions should be considered in the future.

Despite the cited papers being interesting in the theoretical viewpoint, they sin in not considering an even more trivial possibility: the usage of both excitation system and governor based PSSs together, in parallel, with the former being responsible for the damping of the local-area modes, whereas the latter would work on the mitigation of the interarea ones. Theoretically, this simple idea would maximize the damping of both modes, and it was what caught author's attention for a deeper investigation on this topic, what is exploited in details in the following sections of this work.

1.2 Aims of the thesis

The main aim of this thesis, according to the discussion performed throughout the last section, is to investigate new manners to damp out very low frequency oscillations, called interarea modes, in which the current PSS-based approaches either fail or give sub-optimum results.

However, stating by means of words alone, the idea of an "optimum" performance might be misunderstood. In Mathematics, for instance, in order for something to present an "optimum" behavior, a cost function must be minimized. In Control Engineering, this cost is often related to a quadratic function that has a global "optimum", and is minimized in order to obtain the control signal (or system's input signal) of what is called *optimal controller* [30]. Bounded to this idea, the present thesis is promoted.

An interesting idea to develop an optimal controller is to merge both exciter- and governor-based PSSs into a coordinated one, which might also be responsible for regulating turbine's power and generator's terminal voltage. The specialized literature is full of examples of such controllers (see, *e.g.*, [17, 19, 31]).

Notwithstanding, it is also known from practitioners that there exist two major issues for implementing coordinated controllers in practice: the paradigm shift ("Why would we implement such a change if what we have now is already proved to work properly?") and the lack of physical cooperation between the departments responsible for the mechanical and the electrical parts.

Therefore, this thesis does not aim at burden the ongoing solutions. What is specifically proposed here is to keep the current PSS, AVR and governor at the place they already are, and perform a slight modification in governor's software for implementing the proposed decentralized damping solution. In summary, what is being pursued is the development of a device that contributes positively to the damping of systems'

main modes and is able to work in parallel with the current solution. In this thesis we call this device PSS_t, *i.e.*, it is a Power System Stabilizer that acts on the turbine side.

In addition, another important detail that is often neglected in the Power Systems literature is the consideration of the measurement noise. Electrical signals are usually contaminated with noise, mainly near to large machines due to their high electromagnetic fields and vibrations. Figure 1.3 is a very good example of how uncertainty appears in the measurements*. Practitioners are aware of this issue, and what is mostly done is to basically implement a low-pass filter at the input of the governor. In other words, the filter is implemented afterwards and is usually neglected *during* the controller design, regardless of its order.

Although most papers neglect the measurement noise in their implementations (see, *e.g.*, [9, 28, 29, 31]), some regard it only during the simulations (see, *e.g.*, [21, 32, 33]), bounded to the idea of designing the controllers for the deterministic case and check whether it is capable of dealing well when stochasticity plays its role. If not, either the low-pass filter is implemented or, at its best, the controller gains are changed, what for both cases might result in a more conservative approach, since the filter would also attenuate system's high-order dynamics.

This idea seems helpful at a first glance, however what happens in practice is a narrowing in system's bandwidth, changing its characteristics. However, it is known from the Control Theory that *all* available dynamics shall be regarded in order to design controllers that are able to cope properly with all dynamics of the system, otherwise one could run the risk of resulting in either a sub-optimal system behavior (conservative approach) or, and much worse, reducing its stability margins [34, 35].

Besides, another issue arises within all PSSs that use the frequency as input, such as PSS2B and PSS4B: since its variation is usually small (lower than $\pm 0.1\%$ for non-fault cases), the sensor resolution must be high, otherwise a considerable amount of noise comes into play. However, it is known from practitioners that is not common to have encoders with a high number of pulses per revolution on turbine's axis. An usual workaround solution is to use the so-called compensated frequency and apply it on the speed input. The drawback is that adverse torsional interactions cause a mismatch between the angular and terminal frequencies, which is hardly detected in simulations and has the potential to be prejudicial to the actual system [8].

*The author has no information whether such signals are already filtered or not.

Nevertheless, to the best of author's knowledge, there is no control approach implemented at the turbine governor which regards stochasticity *intrinsically* during its design in the Power Systems literature, despite the fact that it is a well known field within the Control Theory. The main idea for making use of such approach is to expand system's bandwidth for enabling the high-order dynamics to act on it (aiming at high-performances) while at the same time, reducing the input signal variance, and consequently increasing the control valve life time.

Regarding noise inherently during controller's design leads necessarily to the field of *Model-based Predictive Control*, short MPC [34, 36]. Controllers designed based on this technique might be, if correctly parametrized, simultaneously optimum and stochastic. Works on MPCs applied to power systems are easily found in literature (see, *e.g.*, [37–40]), however again, to the extent of author's knowledge, there unexist studies on a *complete* stochastic formulation for the MPC in the field so far. Such formulation is another aim to be pursued in this work.

Ultimately, MPC means that system's model must be known, although it is not a trivial task concerning power systems. Most of the commercial softwares turned to the simulation of such plants use a 6th-order nonlinear differential equation system for reproducing generator's dynamical behavior (see, *e.g.*, [41–43]). In spite of being quite reliable when compared to actual systems, this modeling is not suitable for control purposes, since it increases substantially system's complexity. For MPCs it is critical since the size of controller's matrices are given by $z N_y$, with z being the order of the model and N_y the prediction horizon, which is usually equal to system's settling time [36].

As a simple example, a small grid composed by ten generators with prime movers/governors, AVRs and PSSs might be represented by nearly 200 nonlinear differential equations which, when linearized, results in a state matrix of size 200×200 [2]. It is clearly impracticable to solve for its eigenvalues algebraically, and even more difficult to design controllers based on the full model.

On the other hand, methods for simplifying system's complexity are well known in the literature, however most of them cope with system's state matrix reduction based on mathematical techniques where the complete model is always required (see, *e.g.*, [1, 2, 44–46]). On the contrary, an interesting modeling method is the so-called *Steady-State approach* [4, 47] along with its derivation, *Quasi-Steady-State approach* [48–50]. These methods consider basically the dynamics of the mechanical components of the system, *i.e.*, generators' axes, whilst for the terminal voltages static equations are taken into account.

Nonetheless, what has arisen author's interest on simplified modelings for power systems were the works of Wenzel [51] and Nelles [52]. Both present an equivalence between electrical and mechanical systems for performing the modeling of power grids with the aim at their synchronous and transient modes, *i.e.*, small-signal stability, ending up in a small set of differential equations that can be even further simplified aiming control purposes. Important to remark that it is possible to find several lecture notes, scripts, course handbooks, etc. that explain the power system oscillations using mechanical equivalences, since it is relatively easier to think on mechanical oscillating systems rather than on the cause of oscillations in complex electrical ones. The common point between all of these works is that they deliver a didactic explanation for the power system while keep on equating the grid based only on the electrical point of view. Their difference to [51] and [52] is that the latter model the mechanical system showing its equivalence to the power system based on an approach that considers grid's nodes as inertial mechanical bars free to rotate on the plan and connected to each other by springs. The springs represent the transmission lines and the length of the bars are nodes' voltages*.

In fact Wenzel [51] goes a bit forward in his approach than Nelles [52] since the former models also nodes' dynamics from Newton's 2nd Law. The issue in this case is that some assumptions that does not have any relation to the mechanical scheme of oscillating bars must be taken in order to match the results with the common approach presented in the literature. With this information in mind, one may state that the last aim of this work is to fulfill this gap.

By organizing the ideas discussed in this section it is possible to summarize the overall aim of the present thesis:

To contribute to the damping of the interarea modes by implementing a light computing Model-based Predictive Controller at the governor side in order to improve system's performance, while developing a new control-based modeling technique for power systems based on the equivalence between mechanical and electrical systems.

1.3 Contributions of the thesis

During the preparation of this thesis, six papers and one abstract have been published. They are listed in the following, where the main contributions of each are highlighted.

*More details in Chapter 3.

- **R. Trentini**, R. Kutzner, L. Hofmann, A. Campos, and C.S. Furtado Neto, “Modeling, parameter estimation and state-space control of a steam turbine”, in *Proceedings of the 23rd ABCM International Congress of Mechanical Engineering (COBEM 2015)*, Rio de Janeiro, Brazil, 2015. **Conference paper**.
 - Modeling of a steam turbine based on the Mass and Energy Conservation Theory, where the High, Intermediate and Low Pressure sections are regarded as resistive pipes, which simplifies considerably its equating;
 - Parameter identification of the modeled steam turbine based on Particle Swarm Optimization (PSO);
 - Design of turbine’s governor based on the Linear Quadratic Gaussian (LQG), where the measurement noise is taken into account in order to reduce valve’s variance;
- A. Silveira, **R. Trentini**, A. Coelho, R. Kutzner, L. Hofmann, “Generalized minimum variance control under long-range prediction horizon setups”, *ISA Transactions*, vol. 62, pp. 325-332, 2016. **Journal paper**.
 - Authors’ first attempt on developing a fully stochastic, long-range predictive controller with light computational cost.
- **R. Trentini**, R. Kutzner, and L. Hofmann, “State-space generalized minimum variance controller based PSS for damping of inter-area modes”, in *Proceedings of the 18th IEEE Mediterranean Electrotechnical Conference (MELECON 2016)*, Limassol, Cyprus, 2016. **Conference paper***.
 - Reduced black-box identification procedure for power systems.
 - Design of a PSS with only two tuning parameters based on the Generalized Minimum Variance Controller (GMVC).
- **R. Trentini**, R. Kutzner, and L. Hofmann, “Power grid modeling based on the electromechanical energy approach aiming power systems stability studies”, in *Proceedings of the 24th IEEE Mediterranean Conference on Control and Automation (MED’16)*, Athens, Greece, 2016. **Conference paper**.

*Awarded with the 2nd prize in the PhD Students Paper Competition.

- Modeling method for power systems that utilizes the Lagrangian Energy Method in order to simplify the system and aimed at controllers design.
- **R. Trentini**, A. Silveira, R. Kutzner, and L. Hofmann, “On the Unrestricted Horizon Predictive Control – a fully stochastic model-based predictive approach”, in *Proceedings of the European Control Conference (ECC'16)*, Aalborg, Denmark, 2016. **Conference paper.**
 - Definitive authors’ attempt on developing a fully stochastic, long-range and light computing MPC.
 - Intrinsic 2nd Diophantine’s solution through the state-space form.
 - N_y -steps ahead Kalman Filter (KF).
- **R. Trentini**, A. Silveira, M.T. Bartsch, R. Kutzner, and L. Hofmann, “On the design of stochastic RST controllers based on the Generalized Minimum Variance”, in *Proceedings of the 11th UKACC International Conference on Control (CONTROL 2016)*, Belfast, Northern Ireland, 2016. **Conference paper.**
 - Framework for designing any SISO linear controller as a stochastic one, with the aim at reducing control’s signal variance.
- **R. Trentini**, R. Kutzner, and L. Hofmann, “Stochastic speed governor based on the Generalized Minimum Variance Controller”, in *Tagungsband der 43. Kraftwerkstechnisches Kolloquium*, Dresden, Germany, 2016. **Abstract.**
 - Stochastic turbine governor based on the same gains of the current PI ones, aiming at the reduction of valve’s variance.

In addition to the just cited, this thesis also presents its own contributions, which are listed below:

- Extension of the modeling presented in [55] for regarding the transient voltage dynamics, along with the consideration of the prime mover and governor in the modeling and also the simplification of the load-buses.

- Identification of uncertainties and noise dynamics applied to extended power systems based on the Extended Kalman Filter (EKF).
- Development of the PSS_t which works in parallel to the current governor solution.
- Development of the controller presented in [56] for state feedback aiming at the control of complex multivariable systems.
- Development of the multivariable predictive turbine governor with intrinsic ability to damp out interarea modes effectively.

1.4 Organization of the thesis

Additionally to this introduction, this thesis is organized as follows:

Chapter 2 reviews the main topics on power systems with respect to the small signal stability analysis, such as prime movers, governors, synchronous machines, exciters and voltage regulators, besides the basic theory behind Multi-Machine systems.

Chapter 3 presents one of the main contributions of the work, namely the control-based power grid modeling, which makes use of the mechanical-electrical equivalence and is developed through the Lagrangian Energy Method, called *Electromechanical Energy Approach*.

The identification of uncertainties and noise dynamics of the model obtained in Chapter 3 is presented in Chapter 4.

Chapter 5 presents and evaluates the PSS_t, showing its main advantages and drawbacks.

In Chapter 6 the predictive controller to be implemented in turbine's governor is deployed. The UHPC (*Unrestricted Horizon Predictive Controller*) is also a fundamental contribution of this thesis, since it is, at the same time, a stochastic, long-range and light computing MPC.

Computer simulations using two benchmark systems are performed in Chapter 7: Single-Machine Infinite-Bus (SMIB) and Two-Area systems, in order to experiment the proposed modeling and control approaches presented in the latter chapters.

Finally, Chapter 8 presents thesis conclusions and outlooks.

2

Power Systems modeling

This chapter reviews the most relevant topics regarding the Power Systems modeling in a very simplified fashion in order to give a basic understanding on the main components of a power grid that are responsible for the interarea oscillations. It is important to clarify that no new information is given here, rather just a summarized overview based on the literature [1, 2, 4, 47] to situate the reader on the subject is given. All the analysis is performed in the time domain. Also, except for the generator, the modeling here presented is used in all further chapters of this thesis.

To begin with, consider the general model of a generating unit shown in Figure 2.1.

In the cited figure, ω , P , f , V , I and u are the angular speed, active power, frequency, voltage (in RMS), current (in RMS) and controllers' signals, respectively. The super-indexes r , t and \dagger stand for the reference, valve and field actuator signals, respectively. The dashed ellipses represent the measurement devices, while the dashed lines stand for signals that might be used by the devices in which they are connected to.

Still according to the figure, there are basically three regulators acting simultaneously on each generating unit: governor, AVR and PSS. Along with the exciter, the two latter are included in the block "Excitation system", however only the AVR's and PSS's dynamics are regarded in this work since, for a static exciter its time constant is much smaller than generator's one, and hence can be neglected. Similarly,

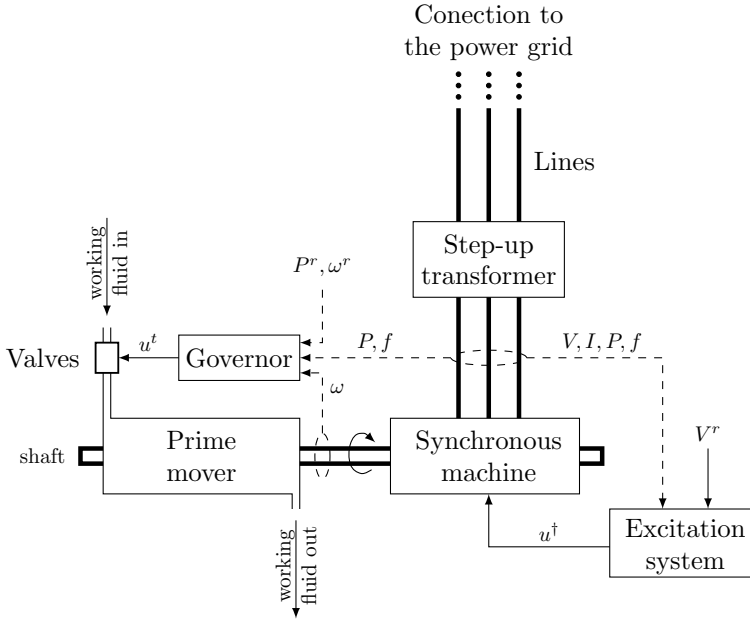


Figure 2.1: Block diagram of a power generating unit (based on [4]).

since the turbine time constant is much greater than the control valve one, the dynamics of the latter may also be neglected. In this case its time constant is comparably smaller to turbine's one [1–4].

Important to highlight is that, in this thesis both the transformers and the lines are considered as simple reactances. In other words, their resistances and capacitances are neglected in order to simplify the modeling. Also, the turbine valve is regarded with a linear behavior and the mechanical limitations and saturation of the concerned devices are neglected. In fact, these are a common simplifications in extended power systems analysis, see, *e.g.*, [1, 2, 4].

A further simplification concerns to the loads, which are regarded static. At last, other components present in power systems are also neglected, such as FACTS, breakers, HVDC transmission lines, etc. Nevertheless, slight modifications on the modeling presented in the following chapters of this thesis would allow the inclusion of the cited components in further studies.

Next sections present the basics on the prime mover, the governor,

the synchronous machine and the excitation system. At last it is also shown the basic modeling assumptions for multi-machine systems.

2.1 Prime mover

An important matter to be overcome in order to represent the overall power system in a simplified manner is the order of its prime movers. Depending upon the type (steam, gas, hydro, etc.), its detailed model might be represented by up to six nonlinear differential equations [4, 53], what increases substantially the final order of the overall power system. However, since the detailed modeling of turbines is beyond the scope of this thesis, here a simplified, linearized and generalized model that might represent either steam, gas or hydro units is regarded [1–4]. Its block diagram is concerned in Figure 2.2, with Δ representing the corresponding linearized variable.

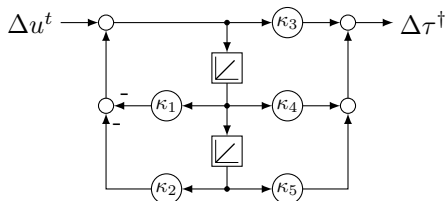


Figure 2.2: Generalized model of a prime mover.

In the time domain, prime mover's generalized model might be given for the k^{th} node by,

$$\begin{aligned}
 \Delta \dot{\vartheta}_{1_k} &= \Delta \vartheta_{2_k}, \\
 \Delta \dot{\vartheta}_{2_k} &= -\kappa_{2_k} \Delta \vartheta_{1_k} - \kappa_{1_k} \Delta \vartheta_{2_k} + \Delta u_k^t, \\
 \Delta \tau_k^\dagger &= \kappa_{3_k} \Delta u_k^t + (\kappa_{5_k} - \kappa_{2_k} \kappa_{3_k}) \Delta \vartheta_{1_k} \\
 &\quad + (\kappa_{4_k} - \kappa_{1_k} \kappa_{3_k}) \Delta \vartheta_{2_k},
 \end{aligned} \tag{2.1}$$

which in essence is a 2nd-order system with two zeros*, being τ^\dagger turbine's output torque (which in p.u. is equivalent to the active power if $\omega \approx 1$ p.u.), ϑ_1 and ϑ_2 are system's internal states and κ_i ($i = 1, \dots, 5$)

*Specifically, the system contains two roots for both the numerator (zeros) and the denominator (poles).

are model's constants that might capture the main parameters of the prime movers.

For instance, according to Kundur *et al.* [2], a tandem-compound steam turbine might be reduced to the model represented by Equations 2.1 if,

$$\kappa_1 = \frac{\tau_{\text{ch}} + \tau_{\text{re}}}{\tau_{\text{ch}}\tau_{\text{re}}}, \quad \kappa_2 = \frac{1}{\tau_{\text{ch}}\tau_{\text{re}}}, \quad \kappa_3 = 0, \quad \kappa_4 = \frac{F_{\text{hp}}}{\tau_{\text{ch}}}, \quad \kappa_5 = \kappa_2,$$

being τ_{ch} and τ_{re} chest's and reheater's time constants, and F_{hp} stands for the fraction of total power generated at turbine's high-pressure section.

Kutzner [59] has shown a simplification for gas turbines, in which may be written in the form of Equations 2.1 as,

$$\kappa_1 = \frac{\tau_v + 1}{\tau_v}, \quad \kappa_2 = \frac{1}{\tau_v}, \quad \kappa_3 = 0, \quad \kappa_4 = \kappa_5 = \kappa_2,$$

with τ_v representing turbine chamber's time constant.

Lastly, Machowski *et al.* [4] demonstrate that for hydro turbines Equations 2.1 also hold if,

$$\begin{aligned} \kappa_1 &= \frac{q_0\tau_{wt} + 2h_0}{q_0\tau_{wt}}, & \kappa_2 &= \frac{2h_0}{q_0\tau_{wt}}, & \kappa_3 &= -2A_t h_0^{3/2}, \\ \kappa_4 &= \frac{2A_t \left(h_0^{5/2} - q_0 h_0^{3/2} \tau_{wt} \right)}{q_0\tau_{wt}}, & \kappa_5 &= \frac{2A_t h_0^{5/2}}{q_0\tau_{wt}}, \end{aligned}$$

where q_0 , h_0 , τ_{wt} and A_t are respectively the flowrate, pressure head, water starting time and a compensation factor for the difference in the base values between generator and turbine.

2.2 Governor

The main Power Systems literature presents mostly speed-based governors, see, *e.g.*, [1–4]. However, VDI/VDE's Standard 3521 sheet 4 [60] cites explicitly a speed/power-based governor which is widely known to be very effective mainly among European practitioners for steam and gas turbines. It is also notorious that the main governor suppliers implement either the full structure or slight modifications of this device, what justifies its use in this thesis. However, despite the fact that usually hydro turbines use different governor structures, the same regulation profile may eventually be reached with the structure presented

in [60]. Figure 2.3 shows the cited governor, which is represented in the k^{th} node by the following linearized equations,

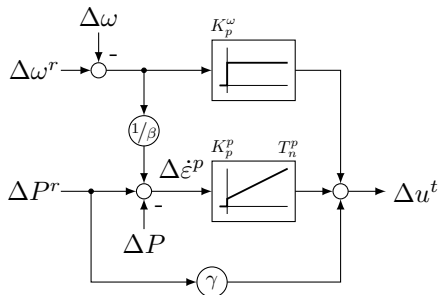


Figure 2.3: Speed/power turbine governor.

$$\begin{aligned} \Delta u_k^t &= \gamma_k \Delta P_k^r + K_{p_k}^p \Delta \varepsilon_k^p + \frac{K_{p_k}^p}{T_{n_k}^p} \Delta \varepsilon_k^p + K_{p_k}^\omega (\Delta \omega_k^r - \Delta \omega_k), \\ \Delta \varepsilon_k^p &= \Delta P_k^r - \Delta P_k + \frac{1}{\beta_k} (\Delta \omega_k^r - \Delta \omega_k), \end{aligned} \quad (2.2)$$

with $K_{p_k}^\omega$ and $K_{p_k}^p$ being respectively the proportional gains of the speed and power governors, whereas $T_{n_k}^p$ is the reset time, β_k is turbine's droop (if applicable), γ_k is governor's feedforward gain and $\Delta \omega^r$ is the speed reference, which is usually equal to zero.

Notice the inclusion of the state variable $\Delta \varepsilon^p$. It means that the model of the governor increases in one unit the overall size of the system, as it is discussed in the following Section 2.5.

2.3 Synchronous machine

Being the core component of the power generating unit, most of the specialized literature sets significant chapters on generator's modeling (see, *e.g.*, [1, 2, 4]). However and as well as for the prime mover, the detailed modeling of this important device is beyond the scope of the present thesis.

Rather, the idea here is to present the most common linearized dynamic models used for the generators in the Power Systems literature. The three models to be presented are obtained from [4].

6th-order model: This model is widely used for Power Systems simulations in specialized softwares (see, *e.g.*, [41–43]), and its differential equations are given for the k^{th} node by,

$$\begin{aligned}\Delta \dot{\lambda}_k &= \Delta \omega_k, \\ 2H_k \Delta \dot{\omega}_k &= \Delta P_k^\dagger - \Delta P_k, \\ \tau'_{d0k} \Delta \dot{e}'_{qk} &= \Delta e_k^\dagger - \Delta e'_{qk} + \Delta i_{dk} (X_{dk} - X'_{dk}), \\ \tau'_{q0k} \Delta \dot{e}'_{dk} &= -\Delta e'_{dk} - \Delta i_{qk} (X_{qk} - X'_{qk}), \\ \tau''_{d0k} \Delta \dot{e}''_{qk} &= \Delta e'_{qk} - \Delta e''_{qk} + \Delta i_{dk} (X'_{dk} - X''_{dk}), \\ \tau''_{q0k} \Delta \dot{e}''_{dk} &= \Delta e'_{dk} - \Delta e''_{dk} + \Delta i_{qk} (X'_{qk} - X''_{qk}),\end{aligned}$$

where ΔP^\dagger is the mechanical power delivered by the prime mover, τ_{i0} ($i = d, q$) is field's time constant, X_i ($i = d, q$) is the internal reactances, and Δe represents generator's internal voltage. The super-indexes ' and '' stand for the transient and subtransient values, respectively, being the latter related to rotor's damper windings.

The terminal voltage V is obtained by,

$$V_k = \sqrt{V_{dk}^2 + V_{qk}^2}, \quad (2.3)$$

with,

$$V_{dk} = e''_{dk} - R_{ak} i_{dk} - X''_{qk} i_{qk}, \quad V_{qk} = e''_{qk} + X''_{dk} i_{dk} - R_{ak} i_{qk},$$

being R_a the armature resistance.

3rd-order model: Despite representing well the generator's dynamics, the 6th-order model is not suitable for modal analysis and control purposes due to its complexity. Hence, a common model simplification is made by neglecting the damper windings, which also reduces $\Delta e'_d = 0$. Thus,

$$\begin{aligned}\Delta \dot{\lambda}_k &= \Delta \omega_k, \\ 2H_k \Delta \dot{\omega}_k &= \Delta P_k^\dagger - \Delta P_k - D_k \Delta \omega_k, \\ \tau'_{d0k} \Delta \dot{e}'_{qk} &= \Delta e_k^\dagger - \Delta e'_{qk} + \Delta i_{dk} (X_{dk} - X'_{dk}).\end{aligned} \quad (2.4)$$

This model is also called *Classical Model*, and Machowski *et al.* [4] cites that it is considered sufficiently accurate to analyse electromechanical oscillations.

Nevertheless, the taken assumption means that the asynchronous torque produced by the damper windings is also neglected. Therefore it is required to add the damping term D at the swing equation for compensating the lack of these windings.

The drawback of this modeling is that, mainly for multi-machine systems, the damping term D must be estimated, since it does not represent an actual damping factor on generator's axis.

The terminal voltage V is still obtained by Equation 2.3 with,

$$V_{d_k} = e'_{d_k} - R_{a_k} i_{d_k} - X'_{q_k} i_{q_k}, \quad V_{q_k} = e'_{q_k} + X'_{d_k} i_{d_k} - R_{a_k} i_{q_k},$$

2nd-order model: This model is widely used for simplified analysis of power systems dynamics [4]. It neglects the voltage dynamics with the justification that, since Δe^\dagger and Δi_d are small and the time constant τ'_{d0} is large, then $\Delta e'_q$ varies slowly. Hence,

$$\begin{aligned} \Delta \dot{\lambda}_k &= \Delta \omega_k, \\ 2H_k \Delta \dot{\omega}_k &= \Delta P_k^\dagger - \Delta P_k - D_k \Delta \omega_k, \end{aligned} \tag{2.5}$$

which represents basically generator's mechanical dynamics.

If the rotor transient saliency is neglected ($X'_q = X'_d$), the terminal voltage V is given for this model simply as,

$$(v_{d_k} + jv_{q_k}) = (e'_{d_k} + je'_{q_k}) - jX'_{d_k} (i_{q_k} + ji_{d_k}).$$

2.4 Excitation system

As previously cited, the excitation systems is composed basically by the Automatic Voltage Regulator (AVR), Power System Stabilizer (PSS) and exciter. Here it is considered that exciter's time constant is much smaller than generator's one, and therefore its dynamics may be neglected. This assumption is common among static exciter types, see, *e.g.*, [2, 4]. For rotating exciters a simple and usual representation is to regard them as 1st-order blocks. However, for the sake of simplicity this thesis does not consider rotating exciters during the excitation system modeling.

Automatic Voltage Regulator: The AVR is regarded here as a PI controller, which is concerned in Figure 2.4, and its mathematical representation is given by,

$$\begin{aligned}\Delta u_k^\dagger &= K_{p_k}^e \Delta \varepsilon_k^e + \frac{K_{p_k}^e}{T_{n_k}^e} \Delta \varepsilon_k^e, \\ \Delta \dot{\varepsilon}_k^e &= \Delta V_k^r - \Delta V_k + \Delta v_{\text{pss}_k},\end{aligned}\tag{2.6}$$

being $K_{p_k}^e$ and $T_{n_k}^e$ AVR's proportional gain and reset time of the k^{th} node, respectively, and Δv_{pss_k} stands for PSS's output.

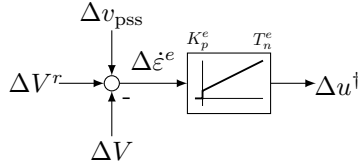


Figure 2.4: Simplified AVR-based PI controller.

Notice that, as well as for the governor, the AVR also introduces a new state variable $\Delta \varepsilon^e$ to system's overall modeling.

Power System Stabilizer: According to Kundur *et al.* [2], for small-signal stability analysis the PSS may be simplified in order to reduce system's state matrix. Also, it is known that speed-based PSSs present problems related to torsional modes and lack of sensor resolution [2, 4]. A clever way to overcome these issues is through the usage of the PSS2B, which is shown in its simplified version with two lead-lag blocks in Figure 2.5.

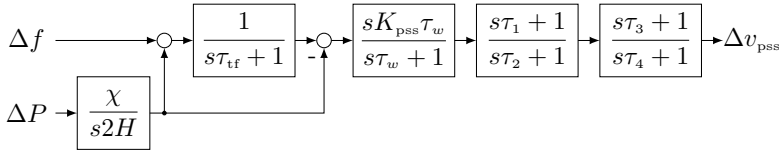


Figure 2.5: Simplified PSS2B.

In the cited figure, H , K_{pss} , τ_{tf} , τ_w and τ_i ($i = 1, \dots, 4$) stand respectively for generator's inertia constant, the PSS gain and the time

constants of the torsional and washout filters and lead-lag compensator. Further, χ is a flag that might be either 1 or 0, depending only upon the number of desired inputs. In the time domain, the simplified PSS2B might be represented as,

$$\begin{aligned}
\Delta \dot{v}_{1k} &= \Delta v_{2k}, \\
\Delta \dot{v}_{2k} &= \Delta v_{3k}, \\
\Delta \dot{v}_{3k} &= \Delta v_{4k}, \\
\Delta \dot{v}_{4k} &= -\mu_{1k} \Delta v_{1k} - \mu_{2k} \Delta v_{2k} - \mu_{3k} \Delta v_{3k} - \mu_{4k} \Delta v_{4k} + \Delta u_{\text{pss}_k}, \\
\Delta v_{\text{pss}_k} &= \sigma_{2k} \Delta v_{2k} + \sigma_{3k} \Delta v_{3k} + \sigma_{4k} \Delta v_{4k}, \\
\Delta u_{\text{pss}_k} &= 2H_k \Delta f_k - \chi_k \tau_{\text{tf}_k} \Delta P_k,
\end{aligned} \tag{2.7}$$

with,

$$\begin{aligned}
\mu_{1k} &= \frac{1}{\tau_{2k} \tau_{4k} \tau_{\text{tf}_k} \tau_{w_k}}, & \mu_{2k} &= \frac{\tau_{2k} + \tau_{4k} + \tau_{\text{tf}_k} + \tau_{w_k}}{\tau_{2k} \tau_{4k} \tau_{\text{tf}_k} \tau_{w_k}}, \\
\mu_{3k} &= \frac{(\tau_{2k} + \tau_{4k} + \tau_{\text{tf}_k}) \tau_{w_k} + (\tau_{2k} + \tau_{4k}) \tau_{\text{tf}_k} + \tau_{2k} \tau_{4k}}{\tau_{2k} \tau_{4k} \tau_{\text{tf}_k} \tau_{w_k}}, \\
\mu_{4k} &= \frac{((\tau_{2k} + \tau_{4k}) \tau_{\text{tf}_k} + \tau_{2k} \tau_{4k}) \tau_{w_k} + \tau_{2k} \tau_{4k} \tau_{\text{tf}_k}}{\tau_{2k} \tau_{4k} \tau_{\text{tf}_k} \tau_{w_k}}, \\
\sigma_{2k} &= \frac{K_{\text{pss}_k}}{2H_k \tau_{2k} \tau_{4k} \tau_{\text{tf}_k}}, & \sigma_{3k} &= \frac{(\tau_{1k} + \tau_{3k}) K_{\text{pss}_k}}{2H_k \tau_{2k} \tau_{4k} \tau_{\text{tf}_k}}, \\
\sigma_{4k} &= \frac{\tau_{1k} \tau_{3k} K_{\text{pss}_k}}{2H_k \tau_{2k} \tau_{4k} \tau_{\text{tf}_k}}.
\end{aligned}$$

2.5 Multi-machine systems

As already cited in the Introduction section, power systems are very complex and coupled structures, in which their mathematical models might easily reach as many as 30,000 states [2, 4]. Therefore, the analysis of such huge systems must be carried out carefully. Thereunto, as well as shown in [4] with the so-called *Steady-State approach**, this thesis regards the voltage and angle of each *active* node of the grid.

By active it is meant the nodes in which at least one generator and/or load is connected to, or in other words, nodes that either generate or consume power. Conversely, *passive* nodes are the nodes where

*Despite the name *Steady-State approach*, this modeling procedure regards a dynamic system (refer to [4]).

neither load(s) nor generator(s) are connected to. Figure 2.6 exemplifies this approach.

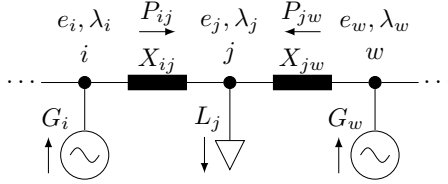


Figure 2.6: Example of power flow through the nodes of a power system.

This analysis is similar to Kirchhoff's Current Law, however in this case we assume that node's entering power is negative while the leaving one is positive. In the example of Figure 2.6, node's i active power is given only by $P_i = P_{ij}$, while node j presents $P_j = -P_{ij} - P_{jw}$. Similarly to node i , at node w holds $P_w = P_{jw}$. The values for the powers, as well for the initial voltages, angles, etc., are obtained by the load flow analysis that must be performed beforehand.

Eventually, each dynamic node (*i.e.*, nodes where one or more generators are connected) may regard the whole generating unit, *i.e.*:

- the prime mover (Equations 2.1, two state variables);
- the governor (Equations 2.2, one state variable);
- the generator (Equations 2.5, two state variables);
- the AVR (Equations 2.6, one state variable) and,
- the PSS (Equations 2.7, three state variables).

The equation that couples consecutive nodes is,

$$P_k = V_k^2 G_{kk} + \sum_{\substack{m=1 \\ m \neq k}}^N V_k V_m [B_{km} \sin(\lambda_k - \lambda_m) + G_{km} \cos(\lambda_k - \lambda_m)],$$

with N being the number of active nodes of the grid and with the admittance between them being given by $Y_{km} = G_{km} + jB_{km}$. Another common simplification among the Power Systems literature is to regard $G_{km} = 0$, *i.e.*, to consider only line's reactance.

Summarizing, each dynamic node is represented by a 10th-order system. It is still a high order, however 63% smaller than the usual mathematical model that most of the commercial power systems softwares implement (see, *e.g.*, [41–43]).

Nevertheless, regarding only Equations 2.5 for representing generator's dynamics leads to an issue: this model does not allow a dynamic change in the voltage. A solution for this matter is, *e.g.*, the usage of the *Quasi-Steady-State approach* [47–50], that considers algebraic equations for the voltage profile. This is an interesting approach for simulations purposes, but it still sins whenever the aim is system's modal analysis, since the state corresponding to the voltage is not regarded in system's matrices.

The most direct possibility is to use Equation 2.4, which increases node's mathematical representation in one order. Further, the d-axis current must be obtained, which complicates the solution as well. In Chapter 3 a solution for this matter that also increases node's model in one order is discussed. Nonetheless, there is shown that the transient voltage dynamic equation might be obtained through the Lagrangian Energy Method using an equivalence between electrical and mechanical systems, being the cited solution equivalent to the one presented in this chapter.

Lastly, it is important to notice that, even though the presented model is considerably reduced compared to others, it does not lose its main features whenever the aim is the assess to interarea oscillations [4].

3

The Electromechanical Energy Approach

This chapter presents one of the main contributions behind the thesis: the modeling of power grids in order to obtain a set of differential equations which describes system's dynamic behavior in a simplified fashion aiming at its further control, *i.e.*, the final obtained model is reduced and control-based. The method is called *Electromechanical Energy Approach*.

Indeed, important to highlight is that the chapter does not aim at achieving a very accurate model for power systems, since control-based models are usually simplified and linearized versions of the complete ones. Instead, the modeling presented here considers simplifications inherently, *e.g.*, the transmission lines resistances are neglected, as well as generators' subtransient and d-axis dynamics (regarded constants).

Also noteworthy is that this chapter presents three slight but substantial extensions of author's publication [55] w.r.t. the consideration of the RMS values of node's voltage dynamics inherently, the simplification of load-buses and the implementation of the prime mover and governor on system's modeling, what was not covered in the cited paper.

The chapter begins with a short clarification on the basis for the development of the presented procedure, where the modeling itself is presented in the following section. Lastly, the modal analysis of one exemplary system is performed in order to evaluate the proposed method.

3.1 Basis for the method

According to the discussion performed throughout the Introduction, the idea of this section was obtained from the works of Wenzel [51] and Nelles [52], which are possibly inspired by Leonhard [61]. Independently and at the same time, both have presented an analogy between the power grid and a mechanical structure consisted of rotating bars. They also have proved that there is an equivalence on the main parameters of both systems, which for completeness are shown in Table 3.1.

Table 3.1: Mechanical-Electrical quantities equivalence [51, 52]

Mechanical quantity	Electrical quantity
length	voltage
spring constant	inductance ⁻¹
torque	active power
radial force	reactive electric charge

Differently from [51] and [52], that regarded only the mechanical equations in their modelings, what is specifically shown here is that when one considers an *electromechanical* scheme of oscillating bars the final result is a complete model for the analyzed node of the power grid, *i.e.* the mechanical and electrical differential equations are directly obtained. It is achieved due to the usage of the so-called *Lagrangian Energy Method*, which is basically an energy-based method that considers system's kinetic and potential energies, and is very suitable for complex systems since it solves for its differential equations at once without further assumptions.

It is important to remark that there are electromechanical devices (generators) involved in the grid, *i.e.*, both electrical and mechanical quantities must be taken into account during the analysis. Hence, our next assumption is that nodes' moments of inertia are given by,

$$\mathbf{J}_k = \begin{bmatrix} J_k^m & J_k^e \end{bmatrix},$$

where \mathbf{J}_k represents simultaneously the inertias of the mechanical (J_k^m – related to axis' moving mass) and the electrical (J_k^e – related to rotor's impedance) parts of the k^{th} node.

For a better picture of the overall problem, the diagram of the proposed electromechanical representation of a Two-Node system is

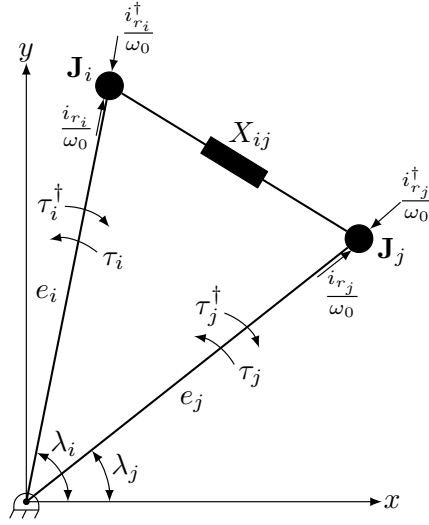


Figure 3.1: Electromechanical diagram for a Two-Node system.

shown in Figure 3.1. This figure, though, will serve as the basis for the modeling of extended power grids consisting of N nodes.

In the cited figure there are two rotating bars with variable lengths e_i , e_j and variable angles λ_i , λ_j^* . The bars represent the grid nodes, whereas X_{ij} is the reactance between them, including transformer's, line's and generator's internal reactances. The combined inertia vector \mathbf{J}_k is, without any loss of generality, arbitrarily represented on the upper part of the bars. A torque τ_k^{\dagger} and a reactive electric charge $i_{r_k}^{\dagger}/\omega_0$ are generated in each bar to oppose the external ones τ_k , i_{r_k}/ω_0 , which come from the connection to the remaining grid. The torque is proportional to the active power such that $P = \omega\tau \approx \omega_0\tau$, being ω_0 generator's angular synchronous frequency. The *transmission angle* is given by $\lambda_{ij} = \lambda_i - \lambda_j$ and it is directly responsible for the transmitted active power over the nodes i, j [1].

*Note: since the aim of this section is to assess the frequency of rotors' oscillations, the voltages, angles, powers, torques and currents to be analyzed are intrinsically regarded as the transient ones.

3.2 The modeling

Let us also assume that the external forces/torques and state vectors are given respectively by,

$$\mathbf{Q}_k = \frac{1}{\omega_0} [P_k^\dagger \quad i_{r_k}^\dagger]^T \quad \text{and} \quad \mathbf{q}_k = [\lambda_k \quad e_k]^T,$$

which in practice represent the active power P_k^\dagger and reactive current $i_{r_k}^\dagger$ generated at the k^{th} node, besides its own voltage e_k and voltage angle λ_k . Notice that e_k is equivalent to generator's transient q-axis emf [4].

The Lagrangian Energy Method states that,

$$\mathcal{L} = \mathcal{T} - \mathcal{U},$$

with \mathcal{T} and \mathcal{U} being the kinetic and potential energies respectively given by,

$$\begin{aligned} \mathcal{T} &= \frac{1}{2} \sum_{k=1}^N \mathbf{J}_k \dot{\mathbf{q}}_k^2, \\ \mathcal{U} &= \frac{1}{2} \sum_{k=1}^N \sum_{m \neq k}^M \frac{1}{\omega_0 X_{km}} (\vec{e}_k - \vec{e}_m)^2, \\ &= \frac{1}{2} \sum_{k=1}^N \sum_{m \neq k}^M \frac{1}{\omega_0 X_{km}} (e_k^2 + e_m^2 - 2 e_k e_m \cos \lambda_{km}), \end{aligned}$$

where there are M connections to the k^{th} node, being $M < N$.

The method also allows the consideration of damping factors for its states. We suppose that there are damping between node k w.r.t. the x -axis and also to each attached node, hence,

$$\mathcal{P} = \frac{1}{2} \sum_{k=1}^N \mathbf{b}_k \dot{\mathbf{q}}_k^2 + \frac{1}{2} \sum_{k=1}^N \sum_{m \neq k}^M \mathbf{b}_{km} (\dot{\mathbf{q}}_k^2 - \dot{\mathbf{q}}_m^2),$$

where,

$$\mathbf{b}_k = [b_k^m \quad b_k^e] \quad \text{and} \quad \mathbf{b}_{km} = [b_{km}^m \quad 0],$$

with the superscripts “ m ” and “ e ” denoting the mechanical and electrical damping, respectively. To be noticed is that no electrical damping

between nodes k and m is regarded, which can be easily seen in Figure 3.1.

Now, re-arranging the external forces and state vectors to be,

$$\mathbf{Q} = \frac{1}{\omega_0} [P_1^\dagger \quad \cdots \quad P_N^\dagger \mid i_{r_1}^\dagger \quad \cdots \quad i_{r_N}^\dagger]^T,$$

$$\mathbf{q} = [\lambda_1 \quad \cdots \quad \lambda_N \mid e_1 \quad \cdots \quad e_N]^T,$$

and using the so-called Lagrange's Equation of the First Kind,

$$\mathbf{Q} = \frac{d}{dt} \left(\frac{\partial \mathcal{L}}{\partial \dot{\mathbf{q}}} \right) - \frac{\partial \mathcal{L}}{\partial \mathbf{q}} + \frac{\partial \mathcal{P}}{\partial \dot{\mathbf{q}}},$$

one obtains,

$$\mathbf{Q} = \mathbf{J} \ddot{\mathbf{q}} + \mathbf{D} \dot{\mathbf{q}} + \boldsymbol{\kappa}(\mathbf{q}), \quad (3.1)$$

where \mathbf{J} and \mathbf{D} are the here defined *inertia* and *damping* matrices, and $\boldsymbol{\kappa}$ is defined as the *coupling* vector. They are given by,

$$\mathbf{J} = \text{diag}(J_1^m \quad \cdots \quad J_N^m \mid J_1^e \quad \cdots \quad J_N^e),$$

$$\boldsymbol{\kappa}(\mathbf{q}) = \frac{1}{\omega_0} [P_1 \quad \cdots \quad P_N \mid i_{r_1} \quad \cdots \quad i_{r_N}]^T,$$

$$\mathbf{D} = \left[\begin{array}{c|c} \mathbf{D}^m & \mathbf{0} \\ \hline \mathbf{0} & \mathbf{D}^e \end{array} \right],$$

with,

$$\mathbf{D}^m = \left[\begin{array}{cccc} b_1^m + \sum_{m \neq 1}^M b_{1m}^m & -b_{12}^m & \cdots & -b_{1N}^m \\ -b_{21}^m & b_2^m + \sum_{m \neq 1}^M b_{2m}^m & \cdots & -b_{2N}^m \\ \vdots & \vdots & \ddots & \vdots \\ -b_{N1}^m & -b_{N2}^m & \cdots & b_N^m + \sum_{m \neq 1}^M b_{Nm}^m \end{array} \right],$$

$$\mathbf{D}^e = \text{diag}(b_1^e \quad \cdots \quad b_N^e),$$

and,

$$P_k = \sum_{m \neq k}^M \frac{1}{X_{km}} e_k e_m \sin \lambda_{km}, \quad (3.2)$$

$$i_{r_k} = \sum_{m \neq k}^M \frac{1}{X_{km}} (e_k - e_m \cos \lambda_{km}), \quad (3.3)$$

being the latter the active power P_k and reactive current i_{r_k} consumed at the k^{th} node due to the connection to the grid. Also, $b_{km} = b_{mk}$.

Important to notice is that the name *coupling* vector stands due to its characteristic of coupling between the analyzed nodes, differently from the *inertia* and *damping* matrices, which are linear. The coupling occurs due to the transmitted power/current between the nodes, as can be directly stated observing the vector $\boldsymbol{\kappa}$.

Finally, assuming that,

$$J_k^m = \frac{2H_k}{\omega_0^2} S_b, \quad J_k^e = \frac{1}{\omega_0^3 X'_{d_k}}, \quad b_k^m = \frac{S_b}{\omega_0^2} D_k,$$

$$b_{km}^m = \frac{S_b}{\omega_0^2} D_{km} \quad \text{and} \quad b_k^e = \frac{\tau'_{d0_k}}{\omega_0} \sum_{m \neq k}^M \frac{1}{X_{km}},$$

being H_k and S_b the inertia constant and apparent power base value [2], D_k and D_{km} the damping coefficients, X'_{d_k} generator's d-axis transient reactance and τ'_{d0_k} generator's open-loop transient time constant. Converting everything to the p.u. system and remembering that $\dot{\lambda} = \omega_0 \bar{\omega}$, Equation 3.1 turns to,

$$\dot{\bar{\omega}}_k = \frac{1}{2H_k} \left[\bar{P}_k^\dagger - \bar{P}_k + \sum_{m \neq k}^M D_{km} \bar{\omega}_m - \left(D_k + \sum_{m \neq k}^M D_{km} \right) \bar{\omega}_k \right], \quad (3.4)$$

$$\ddot{\bar{e}}_k = \omega_0^2 \bar{X}'_{d_k} \left(\bar{i}_{r_k}^\dagger - \bar{i}_{r_k} - \sum_{m \neq k}^M \frac{\tau'_{d0_k}}{\bar{X}_{km}} \dot{\bar{e}}_k \right), \quad (3.5)$$

where the upper bar represents the p.u. values and ω_k is the angular frequency at the k^{th} node.

The set of equations 3.4-3.5 depicts the behavior of the power system at node k with the aim at stability studies. Equation 3.4 is particularly similar to the well-known swing equation [1], however in this case the active power \bar{P}_k represents the contribution from the grid connection rather than from the generator alone.

One should also notice that the sum $D_k + \sum_{m \neq k}^M D_{km}$ is related to node's damping of the synchronous modes and $\sum_{m \neq k}^M D_{km}$ alone to the oscillation damping between nodes k and m .

In comparison to the widely-known *Steady-State* method, the developed electromechanical energy based approach has the clear advantage of being more detailed since it takes into account also the dynamics of the electrical circuit w.r.t. each node, besides of considering also the generated power P_k^\dagger and reactive current $i_{r_k}^\dagger$ as inputs. Nevertheless, in spite of resulting in simple and intuitive equations, the modeling presented so far in this section is not feasible whenever the aim is the stability analysis of very large power grids since each node corresponds to a 4th-order nonlinear system.

A trivial simplification that can be performed in the model is to neglect the electrical second derivative since,

$$\frac{1}{\omega_0^2 \bar{X}'_{d_k}} \ll \sum_{m \neq k}^M \frac{\tau'_{d0_k}}{\bar{X}_{km}}.$$

Therefore, Equation 3.5 turns to,

$$\dot{\bar{e}}_k = \frac{1}{\tau'_{d0_k}} \underbrace{\left(\sum_{m \neq k}^M \frac{1}{\bar{X}_{km}} \right)^{-1}}_{\bar{Y}_k} \left(\bar{i}_{r_k}^\dagger - \bar{i}_{r_k} \right).$$

Substituting Equation 3.3 into the latter, one easily finds,

$$\boxed{\dot{\bar{e}}_k = \frac{1}{\tau'_{d0_k}} \left[\bar{e}_k^\dagger - \bar{e}_k + \bar{Y}_k \sum_{m \neq k}^M \frac{1}{\bar{X}_{km}} \bar{e}_m \cos \lambda_{km} \right]}, \quad (3.6)$$

where $\bar{e}_k^\dagger = \bar{i}_{r_k}^\dagger \bar{Y}_k$ is proportional to generator's field voltage. Notice that if the system is composed by only one generator (SMIB system), then $M = 0$ and Equation 3.6 becomes very similar to the widely-known voltage equation of the so-called *Classical Model* [1–4] (refer to Equation 2.4 with i_{d_k} being the reactive current i_{r_k} of Equation 3.3).

In order to reduce further its complexity, system's linearization will be performed in the following. Applying Taylor's series to equations 3.4-3.5 and truncating it in the first term one obtains,

$$\Delta \dot{\bar{\omega}}_k = \frac{1}{2H_k} \left[\Delta \bar{P}_k^\dagger - \Delta \bar{P}_k + \sum_{m \neq k}^M D_{km} \Delta \bar{\omega}_m - \left(D_k + \sum_{m \neq k}^M D_{km} \right) \Delta \bar{\omega}_k \right], \quad (3.7)$$

$$\Delta \dot{\bar{e}}_k = \frac{1}{\tau'_{d0k}} \left[\Delta \bar{e}_k^\dagger - \Delta \bar{e}_k + \bar{Y}_k \sum_{m \neq k}^M \frac{1}{\bar{X}_{km}} \cos \tilde{\lambda}_{km} \Delta \bar{e}_m - \bar{Y}_k \sum_{m \neq k}^M \frac{1}{\bar{X}_{km}} \tilde{e}_m \sin \tilde{\lambda}_{km} \Delta \lambda_{km} \right], \quad (3.8)$$

with,

$$\begin{aligned} \Delta \bar{P}_k = & \sum_{m \neq k}^M \frac{1}{\bar{X}_{km}} \tilde{e}_m \sin \tilde{\lambda}_{km} \Delta \bar{e}_k + \tilde{e}_k \sum_{m \neq k}^M \frac{1}{\bar{X}_{km}} \sin \tilde{\lambda}_{km} \Delta \bar{e}_m \\ & + \tilde{e}_k \sum_{m \neq k}^M \frac{1}{\bar{X}_{km}} \tilde{e}_m \cos \tilde{\lambda}_{km} \Delta \lambda_{km}, \end{aligned}$$

where the tilde represents the equilibrium points in which the system is linearized around. Hence, grid's state-space representation is given by,

$$\begin{aligned} \Delta \dot{\mathbf{x}}_{c1} = & \underbrace{\begin{bmatrix} \mathbf{0} & \omega_0 \mathbf{I} & \mathbf{0} \\ -\mathcal{H}^{-1} \Phi_\lambda & -\mathcal{H}^{-1} \Phi_\omega & -\mathcal{H}^{-1} \Phi_e \\ -\mathcal{T}^{-1} \Psi_\lambda & \mathbf{0} & -\mathcal{T}^{-1} \Psi_e \end{bmatrix}}_{\mathbf{A}_{n1}} \Delta \mathbf{x}_{c1} \\ & + \underbrace{\begin{bmatrix} \mathbf{0} & \mathbf{0} \\ \mathcal{H}^{-1} & \mathbf{0} \\ \mathbf{0} & \mathcal{T}^{-1} \end{bmatrix}}_{\mathbf{B}_{n1}} \Delta \mathbf{u}_{c1}, \end{aligned}$$

$$\Delta \mathbf{y}_{c1} = \underbrace{\begin{bmatrix} \Phi_\lambda & \Phi_\omega & \Phi_e \\ \mathbf{0} & \mathbf{0} & \mathbf{I} \end{bmatrix}}_{\mathbf{C}_{n1}} \Delta \mathbf{x}_{c1},$$

being $\Delta \mathbf{x}_{c1}$ (size $3N \times 1$), $\Delta \mathbf{u}_{c1}$ and $\Delta \mathbf{y}_c$ (both size $2N \times 1$) the state, input and output vectors respectively, which are given by,

$$\begin{aligned} \Delta \mathbf{x}_{c1} &= [\Delta \lambda_1 \quad \cdots \quad \Delta \lambda_N \mid \Delta \bar{\omega}_1 \quad \cdots \quad \Delta \bar{\omega}_N \mid \Delta \bar{e}_1 \quad \cdots \quad \Delta \bar{e}_N]^T, \\ \Delta \mathbf{u}_{c1} &= [\Delta \bar{P}_1^\dagger \quad \cdots \quad \Delta \bar{P}_N^\dagger \mid \Delta \bar{e}_1^\dagger \quad \cdots \quad \Delta \bar{e}_N^\dagger]^T, \\ \Delta \mathbf{y}_{c1} &= [\Delta \bar{P}_1 \quad \cdots \quad \Delta \bar{P}_N \mid \Delta \bar{e}_1 \quad \cdots \quad \Delta \bar{e}_N]^T. \end{aligned}$$

The first N rows of the output vector $\Delta \mathbf{y}_c$ give nodes' active powers, whereas the remaining N rows provide their voltages. Despite the fact that it is not common in the literature, it is known from practitioners that the choice for the active power as output is natural in Power Systems since it is a controllable variable [4].

The input matrix \mathbf{B}_{n1} is partially composed by the inverse of the inertia and time constant matrices \mathcal{H} and \mathcal{T} , both size $N \times N$, where,

$$\begin{aligned} \mathcal{H} &= \text{diag}(2H_1 \quad \cdots \quad 2H_N), \\ \mathcal{T} &= \text{diag}(\tau'_{d0_1} \quad \cdots \quad \tau'_{d0_N}). \end{aligned}$$

The state matrix \mathbf{A}_{n1} , dimension $3N$, is composed by the following sub-matrices,

$$\Phi_\lambda = \begin{bmatrix} \tilde{e}_1 \sum_{m \neq 1}^M \frac{\tilde{e}_m c \tilde{\lambda}_{1m}}{\bar{X}_{1m}} & -\frac{\tilde{e}_1 \tilde{e}_2 c \tilde{\lambda}_{12}}{\bar{X}_{12}} & \cdots & -\frac{\tilde{e}_1 \tilde{e}_N c \tilde{\lambda}_{1N}}{\bar{X}_{1N}} \\ -\frac{\tilde{e}_2 \tilde{e}_1 c \tilde{\lambda}_{21}}{\bar{X}_{21}} & \tilde{e}_2 \sum_{m \neq 2}^M \frac{\tilde{e}_m c \tilde{\lambda}_{2m}}{\bar{X}_{2m}} & \cdots & -\frac{\tilde{e}_2 \tilde{e}_N c \tilde{\lambda}_{2N}}{\bar{X}_{2N}} \\ \vdots & \vdots & \ddots & \vdots \\ -\frac{\tilde{e}_N \tilde{e}_1 c \tilde{\lambda}_{N1}}{\bar{X}_{N1}} & -\frac{\tilde{e}_N \tilde{e}_2 c \tilde{\lambda}_{N2}}{\bar{X}_{N2}} & \cdots & \tilde{e}_N \sum_{m \neq N}^M \frac{\tilde{e}_m c \tilde{\lambda}_{Nm}}{\bar{X}_{Nm}} \end{bmatrix}$$

$$\begin{aligned}
\Phi_\omega &= \begin{bmatrix} D_1 + \sum_{m \neq 1}^M D_{1m} & -D_{12} & \cdots & -D_{1N} \\ -D_{21} & D_2 + \sum_{m \neq 2}^M D_{2m} & \cdots & -D_{2N} \\ \vdots & \vdots & \ddots & \vdots \\ -D_{N1} & -D_{N2} & \cdots & D_N + \sum_{m \neq N}^M D_{Nm} \end{bmatrix} \\
\Phi_e &= \begin{bmatrix} \sum_{m \neq 1}^M \frac{\tilde{e}_m s \tilde{\lambda}_{1m}}{\tilde{X}_{1m}} & \frac{\tilde{e}_1 s \tilde{\lambda}_{12}}{\tilde{X}_{12}} & \cdots & \frac{\tilde{e}_1 s \tilde{\lambda}_{1N}}{\tilde{X}_{1N}} \\ \frac{\tilde{e}_2 s \tilde{\lambda}_{21}}{\tilde{X}_{21}} & \sum_{m \neq 2}^M \frac{\tilde{e}_m s \tilde{\lambda}_{2m}}{\tilde{X}_{2m}} & \cdots & \frac{\tilde{e}_2 s \tilde{\lambda}_{2N}}{\tilde{X}_{2N}} \\ \vdots & \vdots & \ddots & \vdots \\ \frac{\tilde{e}_{Ns} \tilde{\lambda}_{N1}}{\tilde{X}_{N1}} & \frac{\tilde{e}_{Ns} \tilde{\lambda}_{N2}}{\tilde{X}_{N2}} & \cdots & \sum_{m \neq N}^M \frac{\tilde{e}_m s \tilde{\lambda}_{Nm}}{\tilde{X}_{Nm}} \end{bmatrix} \\
\Psi_\lambda &= \begin{bmatrix} \bar{Y}_1 \sum_{m \neq 1}^M \frac{\tilde{e}_m s \tilde{\lambda}_{1m}}{\tilde{X}_{1m}} & -\frac{\bar{Y}_1 \tilde{e}_2 s \tilde{\lambda}_{12}}{\tilde{X}_{12}} & \cdots & -\frac{\bar{Y}_1 \tilde{e}_{Ns} \tilde{\lambda}_{1N}}{\tilde{X}_{1N}} \\ -\frac{\bar{Y}_2 \tilde{e}_1 s \tilde{\lambda}_{21}}{\tilde{X}_{21}} & \bar{Y}_2 \sum_{m \neq 2}^M \frac{\tilde{e}_m s \tilde{\lambda}_{2m}}{\tilde{X}_{2m}} & \cdots & -\frac{\bar{Y}_2 \tilde{e}_{Ns} \tilde{\lambda}_{2N}}{\tilde{X}_{2N}} \\ \vdots & \vdots & \ddots & \vdots \\ -\frac{\bar{Y}_N \tilde{e}_1 s \tilde{\lambda}_{N1}}{\tilde{X}_{N1}} & -\frac{\bar{Y}_N \tilde{e}_2 s \tilde{\lambda}_{N2}}{\tilde{X}_{N2}} & \cdots & \bar{Y}_N \sum_{m \neq N}^M \frac{\tilde{e}_m s \tilde{\lambda}_{Nm}}{\tilde{X}_{Nm}} \end{bmatrix} \\
\Psi_e &= \begin{bmatrix} 1 & -\frac{\bar{Y}_1 c \tilde{\lambda}_{12}}{\tilde{X}_{12}} & \cdots & -\frac{\bar{Y}_1 c \tilde{\lambda}_{1N}}{\tilde{X}_{1N}} \\ -\frac{\bar{Y}_2 c \tilde{\lambda}_{21}}{\tilde{X}_{21}} & 1 & \cdots & -\frac{\bar{Y}_2 c \tilde{\lambda}_{2N}}{\tilde{X}_{2N}} \\ \vdots & \vdots & \ddots & \vdots \\ -\frac{\bar{Y}_N c \tilde{\lambda}_{N1}}{\tilde{X}_{N1}} & -\frac{\bar{Y}_N c \tilde{\lambda}_{N2}}{\tilde{X}_{N2}} & \cdots & 1 \end{bmatrix},
\end{aligned}$$

in which, for a better readability, $c\tilde{\lambda}_{km} = \cos \tilde{\lambda}_{km}$ and $s\tilde{\lambda}_{km} = \sin \tilde{\lambda}_{km}$.

It is interesting to notice that if nodes' voltages \bar{e}_k are regarded constant, the method presented here becomes very similar to the *Steady-State* one [4, 47], however with a remarkable difference: the damping matrix Φ_ω is full for the *Electromechanical Energy Approach*, whilst it is only diagonal for the former. Indeed, for a SMIB system both methods are equivalent as shown in author's paper [55], and one does not distinguish any difference among them. Conversely, this characteristic is clearly seen in a multi-machine system.

As already briefly cited, the non-diagonal terms of Φ_ω are responsible for the damping factor between node k and the remaining grid, whereas its diagonal terms represent the damping factors of the k^{th} node alone. In other words, the *Electromechanical Energy Approach* gives to the designer more degrees-of-freedom for fitting system's modes. In practice, what is being tackled is the capacity of the model to account for low frequency oscillations of the system.

The next sections present an approach for simplifying the load-buses and also how to regard the governor, turbine and excitation system.

3.2.1 Simplification of the load and passive buses

As observed by Hermans *et al.* [62], for frequency-control relevant time scales and for static loads, load and passive bus angle and voltage dynamics can be ignored since the inertia and time constant at these nodes are negligibly small compared to the generators ones. Hence, the just shown matrices might be represented as,

$$\begin{aligned} \Phi_\lambda &= \begin{bmatrix} \Phi_{\lambda 11} & \Phi_{\lambda 12} \\ \Phi_{\lambda 21} & \Phi_{\lambda 22} \end{bmatrix}, & \Phi_\omega &= \begin{bmatrix} \Phi_{\omega 11} & \Phi_{\omega 12} \\ \Phi_{\omega 21} & \Phi_{\omega 22} \end{bmatrix}, \\ \Phi_e &= \begin{bmatrix} \Phi_{e 11} & \Phi_{e 12} \\ \Phi_{e 21} & \Phi_{e 22} \end{bmatrix}, & \Psi_\lambda &= \begin{bmatrix} \Psi_{\lambda 11} & \Psi_{\lambda 12} \\ \Psi_{\lambda 21} & \Psi_{\lambda 22} \end{bmatrix}, \\ \Psi_e &= \begin{bmatrix} \Psi_{e 11} & \Psi_{e 12} \\ \Psi_{e 21} & \Psi_{e 22} \end{bmatrix}, \end{aligned}$$

with,

$$\begin{aligned} \Delta \mathbf{x}_{e1} &= \left[\Delta \lambda_G \quad \Delta \lambda_L \quad \vdots \quad \Delta \bar{\omega}_G \quad \Delta \bar{\omega}_L \quad \vdots \quad \Delta \bar{e}_G \quad \Delta \bar{e}_L \right]^T, \\ \Delta \mathbf{u}_{e1} &= \left[\Delta \bar{P}_G^\dagger \quad \Delta \bar{P}_L^\dagger \quad \vdots \quad \Delta \bar{e}_G^\dagger \quad \Delta \bar{e}_L^\dagger \right]^T, \\ \Delta \mathbf{y}_{e1} &= \left[\Delta \bar{P}_G \quad \Delta \bar{P}_L \quad \vdots \quad \Delta \bar{e}_G \quad \Delta \bar{e}_L \right]^T, \end{aligned}$$

$$\begin{aligned}\mathcal{H} &= \text{diag}(\mathcal{H}_G \quad \mathcal{H}_L), \\ \mathcal{T} &= \text{diag}(\mathcal{T}_G \quad \mathcal{T}_L),\end{aligned}$$

being the sub-indexes G and L the corresponding vectors/matrices for the generator- and load-nodes respectively.

If $\mathcal{H}_L, \mathcal{T}_L \rightarrow \mathbf{0}$, then $\Delta(\dot{\lambda}_L, \dot{\omega}_L, \dot{e}_L, \bar{\omega}_L) \rightarrow \mathbf{0}$. Remarking that for load-buses $\Delta\bar{e}_L^\dagger = 0$, the voltage and angle corresponding to the load may be represented by algebraic equations with the form,

$$\begin{aligned}\Delta\bar{e}_L &= \alpha_1\Delta\lambda_G + \alpha_2\Delta\bar{\omega}_G + \alpha_3\Delta\bar{e}_G + \alpha_4\Delta\bar{P}_L^\dagger, \\ \Delta\lambda_L &= \beta_1\Delta\lambda_G + \beta_2\Delta\bar{\omega}_G + \beta_3\Delta\bar{e}_G + \beta_4\Delta\bar{P}_L^\dagger,\end{aligned}$$

being,

$$\begin{aligned}\alpha_1 &= -(\Psi_{\lambda 22}\Phi_{\lambda 22}^{-1}\Phi_{e 22} - \Psi_{e 22})^{-1}(\Psi_{\lambda 22}\Phi_{\lambda 22}^{-1}\Phi_{\lambda 21} - \Psi_{\lambda 21}), \\ \alpha_2 &= -(\Psi_{\lambda 22}\Phi_{\lambda 22}^{-1}\Phi_{e 22} - \Psi_{e 22})^{-1}\Psi_{\lambda 22}\Phi_{\lambda 22}^{-1}\Phi_{\omega 21}, \\ \alpha_3 &= -(\Psi_{\lambda 22}\Phi_{\lambda 22}^{-1}\Phi_{e 22} - \Psi_{e 22})^{-1}(\Psi_{\lambda 22}\Phi_{\lambda 22}^{-1}\Phi_{e 21} - \Psi_{e 21}), \\ \alpha_4 &= -(\Psi_{\lambda 22}\Phi_{\lambda 22}^{-1}\Phi_{e 22} - \Psi_{e 22})^{-1}\Psi_{\lambda 22}\Phi_{\lambda 22}^{-1}, \\ \beta_1 &= -\Phi_{\lambda 22}^{-1}(\Phi_{\lambda 21} + \Phi_{e 22}\alpha_1), \\ \beta_2 &= -\Phi_{\lambda 22}^{-1}(\Phi_{\omega 21} + \Phi_{e 22}\alpha_2), \\ \beta_3 &= -\Phi_{\lambda 22}^{-1}(\Phi_{e 21} + \Phi_{e 22}\alpha_3), \\ \beta_4 &= -\Phi_{\lambda 22}^{-1}(\mathbf{I} - \Phi_{e 22}\alpha_4).\end{aligned}$$

Important to notice is that $\Delta\bar{P}_{L_k}^\dagger = 0$ if the k^{th} busbar is passive.

At last, the state-space system representation with simplified load-buses is then given by,

$$\begin{aligned}\Delta\dot{x}_{c0} &= \underbrace{\begin{bmatrix} \mathbf{0} & \omega_0\mathbf{I} & \mathbf{0} \\ -\mathcal{H}_G^{-1}\Phi_{\lambda 1} & -\mathcal{H}_G^{-1}(\Phi_{\omega 1} + \Phi_{\omega 11}) & -\mathcal{H}_G^{-1}\Phi_{e 1} \\ -\mathcal{T}_G^{-1}\Psi_{\lambda 1} & -\mathcal{T}_G^{-1}\Psi_{\omega 1} & -\mathcal{T}_G^{-1}\Psi_{e 1} \end{bmatrix}}_{\mathbf{A}_{n0}} \Delta x_{c0} \\ &+ \underbrace{\begin{bmatrix} \mathbf{0} & \mathbf{0} & \mathbf{0} \\ \mathcal{H}_G^{-1} & \mathcal{H}_G^{-1}\Phi_{P^\dagger 1} & \mathbf{0} \\ \mathbf{0} & \mathcal{T}_G^{-1}\Psi_{P^\dagger 1} & \mathcal{T}_G^{-1} \end{bmatrix}}_{\mathbf{B}_{n0}} \Delta u_{c0},\end{aligned}\tag{3.9}$$

$$\Delta \mathbf{y}_{c0} = \underbrace{\begin{bmatrix} \Phi_{\lambda 1} & \Phi_{\omega 1} + \Phi_{\omega 11} & \Phi_{e1} \\ \mathbf{0} & \mathbf{0} & \mathbf{I} \end{bmatrix}}_{\mathbf{C}_{n0}} \Delta \mathbf{x}_{c0} + \underbrace{\begin{bmatrix} \mathbf{0} & \Phi_{P^\dagger 1} & \mathbf{0} \\ \mathbf{0} & \mathbf{0} & \mathbf{0} \end{bmatrix}}_{\mathbf{D}_n} \Delta \mathbf{u}_{c0}, \quad (3.10)$$

with,

$$\begin{aligned} \Phi_{\lambda 1} &= \Phi_{\lambda 11} + \Phi_{e12} \alpha_1 + \Phi_{\lambda 12} \beta_1, & \Phi_{\omega 1} &= \Phi_{e12} \alpha_2 + \Phi_{\lambda 12} \beta_2, \\ \Phi_{e1} &= \Phi_{e11} + \Phi_{e12} \alpha_3 + \Phi_{\lambda 12} \beta_3, & \Phi_{P^\dagger 1} &= \Phi_{e12} \alpha_4 + \Phi_{\lambda 12} \beta_4, \\ \Psi_{\lambda 1} &= \Psi_{\lambda 11} + \Psi_{e12} \alpha_1 + \Psi_{\lambda 12} \beta_1, & \Psi_{\omega 1} &= \Psi_{e12} \alpha_2 + \Psi_{\lambda 12} \beta_2, \\ \Psi_{e1} &= \Psi_{e11} + \Psi_{e12} \alpha_3 + \Psi_{\lambda 12} \beta_3, & \Psi_{P^\dagger 1} &= \Psi_{e12} \alpha_4 + \Psi_{\lambda 12} \beta_4, \end{aligned}$$

and

$$\begin{aligned} \Delta \mathbf{x}_{c0} &= \begin{bmatrix} \Delta \lambda_G & \Delta \bar{\omega}_G & \Delta \bar{e}_G \end{bmatrix}^T, \\ \Delta \mathbf{u}_{c0} &= \begin{bmatrix} \Delta \bar{P}_G^\dagger & \Delta \bar{P}_L^\dagger & \Delta \bar{e}_G^\dagger \end{bmatrix}^T, \\ \Delta \mathbf{y}_{c0} &= \begin{bmatrix} \Delta \bar{P}_G & \Delta \bar{e}_G \end{bmatrix}^T. \end{aligned}$$

To be noticed is that the simplification of the load-buses leads to the inclusion of matrix \mathbf{D}_n , *i.e.*, the feedforward term, in system's state-space representation.

3.2.2 Regulated system

At last, let us now include the generating unit's controllers (AVR, PSS and governor) and the prime mover equations in the model of Equations 3.9-3.10. To this end, the models presented in Chapter 2 are linearized and their variables are regarded in p.u..

For the prime mover, Equations 2.1 are used with the assumption that, in p.u., the turbine output torque τ^\dagger and power P^\dagger are equivalent for small changes in speed [2, 4].

In the case of the governor, Equations 2.2 are directly referred.

The AVR regards Equations 2.6, however here an issue arises since the device requires terminal voltage's V_k feedback and system's modeling presented so far does not provide this variable.

Hence, a possible solution for this matter is to simply neglect voltage's dynamics in Equations 3.9-3.10. This procedure might seem awkward at a first glance since a strong effort was put on the voltage

dynamics equating throughout this chapter. However, a very good argument in favor of this simplification is that, whenever one remarks that a control-based model is being pursued, this reduction in an extended power system might represent an important advantage in terms of processing and result analysis.

Also, it is not bad practice to consider that AVRs' high gains bring the terminal voltages very quickly to their reference values, and therefore their dynamic are much faster than the mechanical ones, in which the interarea modes lean on. Therefore, one should argue that the voltage dynamics have little or even no effect on the frequency of the modes. In fact, the AVR might affect strongly only the damping of the system [4].

Precisely, the AVR presented in Equations 2.6 increases system's size in one order, and the PSS (Equations 2.7) in four more. Along with the governor, only generating system's regulators represent an increase of six orders per node, being five of them related to the voltage dynamics. Since each node is represented by three differential equations (Equations 3.9-3.10), considering also prime mover's dynamics (Equations 2.1), the overall system would then be depicted by an 11th-order system. As an example, extending the modeling for a ten generators system, we would end up with a state matrix of size 110×110 .

In comparison, if one neglects the internal voltage dynamics \bar{e}_k , AVR's and PSS's ones are naturally neglected as well, resulting eventually in a 5th-order system per node. For the same ten generators system, a state matrix of size 50×50 is to be implemented. It represents a reduction of nearly 55% in system's complexity, and is very important aiming at control-based models.

Another good argument for this reduction is that, what is eventually being pursued in this thesis is the development of a state-space turbine *governor* that is able to damp out interarea modes inherently, so that the voltage dynamics is not required throughout controller's design. In fact this approach is contrasting to the most usual ones in power systems in the sense that, if the main aim is the design of a PSS for damping the same interarea modes, undoubtedly one should also regard the voltage dynamics, otherwise PSS's design loses the variable in which this device acts on.

However, one should be aware that neglecting voltage dynamics means that the overall system is neither able to represent the possible poor damping or even instability caused by the high gains of the AVRs, nor its correction after the implementation of the PSSs. Nonetheless, a possible workaround for this matter is to change the damping coeffi-

coefficients D_k and D_{km} depending upon the case to be analyzed.

Hence, an unregulated system might have different damping factors than the regulated one containing only AVRs, and even different than the same system regarded with PSSs. In spite of seeming exotic at a first glance, one should remark that, as already cited in Chapter 2, indeed the damping coefficients D_k and D_{km} do not have real physical meanings, and they are added to the modeling in order to compensate for the lack of the damping windings. Eventually, the damping coefficients will capture the influence that the AVR and/or the PSS have on the system. Therefore it is possible to conclude that this particularity is inherent to models that neglect the subtransient dynamics, like for example the widely-used Steady-State Approach.

In fact and as already cited in this chapter, the neglecting of the voltage dynamics makes the Electromechanical Energy Approach to be very similar to the Steady-State one. The mainly difference is that the former regards a full damping matrix Φ_ω while for the latter this matrix is only diagonal.

Lastly, one shall notice that the assumption concerned in the former paragraphs on regarding the transient voltage \bar{e}_k constant (*i.e.*, with no dynamics) only holds for regulated systems since then AVRs' high gains come into play. In other words, if the analysis is performed on an unregulated system, Equations 3.9-3.10 may still be used.

Therefore, the complete model of the regulated power system is given by,

$$\begin{aligned}\Delta \dot{\mathbf{x}}_c &= \mathbf{A}_n \Delta \mathbf{x}_c + \mathbf{B}_n \Delta \mathbf{u}_c, \\ \Delta \mathbf{y}_c &= \mathbf{C}_n \Delta \mathbf{x}_c + \mathbf{D}_n \Delta \mathbf{u}_c,\end{aligned}\tag{3.11}$$

with,

$$\begin{aligned}\Delta \mathbf{x}_c &= [\Delta \lambda_G \quad \Delta \bar{\omega}_G \quad \Delta \bar{\vartheta}_1 \quad \Delta \bar{\vartheta}_2 \quad \Delta \bar{\varepsilon}^p]^T, \\ \Delta \mathbf{u}_c &= [\Delta \bar{P}_G^r \quad \Delta \bar{\omega}_G^r \quad \Delta \bar{P}_L^\dagger]^T, \\ \Delta \mathbf{y}_c &= [\Delta \bar{P}_G \quad \Delta \bar{\omega}_G]^T.\end{aligned}$$

For the sake of readability, the full description of matrices \mathbf{A}_n , \mathbf{B}_n , \mathbf{C}_n and \mathbf{D}_n is found in Appendix A.

Next section shows the modal analysis of one exemplary benchmark systems in order to evaluate the main difference between the presented *Electromechanical Energy Approach* and the *Steady-State* one, where it is highlighted the main contribution of the usage of both full damping matrix Φ_ω and nodes' voltage dynamics.

3.3 Modal analysis: 2M/1L system

The Two-Machine One-Load system, short 2M/1L, was first proposed in author's paper [55] to show the effectiveness of the Electromechanical Energy Approach. This section exploits the system beyond what was proposed in the cited work so that not only the modal analysis of the unregulated system is analyzed, but also of the fully regulated one, *i.e.*, with AVR, PSS and governor. The 2M/1L system is shown in Figure 3.2 and its simulation data is detailed in Appendix B.

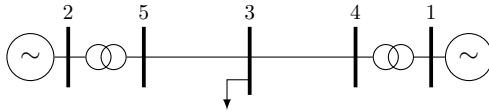


Figure 3.2: Two-Machine One-Load system.

The results for the natural frequency and damping ratio are obtained from the linearization of the original system in Matlab[®] along with its toolbox SimPowerSystems[™]. It is also important to clarify that neither the AVRs nor the PSSs nor the governors are optimally tuned. Instead, their parameters are set to common values just in order to analyze the system without being strict in finding optimal performances for the controlled variables.

For the sake of comparison, in this section the modal analysis for the Steady-State Approach will also be performed. In order to make these comparisons feasible, the damping matrix Φ_ω must be estimated for both models (Electromechanical Energy and Steady-State Approaches). As already mentioned, for the latter only a diagonal matrix is regarded, while for the former the matrix might be full. Also important to remark is that, for the unregulated system, the Electromechanical Energy Approach regards the voltage dynamics of each generating unit, whilst the Steady-State Approach concerns only the mechanical dynamics of the system which eventually reduces system's order in one unit. On the other hand, both methods concerns a 5th-order model per node for the regulated case, according to the previous discussion.

Unregulated system: For the unregulated case, *i.e.*, without AVR, PSS, governor and prime mover, the system presents one interarea mode with natural frequency of 0.7827 Hz and damping ratio of 10%,

while its synchronous oscillations lies on a frequency of 0.0056 Hz and is fully damped. There is also a damped voltage mode at 0.0246 Hz. Table 3.2 shows the results for the actual system*, Steady-State and Electromechanical Energy approaches. Remark that the linearized models are respectively of orders twelve, four and six, and hence only the most relevant modes are depicted in the table.

Table 3.2: Modal analysis - unregulated case

	Natural frequency (Hz)	Damping ratio (%)	Eigenvalues
Actual system	0.7827	10	$-0.49 \pm j4.89$
	0.0246	100	-0.1546
	0.0056	100	-0.035
Steady-State ($D_k = 13.6$)	0.8371	10	$-0.52 \pm j5.23$
	0.1665	100	-1.05
Electromechanical ($D_k = 0.46$) ($D_{km} = 12.8$)	0.8374	10	$-0.53 \pm j5.24$
	0.0201	100	-0.1263
	0.0056	100	-0.035

The cited table shows clearly that, despite achieving similar results for the interarea mode, the Electromechanical Energy Approach differs from the Steady-State one mainly on the synchronous frequencies. This is due to the consideration of the voltage dynamics in the former and also due to the different tuning of the damping coefficients D_k and D_{km} . In fact, this feature allows the designer to perform a fine-tune adjustment on the very slow oscillation modes.

However, one might argue that such a fine adjustment is not required since the synchronous modes are fully damped. Nonetheless, one must remark that these frequencies are very important for the correct dynamical representation of the system. As an illustrative example, consider the dynamic response of generator's active power ΔP_1 for a 2% step in power shown in Figure 3.3.

From the figure it is possible to notice that both approaches reach the correct steady-state value, however only the Electromechanical Energy one is able to depict with a high precision the slowest frequency of the system. As a complement, Figure 3.4 details the first 20 seconds of the previous graph in order to show the fitting of the interarea mode.

*Note: throughout this work, the actual system is regarded as the power grid simulated in a dedicated software.

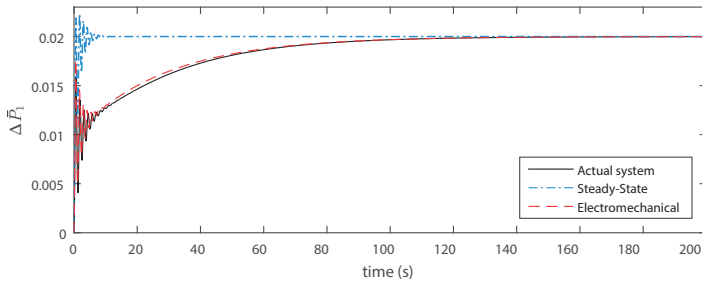


Figure 3.3: Dynamic response of generator's 1 active power for a 2% step in the power input.

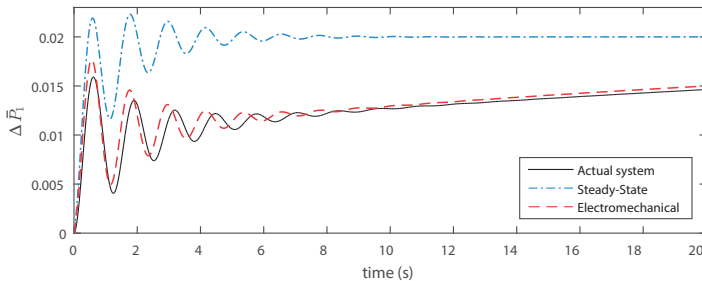


Figure 3.4: Detail of the first 20 seconds of the dynamic response of generator's 1 active power for a 2% step in the power input.

The cited figure shows that the fastest mode of the analysis is well represented by both models despite the offset introduced by the Steady-State Approach.

With that said, it is now very important to remark that, just like for the Steady-State Approach, the Electromechanical Energy one also might sin in representing well the steady-state value of some of its states and outputs. For instance, even though for $\Delta\bar{P}_1$ the fitting to the actual system is good, for $\Delta\bar{P}_2$ there exist a considerably high mismatch for its steady-state value.

This mismatch can be explained by the fact that both methods neglect the dynamic of generators' internal flux linkages, which in practice have a high influence on rotors' speeds. From another viewpoint, what

happens mathematically is that for both the Steady-State and the Electromechanical Energy approaches, the sum of each row of the matrix Φ_λ is zero, what does not occur for the linearized model of the actual system due to the contribution of the cited flux linkages.

However, in spite of being an issue for dynamical simulations, this feature does not have strong consequences for the modal analysis since all main modes of the system can be well represented by the reduced model developed in this chapter, as it is clearly shown in Table 3.2. Furthermore, next chapter presents an identification method for compensating for eventual mismatches between the actual system and the model obtained via the Electromechanical Energy Approach. Moreover, it is important to remark that this matter does not hold for the regulated case with governor, since then the power reference is followed due to the controller and the mismatch tends to be minimized.

The following analysis focus on the regulated system, therefore the model to be implemented from this point onwards neglects the transient internal voltage dynamics, according to the discussion performed in Section 3.2.2.

System with AVR: The influence of the AVR in system's eigenvalues is summarized in Table 3.3 along with the results for the Steady-State and Electromechanical Energy approaches*. Remark that the linearized models are respectively of order fourteen, four and four, and again only the most relevant modes are depicted in the table.

Table 3.3: Modal analysis - with AVR

	Natural frequency (Hz)	Damping ratio (%)	Eigenvalues
Actual system	0.8231	9.8	$-0.51 \pm j5.15$
	0.00012	100	-0.0007
Steady-State ($D_k = 13.3$)	0.8371	9.7	$-0.51 \pm j5.23$
	0.1628	100	-1.02
Electromechanical ($D_k = 0.01$) ($D_{km} = 13.3$)	0.8371	9.73	$-0.51 \pm j5.23$
	0.00012	100	-0.0008

The cited table shows that the AVR reduces slightly the interarea

*The AVR, PSS and governor regarded in this chapter have the structure presented in Chapter 2, whilst for the hydro turbine the nonlinear model presented in [2] is implemented in Matlab[®] for the simulation model.

mode's damping. What can be also concluded from the presented results is that both models represent well this mode, however the Electromechanical Energy Approach has again the advantage of fitting well also system's lowest mode.

Another point important to cite is that the effect of the AVR on system's damping might be correctly represented by the change in the damping coefficients D_k and D_{km} . In other words, the voltage dynamics can be neglected since its influence on the mechanical oscillations is small for the generators that possess AVRs.

System with AVR and governor: The next analysis regards also the governor – and intrinsically a hydro turbine – and its results are presented in Table 3.4. For this study case, the linearized models are represented by an 18th, and two 8th-order systems, respectively.

Table 3.4: Modal analysis - with AVR and governor

	Natural frequency (Hz)	Damping ratio (%)	Eigenvalues
Actual system	0.7245	2.79	$-0.13 \pm j4.55$
	0.0630	22.2	$-0.09 \pm j0.39$
	0.0015	100	-0.0094
Steady-State ($D_k = 12.4$)	0.7277	2.8	$-0.13 \pm j4.76$
	0.1335	53.74	$-0.45 \pm j0.71$
	0.0015	100	-0.0096
Electromechanical ($D_k = 4.5$) ($D_{km} = 11$)	0.7577	2.81	$-0.13 \pm j4.77$
	0.0829	18.9	$-0.098 \pm j0.51$
	0.0015	100	-0.0096

The table shows that the interarea mode is well represented by the two reduced models. On the other hand, the mismatch for the frequency of 0.063 Hz is higher for the Steady-State Approach than for the Electromechanical Energy one.

Notice that, so far $D_1 = D_2$ and $D_{13} = D_{23}$. These two assumptions were sufficient to fit model's modes to the actual system's ones. However, the next analysis implements different constants for each damping coefficient.

System with AVR, PSS and governor: The last analysis of this chapter regards also the positive damping introduced by the PSS in the system, remarking always that PSS's effect is emulated by the tuning

of the model's damping coefficients D_k and D_{km} . Table 3.5 summarizes the obtained results, with the linearized models being depicted respectively by a 24th- and two 8th-order systems.

Table 3.5: Modal analysis - with AVR, PSS and governor

	Natural frequency (Hz)	Damping ratio (%)	Eigenvalues
Actual system	0.7618	15.4	$-0.74 \pm j4.73$
	0.1532	55.5	$-0.53 \pm j0.80$
	0.0064	50.8	$-0.02 \pm j0.04$
	0.0015	100	-0.0094
Steady-State ($D_k = 28$)	0.7578	15.4	$-0.73 \pm j4.70$
	0.1938	86.6	$-1.05 \pm j0.61$
	0.0015	100	-0.0096
Electromechanical ($D_1 = 10, D_2 = 25$) ($D_{13} = 34, D_{23} = -1$)	0.7651	15.5	$-0.75 \pm j4.75$
	0.1403	57.4	$-0.51 \pm j0.72$
	0.0015	100	-0.0096

As well as for the previous analysis, it is possible to observe that both reduced models are able to represent the interarea mode with small mismatches. However, for this case another two modes (0.1532 Hz and 0.0064 Hz) with respectively damping ratios of 55.5% and 50.8% arise. Neither of the both models are able to depict the latter mode. On the other hand, the former is represented with a relatively good accuracy for both the natural frequency and damping ratio by the Electromechanical Energy Approach. As already cited, this is achieved by a tuning on the damping coefficients such as $D_1 \neq D_2$ and $D_{13} \neq D_{23}$.

At last, notice that the parameter D_{23} has a negative value. However, as already cited throughout this work, the damping coefficients does not have a real meaning in practice, and they are tuned in a way to match the most important frequencies of the system. Since the achieved parameter set is not optimal in a strict mathematical sense, it is possible that other parameter set with only positive values for the coefficients exists. Nonetheless, the idea of this section is to show the feasibility of the method regardless the value of the obtained parameters.

Chapter conclusion

This chapter has presented a new approach for the modeling of power systems based on the Lagrangian Energy Method, named here *Electromechanical Energy Approach* since it converts the system to an electromechanical structure for obtaining its differential equations.

Here an expansion to author's work [55] is exploited in the sense that also the voltage dynamics of the generating unit is regarded. Besides, a way for simplifying the load-buses is also presented, as well as a generalized implementation of generating unit's prime mover and governor. AVR's and PSS's contributions are regarded inherently by model's damping coefficients D_k and D_{km} .

Lastly it is shown that the Electromechanical Energy Approach is able to represent relatively well the main modes of the 2M/1L system for all possible cases: unregulated, with only AVR, with AVR and governor, and with AVR, governor and PSS. In contrast to the Steady-State Approach, the method presented throughout this chapter has the intrinsic ability of fitting also the low frequencies of the system due to its tuning of the damping parameters.

In fact, one can state that the Electromechanical Energy Approach is, for the regulated case, a generalization of the Steady-State one that enables the consideration of damping coefficients for the synchronous modes. For the unregulated case, the Electromechanical Energy Approach differs from the Steady-State one in the consideration also of the voltage dynamics of each node of the system.

However, a drawback of the presented method is the difficulty in estimating the matrix Φ_ω , which is responsible for the damping of the modes and does not have a real meaning. For instance, the results shown in Table 3.5 were obtained after nearly 50 simulations due to the number of free tuning parameters, which for this case is four. In the next chapter a method for accounting for system's uncertainties and how to identify them is presented. This identification will eventually help on determining in a more pragmatic way the parameters of the matrix Φ_ω .

Hence, one might also argue that the main goal of this chapter is fulfilled, *i.e.*, the equating of a reduced order model aimed at control purposes. In fact, considering N_g the number of generating units of the power grid, the Electromechanical Energy Approach results in a simplified system of order $3N_g$ for the unregulated case. Additionally, the insertion of simplified versions of prime movers ($2N_g$) and governors

$(N_g)^*$ leads the power grid to be represented by a $5 N_g^{\text{th}}$ -order linear system. In comparison to most of the commercial softwares it represents a reduction of nearly 70% in system's size.

*For the simplified version of the cited devices, please refer to Chapter 2.

4

Uncertainties and parameter identification in Power Systems

This chapter exploits the uncertainties that might arise in a power system, as well as the identification techniques to find its unknown parameters.

In spite of seem two independent topics, actually uncertainties and parameter identification are closely related. It becomes clear whenever one remarks that the first are directly responsible for modeling errors, which one tries to avoid using System Identification techniques for modeling the system.

The questions that this chapter tries to address are specifically:

- which kind of uncertainties arise in Power Systems?
- how could one identify the parameters with such unpredictability?

In order to answer both questions, the chapter starts with a discussion on the uncertainties involved in a power system and follows with the methods for identifying unknown parameters in it. At last, one example is performed to illustrate the presented method.

It is important to highlight that the theory demonstrated here is well-known from literature, however the way it is implemented to Power Systems is also a contribution of this thesis.

4.1 Uncertainties

It is known that the representation of the power grid obtained in Equation 3.11 does not have a very high accuracy when compared to real data. As it was highlighted, the intention of such equating was to find a model to be used in the controller design, *i.e.*, control-based model, which should be simple and linear, rather than developing a precise power system simulation model.

Besides, it is imperative to imagine that a control-based model will not only be simplified w.r.t. each node of the system, but it will in most cases also make use of some simplification technique for reducing system's total number of nodes, such as those presented in [4].

In practice, each performed simplification has the potential to change system's dynamics strongly or slightly. Therefore, even though the designer use real values for the parameters of the power grid model, they are likely to be off compared to real measurements due to the simplifications of both the model itself and the power grid reduction. It means that our first type of *uncertainties* are introduced in the model, which appears as a parameter mismatch [63].

The second type arises naturally due to the intrinsic characteristics of the power system due to its loads. It is widely known that, despite being partially predictable due to past data, the system loading has an inherent stochastic aspect [4].

The third uncertainty type regards to the measurement noise. Indeed, as already cited in the Introduction, this type of uncertainty is rarely addressed in the Power Systems field, in spite of being an established topic in Control Theory [34, 64].

In fact, it is known that measurement devices introduce a certain amount of noise and quantization to the measured data. However, in this work only the former is regarded, since most of current sensors have resolutions equal or higher than 12 bits and hence the latter may be neglected.

As well as for Figure 1.3, Figure 4.1 is introduced in order to better illustrate the measurement noise issue in Power Systems.

The figure presents an on-site measurement of two diesel generators' active power for a step variation. It is clear to see that the actual value for the power is contaminated with noise. In fact, it is known that the great majority of the available measured data presented in papers and books are filtered. Nonetheless, these two examples highlight the fact that even filtered signals still contain a considerable amount of noise.

For now, one shall remark that these noisy signals are fed back

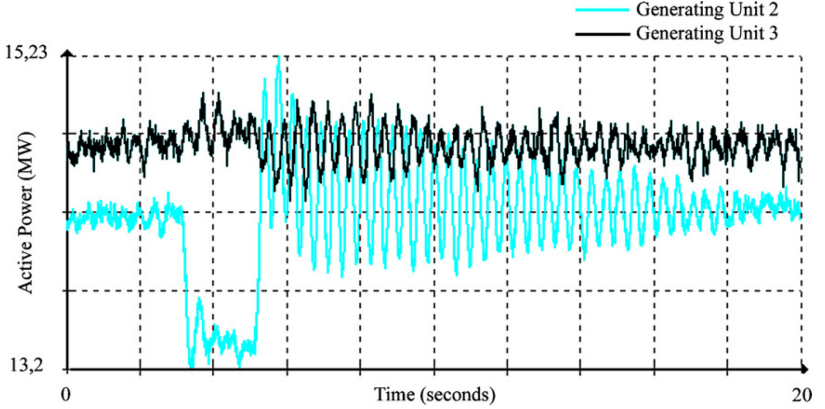


Figure 4.1: Generators 2 and 3 response to a step variation applied to the G2 inlet valve opening - Reproduced from [65] ©2011 Elsevier

to systems' controllers. It means that they are processed within the algorithm and are also responsible for the updated output control signal. Depending upon controller's bandwidth, the noise might be more or less filtered, resulting therefore in a more or less oscillatory control signal. However, as already stated in the Introduction, just applying low-pass filters to mitigate the noise also eliminates system's high-order dynamics, which might deteriorate the control action. In the worst case, system's stability margins might also be reduced [34, 35].

All the cited cases explicit the importance of accounting for the uncertainties during system's modeling, and a way for regarding them is exemplified in the following two sections.

4.1.1 Parameter mismatch

First of all, for simplicity the Δ operator will be from now on neglected in the power grid model represented in Equations 3.11. Further, a deviation on each of its parameters is considered, such as,

$$\begin{aligned}
 \dot{\mathbf{x}}_c &= \underbrace{(\mathbf{A}_n + \delta\mathbf{A}_n)}_{\mathbf{A}_c} \mathbf{x}_c + \underbrace{(\mathbf{B}_n + \delta\mathbf{B}_n)}_{\mathbf{B}_c} \mathbf{u}_c, \\
 \mathbf{y}_c &= \underbrace{(\mathbf{C}_n + \delta\mathbf{C}_n)}_{\mathbf{C}_c} \mathbf{x}_c + \underbrace{(\mathbf{D}_n + \delta\mathbf{D}_n)}_{\mathbf{D}_c} \mathbf{u}_c,
 \end{aligned} \tag{4.1}$$

where δ represent the deviation of the correspondent nominal parameter.

For simplicity, in this work the parametric deviation is only regarded in matrices Φ_λ , Φ_e , Ψ_λ and Ψ_e , since they are the ones which are modified by the linearization procedure, being therefore more susceptible to uncertainties. Also, matrix Φ_ω is fully unknown since it does not have a real physical meaning in the power grid model, Equation 3.11.

It is imperative to highlight that this representation does not ensure zero error w.r.t. the actual power system. Instead, what it really does is to use a parameter deviation in order to try to reach a closer description of the real plant. However, if on one hand one gains in accuracy, a side effect is that the physical meaning of system's parameters might be lost. Nevertheless, it is not a huge drawback since the controller does not require real physical parameters for its design.

In other words, one may use Equation 3.11 for getting insight to the power grid, while Equation 4.1 might be used for simulations and controller design.

4.1.2 Stochasticity

Uncertainties related to the load variations and measurement noise may be represented in Equation 4.1 as stochastic signals using the well-known generalized state-space representation,

$$\begin{aligned}\dot{\mathbf{x}}_c &= \mathbf{A}_c \mathbf{x}_c + \mathbf{B}_c \mathbf{u}_c + \mathbf{w}_c \\ \mathbf{y}_c &= \mathbf{C}_c \mathbf{x}_c + \mathbf{D}_c \mathbf{u}_c + \mathbf{v}_c,\end{aligned}$$

being \mathbf{w}_c and \mathbf{v}_c independent and identically distributed random variables (i.i.d.).

Hence, given the state observer,

$$\begin{aligned}\dot{\hat{\mathbf{x}}}_c &= \mathbf{A}_c \hat{\mathbf{x}}_c + \mathbf{B}_c \mathbf{u}_c + \mathbf{L}_c (\mathbf{y}_c - \mathbf{C}_c \hat{\mathbf{x}}_c - \mathbf{D}_c \mathbf{u}_c) \\ \hat{\mathbf{y}}_c &= \mathbf{C}_c \hat{\mathbf{x}}_c + \mathbf{D}_c \mathbf{u}_c,\end{aligned}$$

where \mathbf{L}_c is the observer gain, the innovation, *i.e.*, the output prediction error, is then,

$$\begin{aligned}\boldsymbol{\xi}_c &= \mathbf{y}_c - \hat{\mathbf{y}}_c, \\ &= \mathbf{y}_c - \mathbf{C}_c \hat{\mathbf{x}}_c - \mathbf{D}_c \mathbf{u}_c,\end{aligned}\tag{4.2}$$

which is also i.i.d. by definition.

Thus, substituting the innovation in the state observer equation one easily obtains,

$$\begin{aligned}\dot{\hat{\mathbf{x}}}_c &= \mathbf{A}_c \hat{\mathbf{x}}_c + \mathbf{B}_c \mathbf{u}_c + \mathbf{L}_c \boldsymbol{\xi}_c \\ \mathbf{y}_c &= \mathbf{C}_c \hat{\mathbf{x}}_c + \mathbf{D}_c \mathbf{u}_c + \boldsymbol{\xi}_c.\end{aligned}$$

Anderson and Moore [63] perform in their book a very thorough proof in order to affirm that if \mathbf{L}_c equals the *Kalman Gain* $\boldsymbol{\Gamma}_c$, the system can be represented by,

$$\begin{aligned}\dot{\mathbf{x}}_c &= \mathbf{A}_c \mathbf{x}_c + \mathbf{B}_c \mathbf{u}_c + \boldsymbol{\Gamma}_c \boldsymbol{\xi}_c \\ \mathbf{y}_c &= \mathbf{C}_c \mathbf{x}_c + \mathbf{D}_c \mathbf{u}_c + \boldsymbol{\xi}_c,\end{aligned}\tag{4.3}$$

which means that the estimated states and outputs are equivalent to the actual ones after filter's convergence. The structure depicted in Equation 4.3 is called *innovation form*, since the innovation $\boldsymbol{\xi}_c$ appears explicit on it. Also, $\boldsymbol{\Gamma}_c$ may be now called as *state disturbance matrix* and $\boldsymbol{\xi}_c$ enters the model as a vector of white noises.

This representation has a very important advantage compared to the generalized one whenever one aims at parameter identification, which is detailed in the next section.

4.2 Parameter identification

System Identification is known to be one of the most important subjects in many engineering fields due to its capacity of describing systems' parameters without possessing much information about it [66].

Especially in Control Engineering, this feature is very welcome since the designers are most of the times seeking for simplified representations of the systems in order to design their controllers. As long as it is clear that system reduction using physical laws often leads to mismatches to the original model, system identification techniques may be implemented. The price to be paid in these cases is that the designer might lose the physical meaning of system's parameters, which is really not a big issue since physical information is usually used to get insight and understanding to the system, which is not required for control purposes.

Further, as a matter of fact, most parameter identification procedures are carried out in the discrete-time domain, which is also the approach to be followed in this work. Another justification for it is

that, since the actual controllers of the generating units are implemented digitally, it is straight forward to use the identified data into the controller design, and hence no time domain conversion is required.

With that said we can rewrite Equation 4.3 in the discrete form,

$$\begin{aligned} \mathbf{x}(k+1) &= \mathbf{A} \mathbf{x}(k) + \mathbf{B} \mathbf{u}(k-d+1) + \mathbf{\Gamma} \boldsymbol{\xi}(k) \\ \mathbf{y}(k) &= \mathbf{C} \mathbf{x}(k) + \mathbf{D} \mathbf{u}(k-d+1) + \boldsymbol{\xi}(k), \end{aligned} \quad (4.4)$$

where the discrete time delay d is considered synchronous in this work.

There are two main issues for identifying the model in Equation 4.4:

1. matrices \mathbf{A} , \mathbf{B} , \mathbf{C} and \mathbf{D} possess parameters that are known (from the original model, Equation 3.11) and unknown (due to the parameter uncertainties), and
2. the state disturbance matrix $\mathbf{\Gamma}$ is fully unknown.

These statements should lead the designer directly to System Identification's sub-field called *grey-box identification* where one is aware of some parameters and the identification procedure must be performed in order to determine the remaining ones [66, 67].

With this information in mind one should remark that in fact only few information is known beforehand, since both states and parameters must be estimated. A clever way to overcome these issues is through the usage of the *Extended Kalman Filter*, short EKF.

In brief, the procedure is implemented in a way where the state vector $\mathbf{x}(k+1)$ is augmented using the unknown parameters, that are considered static. Besides, since the unknown parameters become states, the overall model becomes nonlinear, and this is the justification for applying the EKF [67].

More specifically,

$$\underbrace{\begin{bmatrix} \mathbf{x}(k+1) \\ \boldsymbol{\theta}(k+1) \end{bmatrix}}_{\mathbf{x}_i(k+1)} = \begin{cases} f(\mathbf{x}(k), \boldsymbol{\theta}(k), \mathbf{u}(k), \boldsymbol{\xi}(k)) \\ \boldsymbol{\theta}(k) \end{cases}$$

$$\mathbf{y}(k) = h(\mathbf{x}(k), \boldsymbol{\theta}(k), \mathbf{u}(k)) + \boldsymbol{\xi}(k),$$

being $\boldsymbol{\theta}(k)$ the vector of unknown parameters.

For applying the filter, the *Jacobian matrices*, *i.e.*, the linearization around the equilibrium points, are calculated by,

$$\mathbb{J}_f = \begin{bmatrix} \frac{\partial f_1}{\partial x_1} & \cdots & \frac{\partial f_1}{\partial x_n} & \frac{\partial f_1}{\partial \theta_1} & \cdots & \frac{\partial f_1}{\partial \theta_m} \\ \vdots & \vdots & \vdots & \vdots & \vdots & \vdots \\ \frac{\partial f_n}{\partial x_1} & \cdots & \frac{\partial f_n}{\partial x_n} & \frac{\partial f_n}{\partial \theta_1} & \cdots & \frac{\partial f_n}{\partial \theta_m} \\ \vdots & \vdots & \vdots & \vdots & \vdots & \vdots \\ \frac{\partial f_m}{\partial x_1} & \cdots & \frac{\partial f_m}{\partial x_n} & \frac{\partial f_m}{\partial \theta_1} & \cdots & \frac{\partial f_m}{\partial \theta_m} \end{bmatrix} \bigg|_{\mathbf{x}_i(k) = (\hat{\mathbf{x}}, \hat{\boldsymbol{\theta}}, \hat{\mathbf{u}}, \mathbf{0}),}$$

$$\mathbb{J}_h = \begin{bmatrix} \frac{\partial h_1}{\partial x_1} & \cdots & \frac{\partial h_1}{\partial x_n} & \frac{\partial h_1}{\partial \theta_1} & \cdots & \frac{\partial h_1}{\partial \theta_m} \\ \vdots & \vdots & \vdots & \vdots & \vdots & \vdots \\ \frac{\partial h_n}{\partial x_1} & \cdots & \frac{\partial h_n}{\partial x_n} & \frac{\partial h_n}{\partial \theta_1} & \cdots & \frac{\partial h_n}{\partial \theta_m} \end{bmatrix} \bigg|_{\mathbf{x}_i(k) = (\hat{\mathbf{x}}, \hat{\boldsymbol{\theta}}, \hat{\mathbf{u}}).$$

with n and m representing the number of states and unknown parameters respectively.

The EKF identification algorithm is then given by,

$$\begin{cases} \mathbf{K}(k) = \mathbf{P}(k) \mathbb{J}_h^T [\mathbb{J}_h \mathbf{P}(k) \mathbb{J}_h^T + \boldsymbol{\Lambda}]^{-1}, \\ \hat{\mathbf{x}}_i(k+1) = f(\mathbf{x}_i(k), \mathbf{u}(k), \boldsymbol{\xi}(k)) + \mathbf{K}(k) [\mathbf{y}(k) - h(\hat{\mathbf{x}}_i(k), \mathbf{u}(k))], \\ \mathbf{P}(k+1) = \boldsymbol{\Lambda}^{-1} \mathbb{J}_f [\mathbf{P}(k) - \mathbf{K}(k) \mathbb{J}_h \mathbf{P}(k)] \mathbb{J}_f^T, \end{cases}$$

where \mathbf{K} is the filter gain, \mathbf{P} is its covariance matrix and $\boldsymbol{\Lambda}$ is a diagonal weighting matrix for the confidence on the parameters so that the higher the entry the more confidence one has on the initial parameter.

The engineering software Matlab[®] implements a similar, but optimized, algorithm in its function `greyest()`, where \mathbb{J}_f and \mathbb{J}_h are calculated numerically and the identified model has the same form as Equation 4.4. Therefore, this function will be used throughout the present thesis for implementing the required parametric identification.

Next section exemplifies the identification procedure presented in this chapter using the same exemplary 2M/1L system implemented in Chapter 3 in order to demonstrate the importance of taking the uncertainties into consideration in power systems.

4.3 Identification results: 2M/1L system

This section exploits the parameter identification of the 2M/1L system presented in Figure 3.2 making use of the procedures introduced in this chapter. The focus is on the regulated system case with AVR, PSS and

governor (Equations 3.11) since this is the case to be exploited for the new governor to be developed in Chapters 5 and 6. However one shall keep in mind that the identification procedure here presented holds for all cases analyzed in Chapter 2.

In the following, comparisons between the actual power grid and the nominal model (Equations 3.11) with both the noiseless (Equations 4.1) and the innovation models (Equations 4.3) are performed.

The main goal of the section is to obtain more accurate models that are fully based on the structure of the phenomenological one (Equations 3.11) aiming at the further control of the system. Hence, what is eventually being pursued is the identification of system's parameters that are either unknown or have uncertainties in order to have a more reliable control-based model.

For performing the identification, firstly dynamical simulations of the actual system must be carried out. These simulations shall excite all system's inputs with suitable signals (white noise, PRBS, etc.) and measure simultaneously its outputs. An usual practice within the System Identification field is to apply random inputs signals with different levels in order avoid biased identifications. Also, the data used for the parameter determination is usually not the same as the data used for the identified model validation. Thus, two data sets are to be obtained beforehand through the simulation of the actual system.

For the present thesis, the input variation is limited to the range $\pm 5\%$ on their equilibrium ones in order to keep the actual system close to its linear equivalent model. Besides, the fitting percentage for the analyzed models is given by the Normalized Root-Mean-Square Error (NRMSE) function, being,

$$\text{fit} = 100\% \left(1 - \frac{\|y - \hat{y}\|}{\|y - \bar{y}\|} \right), \quad (4.5)$$

where y , \hat{y} and \bar{y} hold respectively for the actual, estimated and mean values.

Noiseless case: For the first analysis, let us consider the 2M/1L system without any measurement noise. Figure 4.2 shows the results for the active powers for the actual, nominal and identified systems, while Figure 4.3 details the time slot between 84 and 96 seconds in order to highlight the difference between the models.

The figures show that, despite achieving also a good fitting, the nominal system still presents a higher mismatch with the actual data

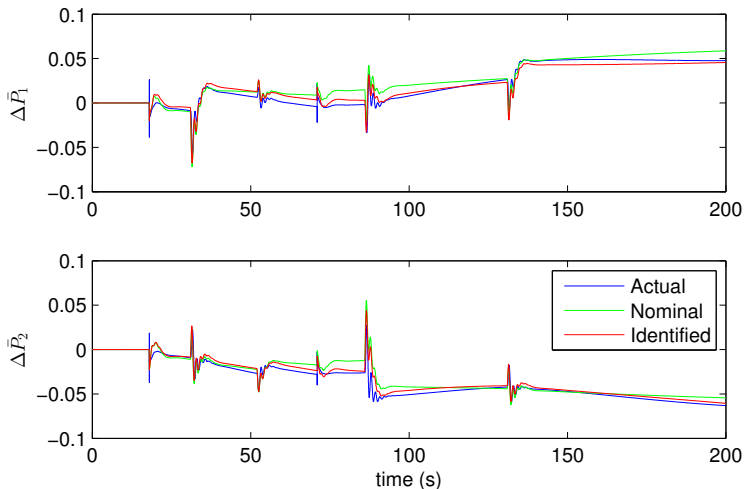


Figure 4.2: Comparison of the active power outputs for the actual, nominal and identified systems for the noiseless case.

when compared with the identified one. In fact, the fitting percentages state it, and for this simulation they are summarized in Table 4.1.

Table 4.1: Fitting percentages for the 2M/1L system (noiseless case)

Nominal		Identified	
$\Delta \bar{P}_1$	$\Delta \bar{P}_2$	$\Delta \bar{P}_1$	$\Delta \bar{P}_2$
63%	60%	77%	74%

However, at this point it is important to highlight that the identification procedure was unable to fit well the actual data with the model for the speed output. It happens due to the fact that the model does not capture one of system's mode (0.0064 Hz). For this reason, both the nominal and the identified models present relatively high steady-state errors. As an exemplification, the results for $\Delta \bar{\omega}_2$ of the actual system vary over a range of $\pm 6e^{-3}$ p.u., while the same output for both the nominal and the identified models varies over $\pm 9e^{-3}$ p.u..

On the other hand, just for the sake of comparison, if one filters this frequency the fitting enhances substantially, proving that the speed

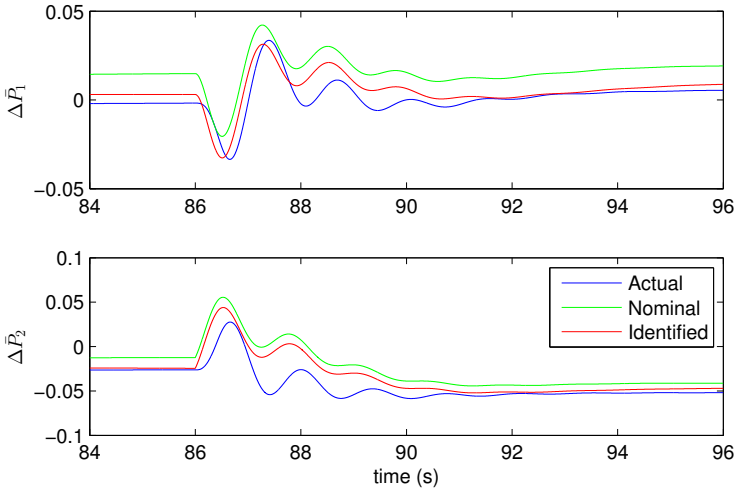


Figure 4.3: Detail of the comparison of the active power outputs for the actual, nominal and identified systems for the noiseless case.

profiles of the model are able to capture the remaining modes of the actual system. Figure 4.4 exemplifies the filtered results for the speed output $\Delta \bar{\omega}_2$ for the same inputs as in Figure 4.2, where the nominal system data is omitted due to the fact that it is very similar to the identified one.

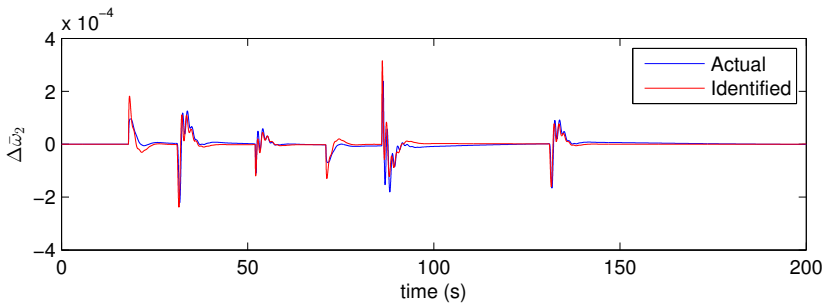


Figure 4.4: Comparison of the filtered outputs $\Delta \bar{\omega}_2$ for the actual and identified systems for the noiseless case.

The analysis of the figure states that, in spite of the frequency 0.0064 Hz, the other modes of the actual system are well represented by the identified model. As a matter of fact, one shall notice that the influence of speeds' steady-state error is small on the overall behavior of the system due to its small amplitude, and therefore does not harm strongly the analysis performed so far. Also it is important to notice that these mismatches in the speed outputs are directly responsible for the mismatches in the power ones (see Equations 3.9-3.10). By being of small amplitudes they are reflected as small deviations in power as well, as exemplified in Figures 4.2 and 4.3.

For completeness, Table 4.2 shows the modal analysis for the concerned systems, where it is interesting to notice that there is only a slight enhancement on the results of the identified system when compared to the nominal one. This information is eventually important due to the fact that it proves that the identification procedure has focused more on the reduction of the steady-state error between the model and the actual system than on the adjustment of model's modes. This is in fact relevant since these modes were already well depicted by the nominal model, whilst the greater issue laid on its steady-state condition.

Table 4.2: Modal analysis of the identified system

	Natural frequency (Hz)	Damping ratio (%)	Eigenvalues
Actual system	0.7618	15.4	$-0.74 \pm j4.73$
	0.1532	55.5	$-0.53 \pm j0.80$
	0.0064	50.8	$-0.02 \pm j0.04$
	0.0015	100	-0.0094
Nominal system	0.7651	15.5	$-0.75 \pm j4.75$
	0.1403	57.4	$-0.51 \pm j0.72$
	0.0015	100	-0.0096
Identified system	0.7605	15.7	$-0.75 \pm j4.72$
	0.1339	59.9	$-0.50 \pm j0.67$
	0.0015	100	-0.0096

System with measurement noise: Differently from the last analysis, now each output ($\Delta \bar{P}_k$ and $\Delta \bar{\omega}_k$) is to be considered with an independent Gaussian noise. For the former the variance is given by $\sigma_P^2 = 4e^{-6}$ and for the latter $\sigma_\omega^2 = 4e^{-8}$. Notice that the variances

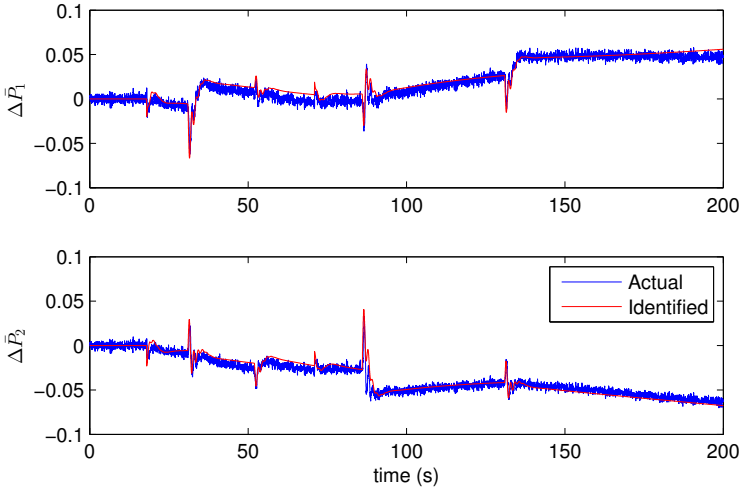


Figure 4.5: Comparison of the active power outputs for the actual and identified systems for the noisy case.

represent a white noise with amplitude varying nearly in the range of ± 0.005 p.u. and ± 0.0005 p.u. respectively, which means that these noisy signals are relatively small.

Noticeable is that these noises are processed within system's regulators (AVRs, PSSs and governors) and therefore they are also responsible for the dynamical behavior of the outputs. According to the discussion performed in the Introduction of this thesis, depending upon regulators' bandwidths these noisy signals might be more or less filtered. Within the Classical Control field, which is the case for the implemented controllers of the 2M/1L, a more filtered noise means a narrower bandwidth, which might make the system to respond slower to input signals. On the other hand, a broader bandwidth might lead the system to work nearer to its stability limits. Therefore, the determination of system's response for external noises is an important analysis to be performed aiming at controllers' design.

Thus, Figure 4.5 shows the results for the active powers of the 2M/1L system implemented with the same inputs as for the noiseless case in order to allow an easier comparison between the outcomes. Figure 4.6 details the results for the time slot between 84 and 96 seconds.

The nominal model is omitted from the figures since its results are the same as those shown in Figures 4.2 and 4.3.

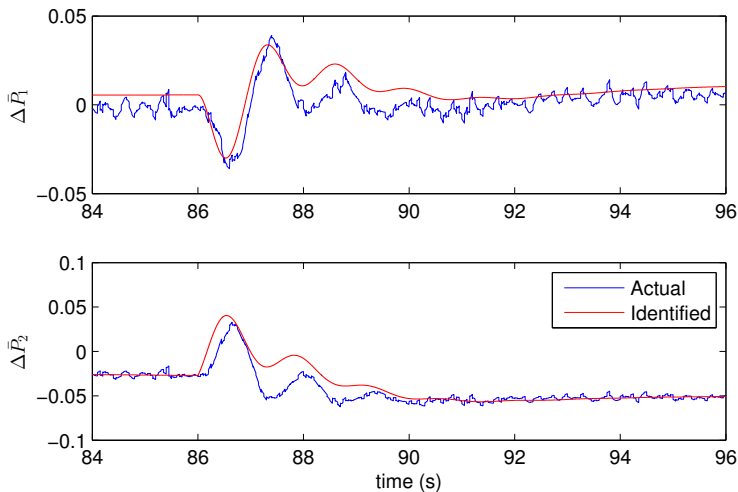


Figure 4.6: Detail of the comparison of the active power outputs for the actual and identified systems for the noisy case.

The fitting percentages for system's power outputs $\Delta \bar{P}_1$ and $\Delta \bar{P}_2$ are 75% and 73% respectively. It is clear to conclude that the identification procedure is robust enough to “understand” what is noise and what is signal among the contaminated noisy data obtained from measurements on the actual system.

Chapter conclusion

This chapter has exploited the potential uncertainties that might arise in power systems. Besides, it has been also shown a technique for identifying parameter deviations in the nominal model developed in Chapter 2. To reach this aim, Equations 3.11 are first written in the so-called *innovation form* (Equation 4.3) and then discretized (Equation 4.4).

The parametric identification is fully based on the EKF algorithm for ensuring both state and parameter convergence, and is called *grey-box identification* since the model to be identified has both known and

unknown parameters, given that its structure is fixed and fully based on phenomenological equations.

Lastly, the procedure presented throughout the chapter is evaluated through the 2M/1L system. It is shown that the identified model is able to depict system's power outputs both for the noiseless and noisy cases in a more accurate fashion than the nominal one.

The drawback of the identification technique is that it is unable to represent well speed steady-state values due to the lack of one of actual system's modes in the nominal model. However, as already explained in the chapter, this feature has just a little impact on power outputs due to the small deviation of the speed, what does not influence highly the power evolution. Important to remark is that all the remaining modes are well depicted in system's speeds, see Figure 4.4.

In the next chapter a new device aimed to help on the damping of system's oscillations is presented. The design of this device is fully based on the identified model obtained through the procedure presented in this chapter.

5

The Power System Stabilizer at the turbine side

In this chapter one of the core ideas behind the thesis is developed and evaluated, *i.e.*, a slight modification on the turbine governor structure to make it able to damp out the low frequency power oscillations. The modification here proposed is named simply PSS_t, where the lower case “t” stands for the turbine and is detailed throughout the chapter.

However, before we start with the proper evaluation of the PSS_t it is important to define how it should be implemented in the current power grids. There are basically two possibilities: either to add the PSS_t on all governors of the system or to add it just on the governor(s) that is(are) allocated in the generating unit(s) that suffer(s) more the effects of the cited oscillations.

In spite of being tempting to modify the governors of all generating units, this possibility does not reflect the reality in power system implementations, where it is known from practitioners that a paradigm shift with such a dimension is often seen with reluctance. Accordingly, this work will focus the PSS_t implementation mainly on the generating units that have more influence on the underdamped low frequency modes.

For this purpose, system’s modal analysis may be performed in order to check where the modes that require a more effective damping action are located. This is done by the direct analysis of system’s participation factors, which is an indication of the states that influence

more or less in each mode (for details refer, *e.g.*, to [2, 4]).

The following sections present the PSSSt, its insertion in plant's model and evaluation w.r.t. its modal analysis, singular values and dynamic simulations using the 2M/1L system as example.

5.1 The PSSSt

As already cited in the Introduction, Wang *et al.* [28] and Milanovic [29] have presented ideas for governor-based PSSs. Both works deal with the situation where the excitor-based PSS is not concerned and the damping of system's modes is performed uniquely by the governors. Moreover, Machowski *et al.* [4] has cited that such a solution was never implemented in practice and should be considered in the future.

Nevertheless, the main problem of this idea is that nowadays the great majority of the generating units have PSSs and hence the disregarding of them is not realistic in a practical viewpoint. What is actual, important and even worrying is Taylor's statement on the condition of the several PSSs during the USA blackouts of 1996. After a deep investigation it was found that important PSSs were either out of service or simply ineffective, and there is a strong suspicion among power engineers that this might also be the case of several PSSs worldwide [23].

Besides, PSS's tuning is not trivial as long as a mathematical representation of the concerned system is not available. What is usually done is to regard the generating unit where the PSS will be implemented as being connected to an infinite bus. Although this approach may be effective for small generating units, it does not hold for large power plants since their influence on the remaining grid is not neglectable.

Moreover, even with system's model the PSS tuning is not straight forward yet due to its number of parameters, which might range from seven (PSS2B) to twenty-six (PSS4B)*.

Thus, for the development of the PSSSt it is important to keep in mind that this device should not impose difficulties for its tuning, otherwise the pure retuning of the current PSSs would be an easier and faster solution.

Therefore, the main idea behind the PSSSt is that it should be used along with the current exciter-based PSS of the generating unit. Hence, the PSSSt might be tuned to damp out the interarea modes in which the PSS is not effective.

*For the simplified versions of the PSS2B and PSS4B.

Remark now that the governor already regards the active power \bar{P} in its structure, which is used for the exciter-based PSS as well, being therefore a natural and suitable variable for the PSS_t.

Notice that the PSS_t should not damp the synchronous frequencies, otherwise governor's performance might be harmed. Therefore, an important feature of the PSS_t is to damp out only the frequencies *from* the interarea modes, *i.e.*, from nearly 0.05 Hz up to nearly 1.5 Hz.

The idea is the same as for the exciter-based PSSs: in order to damp out these modes, one should recognize them among all others. Recognition means filtering, and here one of the main advantages of using the active power as the PSS_t variable is highlighted: there is no need for amplification like in the exciter-based PSS, and hence a pure high-pass filter is expected to be enough for the task.

This signal should be then included somehow in governor's output. Remark that PSS's output signal, which has a small amplitude, enters in AVR's input. Since the AVRs work usually with high gains, the relatively small amplitudes of the PSS output does not influence strongly the voltage set-point tracking.

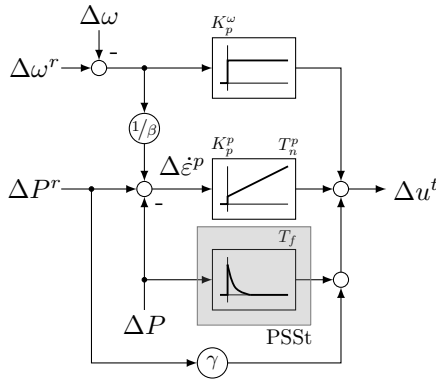
On the other hand, if this same technique is implemented for the PSS_t, due to its relatively small gain a non desirable change in governor's regulation would happen. Thence, a suitable place for PSS_t's insertion is directly at governor's output.

With this said, we can finally summarize the PSS_t as being a high-pass filter having \bar{P} as input, tuned to damp mainly the frequencies from nearly 0.05 Hz and with its output being summed to governor's one. Figure 5.1 exemplifies PSS_t's implementation with T_f being its time constant.

PSS_t's implementation changes k^{th} 's governor control signal of Equation 2.2 to,

$$\begin{aligned} \Delta \bar{u}_k^t &= \gamma_k \Delta \bar{P}_k^r + K_{p_k}^p \Delta \dot{\bar{e}}_k^p + \frac{K_{p_k}^p}{T_{n_k}^p} \Delta \bar{e}_k^p + K_{p_k}^\omega (\Delta \bar{\omega}_k^r - \Delta \bar{\omega}_k) \\ &\quad - \frac{1}{T_{f_k}} \Delta \bar{e}_k^f + \Delta \bar{P}_k, \\ \Delta \dot{\bar{e}}_k^p &= \Delta \bar{P}_k^r - \Delta \bar{P}_k + \frac{1}{\beta_k} (\Delta \bar{\omega}_k^r - \Delta \bar{\omega}_k), \\ \Delta \dot{\bar{e}}_k^f &= -\frac{1}{T_{f_k}} \Delta \bar{e}_k^f + \Delta \bar{P}_k. \end{aligned} \tag{5.1}$$

In summary, the PSS_t acts like a break for system's oscillations. It is implemented in a similar way as the differential action of an Output

Figure 5.1: Governor structure with PSS_t.

Feedback controller, *i.e.*, filtering directly the measured output in order to prevent the high control signal amplitudes due to fast changes in the system reference*. However, one should remark that this solution might harm system's reference tracking, and therefore PSS_t's time constant T_f must be chosen carefully. Notice also that the implementation of the PSS_t increases system's overall order in one unit due to the new state variable $\Delta\bar{\varepsilon}^f$.

The next section evaluates the proposed governor structure using the 2M/1L system as example.

5.2 2M/1L system: Evaluation of the PSS_t

The evaluation of the PSS_t under the 2M/1L system is performed through system's singular values, modal analysis and dynamic simulations, which are presented in the following.

Besides, it is also important to distinguish that, for the 2M/1L, the analysis of system's closed-loop singular values shall be target on the mode with the smallest damping factor among all. The examination of system's participation factors, performed using the identified model presented in Chapter 4 and based on the modeling introduced in Chapter 2, shows that both machines are equally responsible for the cited mode and thus both governors will be modified by the inclusion of two

*Also called *derivative kick*.

PSSSts. This result was particularly expected since the analyzed system is symmetric.

5.2.1 Singular values behavior

The analysis of the singular values for multivariable systems is equivalent to the Bode analysis for SISO ones. The difference lies on the fact that for the multivariable case the phase graph is not obtained. Nevertheless, a deeper explanation about its technique is beyond the scope of the present thesis. For more details, the reader may refer to references [68–70] among many others mainly on the field of Robust Control.

Also, for performing the singular values analysis, at first it is necessary to regard the PSSSt in system's modeling, which augments grid's overall order in one unit and modifies the state vector of Equation 3.11 to,

$$\mathbf{x}_c = [\lambda_G \quad \bar{\omega}_G \quad \bar{\vartheta}_1 \quad \bar{\vartheta}_2 \quad \bar{\varepsilon}^p \quad \bar{\varepsilon}^f]^T.$$

With this said, let us now examine system's singular values for changes in PSSSt's time constant T_f , which is shown in Figure 5.2.

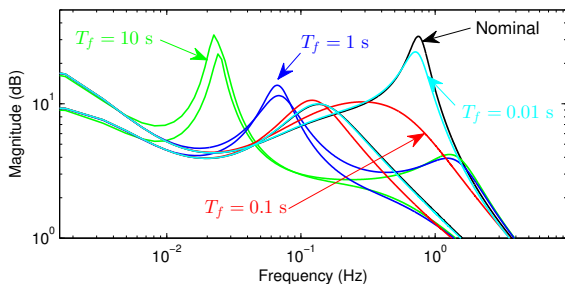


Figure 5.2: System's singular values for different T_f .

The cited figure shows the singular values for the active power output \bar{P} of each generating unit of the power system. It is possible to observe that, according to the expectation, the smaller the time constant T_f , the less influence the PSSSt has on the damping of system's main mode, *i.e.*, the closer the response is to the nominal one.

Notice also that the change in PSSSt's time constant does not harm system's synchronous modes. In other words, system's ability for track-

ing the reference is maintained, with the obvious contribution of the damping of the system's main modes through the PSS_t.

On the other hand, an increase in T_f damps this mode properly. However it creates another resonance peak in the system, and therefore care must be taken during PSS_t's design. In the conclusion of the present chapter a case where this peak is prejudicial to system's performance is shown.

Specifically, for the 2M/1L system the tuning $T_f = 0.05$ s presents a good compromise between the damping of system's main oscillatory frequency and its stability, and therefore this value will be used in the next sections of this chapter.

5.2.2 Modal analysis

Table 5.1 shows the modal analysis of the regulated system with the turbine governor presented in Figure 2.3 and its modification with the PSS_t shown in Figure 5.1. The PSS_t time constant T_f is set to 0.05 s according to the just presented singular values analysis.

Table 5.1: Modal analysis -regulated system

	Natural frequency (Hz)	Damping ratio (%)	Eigenvalues
Nominal governor	0.7605	15.7	$-0.75 \pm j4.72$
	0.1339	59.9	$-0.50 \pm j0.67$
	0.0015	100	-0.0096
Governor with PSS _t ($T_f = 0.05$ s)	0.6645	43.8	$-1.83 \pm j3.75$
	0.1316	52.1	$-0.43 \pm j0.71$
	0.0015	100	-0.0096

From the table it is possible to conclude that the PSS_t damps well system's main mode (0.7605 Hz, 15.7%). In fact, this mode changes to 0.6645 Hz with damping percentage of 43.8%, which means that it is damped after around 540 ms. However, the price to be paid for this increase in damping is a slight decrease of system's second mode (0.1339 Hz) damping: from 59.9% to 52.1%. Nevertheless, despite this reduction the mode is considered still well damped and it does not harm system's overall stability. Anyhow, this feature is important to be kept in mind for further PSS_t's design.

5.2.3 Dynamic simulation

This section explores system's dynamic simulation aiming at the evaluation of the proposed turbine governor with the PSSSt.

Three simulations are performed under the actual system:

- step of 2% in reference voltage \bar{V}_1^r ;
- step of 3% in reference power \bar{P}_2^r .
- short-circuit between nodes 3 and 5 with duration $t_{sc} = 250$ ms.

The two first simulations regard the small-signal stability analysis and the latter concerns the transient stability one. The analyzed variables are generators' speeds $\bar{\omega}_{1,2}$, active powers $\bar{P}_{1,2}$, terminal voltages $\bar{V}_{1,2}$ and governors' outputs $\bar{u}_{1,2}$.

It is important to cite that all implemented simulations in this thesis have regarded the physical limitations of the corresponding components. In other words, saturation blocks for the governor output, control valve, AVR and PSS are concerned.

Step in reference voltage: Figure 5.3 shows the simulation for a 2% step in \bar{V}_1^r at $t = 10$ s for both nominal and PSSSt solutions. The left and right hand sides present the results for generating units 1 and 2, respectively.

The main difference may be seen in the active power graphs, where it is clear the positive contribution of the PSSSt to the damping of system's main mode at 0.7605 Hz, whilst system's steady state values are unchanged. Notice that, for the sake of visualization, the graph time slot does not show the convergence of the variables, which happens after nearly 40 s.

It is also possible to observe that, despite being relatively well damped, the mode which corresponds to the frequency of 0.1339 Hz still persists. One should be aware that this fact is not problematic for the 2M/1L, however it might become an issue in other system configurations whenever a slower mode is not well damped.

Step in reference power: The results for a 3% step in \bar{P}_2^r at $t = 10$ s is presented in Figure 5.4.

Again, the positive damping contribution of the PSSSt to system's overall stability is highlighted mainly on the active power graphs. Notice that the reference tracking profile for \bar{P}_2^r is maintained regardless of the PSSSt. In other words, it means that for the 2M/1L system the PSSSt does not harm this feature of the system.

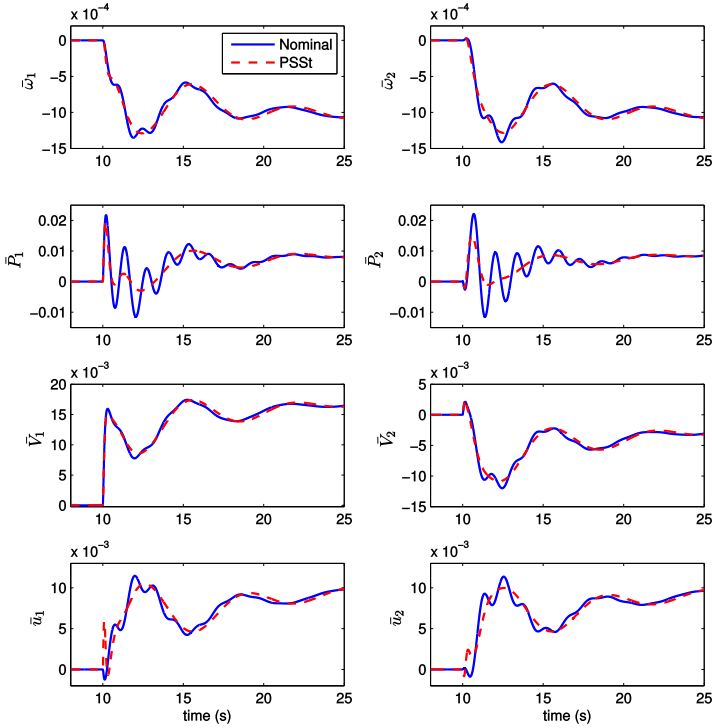


Figure 5.3: Step of 2% in reference voltage \bar{V}_1^r .

Short-circuit: System's transient behavior is evaluated through the enforcement of a short-circuit in half of line's length between busbars 3 and 5, with duration of $t_{sc} = 250$ ms and applied at $t = 10$ s.

This simulation is very important since all the analysis performed so far in this thesis have regarded the linearized system, *i.e.*, it has covered only the small-signal stability field.

Nevertheless, since power systems are intrinsically non-linear, the simulation of a short-circuit has the potential of exciting modes that are not represented in the modal analysis, and therefore its study is called *transient stability analysis*.

Hence, differently from the simulations where small changes in the

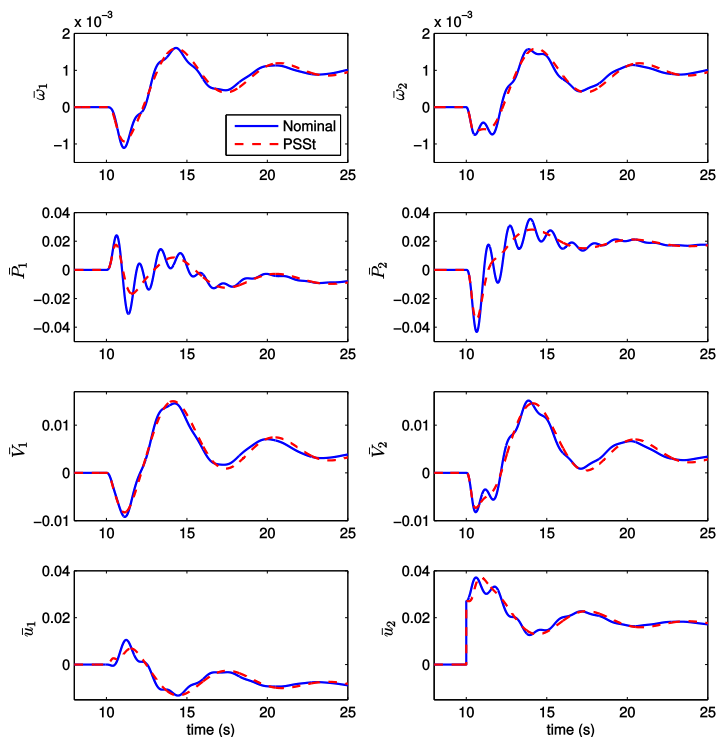


Figure 5.4: Step of 3% in reference power \bar{P}_2^r .

variables are performed, it is difficult for the power engineers to predict the exact behavior of the system whenever a large disturbance occurs, being therefore the short-circuit case a key simulation that must be performed for the evaluation of any modification in the power grid [2]. With this said, consider the cited simulation results in Figure 5.5.

From the figure interesting results may be obtained. For instance, it is observable that an oscillation with 120 Hz happens (2nd harmonic) in the active power and terminal voltage, which is quickly damped.

Notice also that, differently from the current PI-based solution, the new approach with the PSS_T forces the control signal to reduce drastically its amplitude when the short-circuit happens. This is in fact a

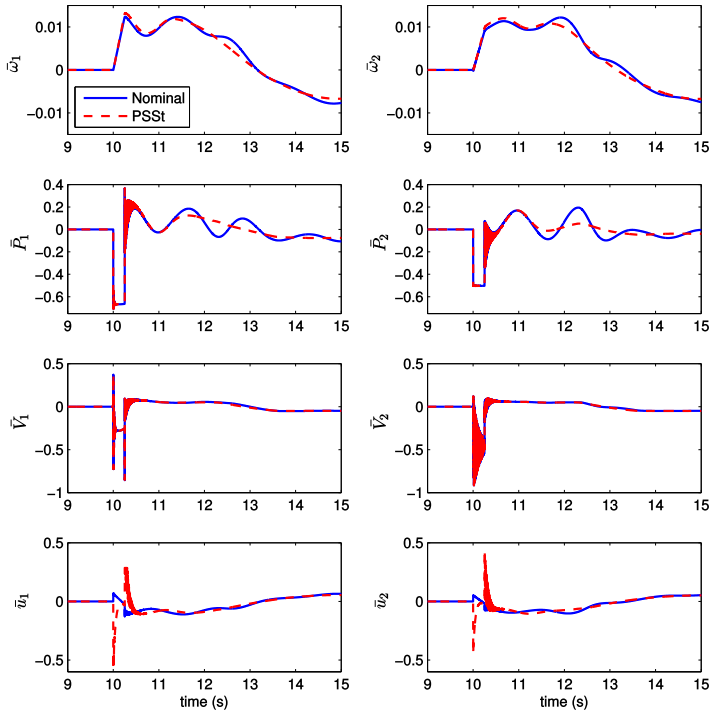


Figure 5.5: Short-circuit between busbars 3 and 5.

very welcome result aiming at system's transient stability since a large increase in speed with a further opening of the turbine valve might lead the overall system to instability.

Lastly, system's main oscillatory mode (0.7605 Hz) is also well damped through the PSS_t, whilst the mode that corresponds to the frequency of 0.1339 Hz still persists with similar amplitude as for the nominal system, which is slightly increased due to the PSS_t.

Chapter conclusions

This chapter has developed the main concept behind the present thesis, *i.e.*, the PSSSt. The idea for its implementation is to perform a slight modification in governor's current structure in order to allow the damping of oscillatory modes that are not well damped through the common exciter-based PSS.

It was shown that the PSSSt is nothing but a high pass filter which acts as the derivative part of an Output Feedback controller. What the PSSSt in fact does is to add a signal that opposes system's oscillations at governor's output \bar{u} . Its main advantage to the exciter-based PSS relies on the fact that the PSSSt has only one tuning parameter (T_f), which represents its time constant.

Computer simulations have shown that the PSSSt is able to damp very well the main oscillatory mode of the 2M/1L system (increase in damping from 15.7% to 43.8%). On the other hand, a slower mode had its damping percentage slightly reduced (reduction in damping from 59.5% to 52.1%), which has not harmed system's overall behavior.

At this point, it is important to remark that the singular values and modal analysis that took place throughout the chapter were only possible due to system's model obtained from the Electromechanical Energy Approach (Chapter 2). Without the model the PSSSt tuning would be performed only via dynamical simulations by trial and error, which is trivial for small systems, but not feasible for large interconnected ones.

With this said, remark that the PSSSt acts like a derivative element. Therefore care must be taken when the design of its time constant since a bad choice might reflect either in the amplification of another oscillatory mode or in a poor reference tracking profile.

As an example, consider for a moment the singular values of a SMIB system with PSSSt shown in Figure 5.6*.

Notice that the damping of nominal system's oscillatory mode through the PSSSt comes with the price of a large increase of the gain in low frequencies, which is absolutely not desirable.

A change in system's gains might be a solution for this matter. However, regardless the gains, governor's current PI structure does not give a natural and easy solution for the posed problem. For instance, an increase in K_p^p amplifies system's main oscillatory mode, as well as a reduction in T_n^p . On the other hand, a reduction in K_p^p and an increase in T_n^p harm system's reference tracking behavior.

*More details of the simulation of this system is given in Chapter 7.

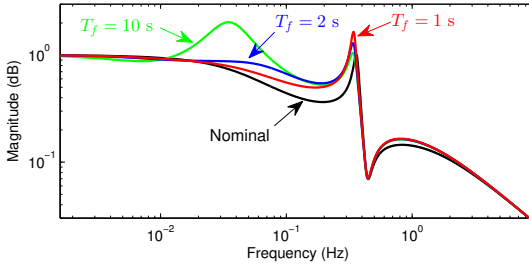


Figure 5.6: System's singular values for different T_f – SMIB.

Hence, the final conclusion of this chapter is that, despite being a simple solution, the PSS_t implementation alone in the current governor architecture does not ensure the improvement of system's stability margins for all power system configurations.

Thus, a new governor structure should be developed in order to achieve this aim. Among the possible architectures, the Model-based Predictive Controller (MPC) is one of the leading approaches that is being implemented nowadays in several different type of plants. A short inquiry at the IEEE web-based library results in nearly 11500 published papers on MPCs from the year 2010*. However, less than ten researches have shown MPC's implementation as turbine governors.

One clear reason for it is MPC's high computational effort when dealing with huge systems and large prediction horizons. As an example, one complete generating unit might reach easily a order of $z = 15$. Since system's settling time is in the order of 15-30 s and a typical sampling time for the turbine governor is 10 ms, GPC's** prediction horizon N_y lays between 1500 and 3000 samples. Given that the size of the matrices that compose GPC's control signal is given by $z N_y$, one concludes that the GPC must solve a calculation with matrices with 22500-45000 of length at each sampling period. Remark that what is said here is for only one generating unit, so that an extension of the power system would hamper the implementation of MPCs even further.

Therefore, in order to exploit the widely known advantages of the predictive controllers in power systems, a light computing MPC should be developed, being what is explored in the next chapter with the new *Unrestricted Horizon Predictive Controller* (UHPC).

*Access on 11.12.2016 at 12:32h.

**The GPC is one of the most implemented MPC type.

6

The Unrestricted Horizon Predictive Controller

This chapter introduces the *Unrestricted Horizon Predictive Controller*, short UHPC, which is one of the leading contributions of the current thesis. As well as in Chapter 3, the theory here demonstrated is improved over author's papers (refer to [35, 56]) in that the present chapter develops the referred controller in a state feedback fashion.

From there and according to the discussion performed throughout the Introduction, the UHPC is to be applied at the turbine side of the generating unit, becoming in this specific case a novel governor type. Since the UHPC may be regarded as a model-based state feedback controller — *i.e.*, it requires system's model during the design — it has the ability of improving system's reference tracking and active power perturbations more efficiently than the widely-used polynomial-based controllers, such as the PID and its derivations [71].

However, the UHPC is not *only* a state feedback controller to be applied as a turbine governor. Additionally, as it will be detailed in this chapter, it is simultaneously fully stochastic and long-range predictive, carrying unprecedented contributions to the Linear Control Theory.

In fact, despite fitting into the category of the *Predictive Functional Controllers*, short PFC, the UHPC is developed under the Minimum Variance (MV) concept, therefore controller's stochasticity is preserved, what is shown in details next.

The chapter begins with a short review on the related researches to

situate the reader on the topic, and continues with UHPC's mathematical development. Lately simulations are performed in order to prove controller's feasibility.

6.1 Related researches

The Model-based Predictive Controllers (MPCs) have been developed in order to overcome some issues that the common controllers (PID, output feedback, etc.) have problems in dealing with, such as input-output constraints, wind-up effect and optimality in the sense of control objectives [72]. In fact, MPCs implement what humans do inherently in daily-life: for instance, while driving a car the driver must *estimate* the acceleration and speed levels in order to reach a destination in a safe way, within a certain time and using a specific amount of fuel. MPC's natural behavior along to its well-posed mathematical fashion on dealing with constraints became the main reason why their are so well accepted both in academia and industry [36].

The MPCs evolved independently in mainly two fronts: while Richalet [73] and others worked on the basic deterministic principles of it, Åström [34] developed the interesting (and stochastic) Minimum Variance Regulator (MVR).

Eventually Richalet ended up developing a sub-class of light computing MPCs called Predictive Functional Control (PFC) — which was successfully implemented in many industrial applications [71] — whereas the evolution of Åström's MVR was more intense and has been directly responsible for new important developments in the MPC field.

However, the lack of computational power back to 30-40 years has indeed limited the full exploitation of the MVR. For instance, the Generalized Minimum Variance Controller (GMVC) presented by Clarke *et al.* [74] has helped on the feasibility of the MVR aiming real processes, however there was still a huge issue whenever the process had large transport delays caused by the difficulty of solving the polynomial equality which arises due to MVR/GMVC's stochasticity during its derivation, named Diophantine equation.

In fact, this matter was dealt by Clarke a couple of years later when he and his colleagues have presented the Generalized Predictive Controller (GPC) with its interesting receding horizon [75] which solves an optimization problem at each time step in order to determine the action plan from k (current time) until N_y (future fixed horizon), applying just

the first calculated input of this plan. At the next time step the optimization procedure is solved again using updated data giving then the feedback action to the system, though it is now performed from $k + 1$ (new current time) until $N_y + 1$ (new future horizon). In other words, despite the difference between the current and future horizon is fixed to N_y , the time horizon is shifted one step forward at each sample.

This new control approach was shown to be quite robust, and then highly reliable for real process applications, which actually happened and still happens nowadays with several derivations of it [76]. One could affirm that one of the reasons for such success in industrial applications is the free-Diophantine solution through the internal simulation of the plant, which has eased substantially the search for the control law, and at the same time, as a consequence, it has diminished the interest on the pure MVR.

Nonetheless, even being a stochastic MPC algorithm, the GPC is rarely applied due to its stochastic properties and the noise model is often simplified. Not even Clarke and Mohtadi [77] when presenting the properties of the GPC considered the usage of a complete stochastic model in their examples, probably avoiding the difficulty introduced by the model of the noise in GPC's equating.

The outcome of this avoidance is that it led, in the course of time, to a much more conservative design, since the main aim became to tune the GPC bounded to the idea of washing out high frequency dynamics and noise with a low-pass filtering fashion instead of exploiting the full potential of the stochastic prediction. According to the discussion performed in the Introduction, by doing this the designer might run the risk of resulting in either a sub-optimal closed-loop behavior (conservative approach) or, and much worse, reducing system's stability margins [34, 35].

With this said, one might notice that without its stochastic potential the GPC and the PFC may become similar. Indeed, the main difference between both is that the former optimizes the full trajectory from time step k to N_y , while the latter looks only at the specific point N_y ahead. This feature reduces dramatically PFC's computational effort, and is the main reason for its successful implementations in real plants. On the other hand, this same particularity inherits the GPC with a more complete description of the system, delivering also more degrees-of-freedom to the designer and as consequence, a better regulation characteristics [72].

However, the price paid by the GPC is high: the computation effort increases with the order of the system and the prediction horizon, z and

N_y respectively. For power system applications, z may be easily greater than 15 for only one generating unit and then even for a short prediction horizon $N_y = 100$ samples, GPC's control law matrices may reach a length of 1500. On the other hand, notice that a prediction horizon of 100 samples is nothing compared to the requirement in power systems, which lays in the range of $2000 \leq N_y \leq 4500$ samples*. Hence, GPC's matrices may reach an incredible length of 30000-45000. Remark that this length increases for extended power grids, which makes GPC's control algorithm clearly unfeasible to solve at each sampling time.

Further, Rossiter [72] has cited in his reference book that for several practical applications there is just a slight enhancement in GPC's closed-loop behavior when compared to the PFC. On the other hand, the PFC is basically a SISO and deterministic controller, so that its implementation in power systems is hampered.

With this information in mind the development of the UHPC has started. What is specifically shown in the next sections is UHPC's ability on dealing with stochastic signals using a very long prediction horizon in a state feedback fashion, without overloading computer's memory.

6.2 UHPC in power systems

As already cited in the previous chapter, the procedure here implemented and followed in the remaining of this thesis is to replace the current PI-based governors with the proposed state-space-based UHPC (one for each turbine), which will act as a turbine governor with an intrinsic capability for damping low frequencies out without the need for PSSs' retuning.

With that said, it is also important to highlight that a decentralized UHPC means that the controller of a certain generating unit is only able to control its own outputs. Hence, despite the access of all system states through the Kalman Filter estimation, in practice it implies that the UHPC will not be fed back with the output signals from other units and thus it shall be given for the k^{th} node solely by $\mathbf{y}(k) = [\bar{P}_k(k) \quad \bar{\omega}_k(k)]$, remarking also that system's state and input matrices \mathbf{A} and \mathbf{B} , as well as its state and input vectors $\mathbf{x}(k)$ and $\mathbf{u}(k)$, shall change depending upon the polynomial-based governor(s) that will be replaced.

Further, the UHPC shall substitute *only* the PI and P structures of the governor, *i.e.*, the remaining structure of the governor is kept

*It is considered $t_s = 10$ ms and a settling time between 20-50 s.

with the compensation of the speed deviation and also with the PSS_t presented in Chapter 5.

Also important to observe is that the model of the regulated system developed in Chapter 3 (Equation 3.11) presents inputs that are not controllable via a decentralized regulator, namely the load active power \bar{P}_L^{\dagger} . Therefore, this input may be considered as an external input disturbance for the *design model*. This assumption eventually reduces Equation 4.4 to,

$$\begin{aligned} \mathbf{x}(k+1) &= \mathbf{A} \mathbf{x}(k) + \mathbf{B} \mathbf{u}(k-d+1) + \mathbf{\Gamma} \boldsymbol{\xi}(k) \\ \mathbf{y}(k) &= \mathbf{C} \mathbf{x}(k) + \boldsymbol{\xi}(k), \end{aligned} \quad (6.1)$$

which will be used from now on in this thesis.

Conclusively, given that the implementation of the UHPC is conditioned upon the substitutable governors, the identification procedure presented in Chapter 4 ought change too, since now the system must be represented without them for its further control via the UHPCs. However, it is known that the actual system still contains all governors, and one is not able to disconnect them in order to perform the identification.

Thence, what is being proposed here is to simply modify the input signals for the identification procedure. In other words, for the polynomial-based governors that will be replaced by UHPCs, instead of using the inputs of node k as its power \bar{P}_k^r and speed $\bar{\omega}_k^r$ references, for these nodes one should use governor's output signal \bar{u}_k^t . This simple modification creates a kind of *by-pass* over the k^{th} governor without disconnecting it from the actual system. Eventually, the system will now be identified in *open-loop**, *i.e.*, the identification will not be able to "see" the governor, thus it will not be identified. In fact, this procedure of *by-passing* the actual controllers of the plant is well-known within the System Identification field, being the most applied technique for identifying inherently unstable systems, see [66, 67, 78]. Figure 6.1 illustrates the difference between the two cases using a single machine as example, where the AVR and PSS are omitted for the sake of simplicity.

To be noticed is that, for the decentralized case the system becomes a SIMO one (*Single-Input Multiple-Outputs*), being its input and outputs given respectively by \bar{u}_k and $\bar{P}_k, \bar{\omega}_k$.

In the next section the UHPC equating is developed expanding author's work [56] to the state-space case.

*This term is employed here with the view on the governor, however the other regulators are still acting on the generator, namely the AVR and PSS.

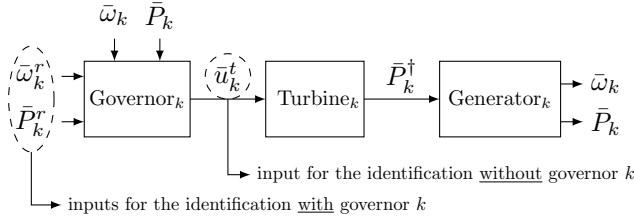


Figure 6.1: Example of the identification procedure: with and without the k^{th} governor.

6.3 UHPC's equating

In this section the UHPC equating is developed, including the regulatory ($\mathbf{y}_r = 0$), reference tracking and reference tracking with integrator cases. At last the UHPC-based governor is presented, which includes also the PSS_t and the compensation for the speed deviation in UHPC's control law.

Differently from the most common MPCs, and at the same time similarly to the PFC, the UHPC regards a quadratic cost function which considers *only* one specific point in the future, being this cost given by,

$$\mathcal{J} = \mathbf{x}(k + N_y)^T \mathbf{Q} \mathbf{x}(k + N_y) + \mathbf{u}(k)^T \mathbf{R} \mathbf{u}(k), \quad (6.2)$$

subjected to the diagonal weighting matrices $\mathbf{Q} = \mathbf{Q}^T \geq 0$ and $\mathbf{R} = \mathbf{R}^T \geq 0$. At this first moment, the reference $\mathbf{y}_r(k)$ is regarded as zero for the sake of simplicity, and it will be inserted throughout the section.

By regarding a point N_y in the future in system's states (Equation 6.1), one easily obtains,

$$\begin{aligned} \mathbf{x}(k + N_y) &= \mathbf{A}^{N_y} \mathbf{x}(k) + \sum_{i=d}^{N_y} \mathbf{A}^{N_y-i} \mathbf{B} \mathbf{u}(k - d + i) \\ &+ \sum_{i=1}^{d-1} \mathbf{A}^{N_y-i} \mathbf{B} \mathbf{u}(k - d + i) + \sum_{i=1}^{N_y} \mathbf{A}^{N_y-i} \mathbf{\Gamma} \boldsymbol{\xi}(k - 1 + i). \end{aligned} \quad (6.3)$$

Clearly the term related to $\boldsymbol{\xi}(k)$ is unknown because it represents

the future of the noise, and therefore can be expressed by present and future parts:

$$\sum_{i=1}^{N_y} \mathbf{A}^{N_y-i} \mathbf{\Gamma} \boldsymbol{\xi}(k-1+i) = \underbrace{\mathbf{A}^{N_y-1} \mathbf{\Gamma} \boldsymbol{\xi}(k)}_{\text{present}} + \underbrace{\sum_{i=2}^{N_y} \mathbf{A}^{N_y-i} \mathbf{\Gamma} \boldsymbol{\xi}(k-1+i)}_{\text{future}}.$$

As well as for the stochastic term, since $N_y \geq d$ the future of the control signal $\mathbf{u}(k)$ in Equation 6.3 is also unknown. Then, similarly to the GPC, the UHPC splits this signal into present and future parts, however applies only the known data, *i.e.*, the terms which contains $\mathbf{u}(k)$. More specifically,

$$\begin{aligned} \sum_{i=d}^{N_y} \mathbf{A}^{N_y-i} \mathbf{B} \mathbf{u}(k-d+i) &= \underbrace{\mathbf{A}^{N_y-d} \mathbf{B} \mathbf{u}(k)}_{\text{present}} \\ &+ \underbrace{\sum_{i=d+1}^{N_y} \mathbf{A}^{N_y-i} \mathbf{B} \mathbf{u}(k-d+i)}_{\text{future}}. \end{aligned}$$

Now, remembering that $\boldsymbol{\xi}(k) = \mathbf{y}(k) - \mathbf{C} \hat{\mathbf{x}}(k)$ (refer to Equation 4.3) and using only the available data, the predicted state vector is given by,

$$\hat{\mathbf{x}}(k+N_y) = (\mathbf{A}^{N_y} - \mathbf{F}\mathbf{C}) \hat{\mathbf{x}}(k) + \mathbf{H} \mathbf{u}(k) + \mathbf{\Upsilon}_1 \underline{\mathbf{u}}(k) + \mathbf{F} \mathbf{y}(k), \quad (6.4)$$

where $\mathbf{F} = \mathbf{A}^{N_y-1} \mathbf{\Gamma}$, $\mathbf{H} = \mathbf{A}^{N_y-d} \mathbf{B}$, $\underline{\mathbf{u}}(k)$ is a vector with input's past data given by $\underline{\mathbf{u}}(k) = [\mathbf{u}(k-1) \ \cdots \ \mathbf{u}(k-d+1)]^T$ and $\mathbf{\Upsilon}_1 = [\mathbf{A}^{N_y-d+1} \mathbf{B} \ \cdots \ \mathbf{A}^{N_y-1} \mathbf{B}]$.

At this point two valuable contributions of the thesis must be highlighted:

1. Equation 6.4 gives the prediction of the system state N_y -steps ahead using only the current information from the control signal and the output itself. Therefore, what we *really* have obtained is a generalization of the Kalman Filter, which is here called *N_y -steps ahead Kalman Filter*, and is detailed in Appendix C;

2. As well as already demonstrated by Silveira and Coelho [79], \mathbf{F} is the intrinsic solution of noise's Diophantine Equation from GMVC's polynomial formulation. Using the same principle, we can show that \mathbf{H} is the solution of GPC's control signal Diophantine Equation, what is demonstrated in Appendix D.

Besides, from now onwards the following equating will consider $d = 1$, which makes the term Υ_1 to disappear. There are mainly two reasons for this assumption: 1) the transport delay in power systems is usually very small whenever the system is operating around its equilibrium points, and 2) the assumption reduces the complexity of the controller without harming severely its performance.

Hence, one ought also notice that Equation 6.2 requires $\mathbf{x}(k + N_y)$. However, since this information is not directly available due to the future of the noise and control signals, what is done here is to use the available information from the N_y -steps ahead Kalman Filter, turning the cost function to,

$$\begin{aligned} \hat{\mathcal{J}} &= \mathbb{E} \{ \mathcal{J} \} = \mathbb{E} \{ \mathbf{x}(k + N_y)^T \mathbf{Q} \mathbf{x}(k + N_y) + \mathbf{u}(k)^T \mathbf{R} \mathbf{u}(k) \}, \\ &= \hat{\mathbf{x}}(k + N_y)^T \mathbf{Q} \hat{\mathbf{x}}(k + N_y) + \mathbf{u}(k)^T \mathbf{R} \mathbf{u}(k), \end{aligned} \quad (6.5)$$

where $\mathbb{E} \{ \cdot \}$ denotes the mathematical expectation operator.

The UHPC control law is thus obtained through the minimization of $\hat{\mathcal{J}}$ such that $\partial \hat{\mathcal{J}} / \partial \mathbf{u}(k) = 0$, which after some algebraic manipulations results in,

$$\mathbf{u}(k) = - \underbrace{(\mathbf{R} + \mathbf{H}^T \mathbf{Q} \mathbf{H})^{-1} \mathbf{H}^T \mathbf{Q}}_{\mathbf{K}_0} [\Upsilon_0 \hat{\mathbf{x}}(k) + \mathbf{F} \mathbf{y}(k)],$$

with $\Upsilon_0 = \mathbf{A}^{N_y} - \mathbf{F} \mathbf{C}$.

Merging the constant terms one obtains,

$$\boxed{\mathbf{u}(k) = -\mathbf{K}_x \hat{\mathbf{x}}(k) - \mathbf{K}_y \mathbf{y}(k)}, \quad (6.6)$$

and,

$$\mathbf{K}_x = \mathbf{K}_0 \Upsilon_0, \quad \mathbf{K}_y = \mathbf{K}_0 \mathbf{F}.$$

Reference tracking: So far we have considered only the regulatory case ($\mathbf{y}_r(k) = 0$). For reference tracking, UHPC's cost function (Equation 6.2) modifies to,

$$\mathcal{J} = [\mathbf{y}(k + N_y) - \mathbf{y}_r(k + d_e)]^T \mathbf{Q} [\mathbf{y}(k + N_y) - \mathbf{y}_r(k + d_e)] + \mathbf{u}(k)^T \mathbf{R} \mathbf{u}(k),$$

where d_e might be either an *emulated* delay for improving system's closed-loop performance or simply $d_e = 0$.

Following the previous steps for obtaining the output predictor $\hat{\mathbf{y}}(k + N_y)$ and substituting it in the cost function, the control law becomes,

$$\boxed{\mathbf{u}(k) = \mathbf{K}_0^r \mathbf{y}_r(k + d_e) - \mathbf{K}_x^r \hat{\mathbf{x}}(k) - \mathbf{K}_y^r \mathbf{y}(k)}, \quad (6.7)$$

with,

$$\begin{aligned} \mathbf{K}_0^r &= (\mathbf{R} + \mathbf{H}^T \mathbf{C}^T \mathbf{Q} \mathbf{C} \mathbf{H})^{-1} \mathbf{H}^T \mathbf{C}^T \mathbf{Q}, \\ \mathbf{K}_x^r &= \mathbf{K}_0^r \mathbf{C} \mathbf{T} \mathbf{y}_0, \quad \mathbf{K}_y^r = \mathbf{K}_0^r \mathbf{C} \mathbf{F}. \end{aligned}$$

Reference tracking with integrator: For ensuring zero steady-state error whenever a perturbation acts on the system, an integrator may be inserted, which increases system's order in one unit per output [80].

In the digital synthesis, the inverse of the integral action – *i.e.*, the difference operator – is represented by $\Delta = 1 - q^{-1}$, with q^{-n} being the backward shift operator for n samples [81]. Hence, Equation 6.1 may be represented for $d = 1$ by,

$$\Delta \mathbf{x}(k + 1) = \mathbf{A} \Delta \mathbf{x}(k) + \mathbf{B} \Delta \mathbf{u}(k) + \mathbf{\Gamma} \Delta \boldsymbol{\xi}(k).$$

Wang [82] cites that if one chooses a state vector to be $\mathbf{x}_a(k) = [\Delta \mathbf{x}(k)^T \quad \mathbf{y}(k)^T]^T$ the augmented system becomes,

$$\begin{aligned} \mathbf{x}_a(k + 1) &= \underbrace{\begin{bmatrix} \mathbf{A} & \mathbf{0} \\ \mathbf{C} \mathbf{A} & \mathbf{I} \end{bmatrix}}_{\mathbf{A}_a} \mathbf{x}_a(k) + \underbrace{\begin{bmatrix} \mathbf{B} \\ \mathbf{C} \mathbf{B} \end{bmatrix}}_{\mathbf{B}_a} \Delta \mathbf{u}(k) + \underbrace{\begin{bmatrix} \mathbf{\Gamma} \\ \mathbf{C} \mathbf{\Gamma} \end{bmatrix}}_{\mathbf{\Gamma}_a} \Delta \boldsymbol{\xi}(k), \\ \mathbf{y}(k) &= \underbrace{\begin{bmatrix} \mathbf{0} & \mathbf{I} \end{bmatrix}}_{\mathbf{C}_a} \mathbf{x}_a(k) + \boldsymbol{\xi}(k). \end{aligned} \quad (6.8)$$

Equation 6.8 will be used from now onwards as being our *design model* for the UHPC, *i.e.*, all matrices and vectors presented so far shall be changed to their augmented versions in order to have the integral effect inserted in the control algorithm.

Consequently, the insertion of the integral action modifies UHPC's control law to,

$$\Delta \mathbf{u}(k) = \mathbf{K}_0^i \mathbf{y}_r(k + d_e) - \mathbf{K}_x^i \hat{\mathbf{x}}_a(k) - \mathbf{K}_y^i \mathbf{y}(k), \quad (6.9)$$

remarking that $\mathbf{u}(k) = \Delta \mathbf{u}(k) + \mathbf{u}(k - 1)$ and given that,

$$\begin{aligned} \mathbf{K}_0^i &= (\mathbf{R} + \mathbf{H}_a^T \mathbf{C}_a^T \mathbf{Q} \mathbf{C}_a \mathbf{H}_a)^{-1} \mathbf{H}_a^T \mathbf{C}_a^T \mathbf{Q}, \\ \mathbf{K}_x^i &= \mathbf{K}_0^i \mathbf{C}_a \Upsilon_{0_a}, \quad \mathbf{K}_y^i = \mathbf{K}_0^i \mathbf{C}_a \mathbf{F}_a, \end{aligned}$$

with,

$$\begin{aligned} \mathbf{F}_a &= \mathbf{A}_a^{N_y - 1} \Gamma_a, \\ \mathbf{H}_a &= \mathbf{A}_a^{N_y - d} \mathbf{B}_a, \\ \Upsilon_{0_a} &= \mathbf{A}_a^{N_y} - \mathbf{F}_a \mathbf{C}_a, \end{aligned}$$

and the Kalman Filter turns to,

$$\hat{\mathbf{x}}_a(k + 1) = (\mathbf{A}_a - \Gamma_a \mathbf{C}_a) \hat{\mathbf{x}}_a(k) + \mathbf{B}_a \Delta \mathbf{u}(k) + \Gamma_a \mathbf{y}(k).$$

Figure 6.2 illustrates UHPC's block diagram implementation, where plant, controller and Kalman Filter are highlighted.

Some remarkable points regarding the development presented so far in this chapter are noteworthy:

- the UHPC is a state feedback controller since system's states appear explicitly in the control law (Equations 6.6, 6.7 and 6.9);
- UHPC's ability of dealing with noise is inherited from the Kalman Filter;
- differently from the GPC and most MPCs, the matrices which form $\Delta \mathbf{u}(k)$ does not grow with the increase of the prediction horizon N_y , meaning that UHPC's computational effort grows solely with the order of the system;
- eventually, UHPC's implementation doubles system's order due to the need for the Kalman Filter, unless all the states are available for measurement. Since this is not the case in power systems,

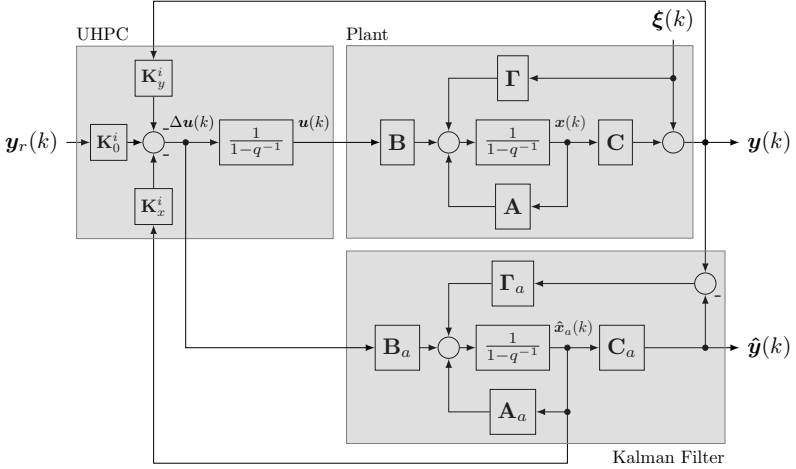


Figure 6.2: UHPC's closed-loop diagram for the reference tracking with integral action ($d = 1$ and $d_e = 0$).

this is the price to be paid whenever one requires a state-space controller. In fact, not only the UHPC, but *any* state-space controller would face the same issue;

- for completeness, one might notice that UHPC's control law (Equation 6.6) equals to the LQR* ones for the regulatory case ($\mathbf{y}_r(k) = 0$) if for both $N_y = d = 1$ and $\mathbf{\Gamma} = 0$ (deterministic case), since then $\mathbf{F} = \mathbf{\Gamma}$, $\mathbf{H} = \mathbf{B}$ and $\mathbf{\Upsilon}_1 = 0$. Specifically,

$$\mathbf{u}(k) = - \underbrace{(\mathbf{R} + \mathbf{B}^T \mathbf{Q} \mathbf{B})^{-1} \mathbf{B}^T \mathbf{Q} \mathbf{A}}_{\mathbf{K}_{\text{LQR}}} \mathbf{x}(k),$$

which is the most fundamental result of the Optimal Control Theory. Without any loss of generality, the equivalence also holds for the LQG** control.

UHPC-based governor: Finally, adding the PSS_t and the compensation for the speed deviation (refer to Equation 5.1) to UHPC's control

* Linear Quadratic Regulator

** Linear Quadratic Gaussian

signal in Equation 6.9, the new turbine governor control law for the k^{th} generating unit becomes,

$$\Delta \bar{u}_k^t(k) = K_{0_k}^i [\bar{P}_k^r(k) - K_{\omega_k} \bar{\omega}_k(k)] - \mathbf{K}_{x_k}^i \hat{\mathbf{x}}_a(k) - K_{y_k}^i \bar{P}_k(k) - T_{f_k}^{-1} \bar{\varepsilon}_k^f(k) + \bar{P}_k(k), \quad (6.10)$$

with K_{ω} being the compensation for the speed deviation and with the augmented state as,

$$\bar{\varepsilon}_k^f(k+1) = \bar{\varepsilon}_k^f(k) - T_{f_k}^{-1} \bar{\varepsilon}_k^f(k) + \bar{P}_k(k). \quad (6.11)$$

Equation 6.10 is the control law to be used throughout the remaining of this thesis. Figure 6.3 shows the proposed governor structure.

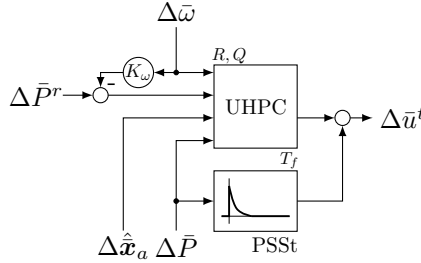


Figure 6.3: UHPC-based governor with PSS.

Notice that the UHPC is to be applied as a decentralized controller and the system is regarded as SIMO. Therefore, $\mathbf{K}_0^i = K_0^i$ and $\mathbf{K}_y^i = K_y^i$, *i.e.*, both are scalars (see Equation 6.10).

At this point it is important to remark that the approach here presented of inserting the speed deviation compensation and the PSS afterwards in the control law might be regarded as sub-optimum since they are not concerned in UHPC's cost function. However, the previous inclusion of these filters would increase substantially UHPC's design complexity, and therefore their inclusion afterwards is a practical alternative for the matter.

Next section presents UHPC-based governor simulations using the assumptions discussed throughout this chapter in the 2M/1L system in order to ascertain the proposed UHPC-based governor feasibility.

6.4 2M/1L system with the UHPC

This section evaluates the just presented UHPC-based governor under the 2M/1L system. It is split into two parts: first the UHPC- and PI-based governors are compared for the case without PSSst and compensation for the speed deviation in order to give insight to UHPC's behavior.

The PSSst is inserted in the governors' outputs in the following, whereas system's singular values, modal analysis and dynamic simulations are performed in order to analyze and compare its impact in system's damping for both governors structures.

6.4.1 UHPC evaluation

The behavior of the singular values of the closed-loop system with the increase of the prediction horizon N_y is exploited in the following. In the sequence, dynamic simulations are performed in order to compare the UHPC ability for rejecting noise.

Therefore, this section aims to compare solely the new UHPC with the current PI governor without PSSst and compensation for the speed deviation in order to verify the main differences of both structures. Also, the output error and control signal weighting matrices will be respectively set to $\mathbf{Q} = \mathbf{I}$ and $\mathbf{R} = 0$, *i.e.*, there is no restriction on the control effort. Further, this section regards only the identified model instead of the actual system in order to ease the analysis due to model's linearity.

Prediction horizon: Figure 6.4 shows the singular values for five different system conditions: open-loop, *i.e.*, without governors; UHPC with $N_y = 1$; UHPC with $N_y = 10$; UHPC with $N_y = 100$; and UHPC with $N_y = 1000$ samples*.

The figure shows explicitly that the increase in UHPC's prediction horizon leads the closed-loop system to present the same behavior as the open-loop one, whereas some intermediate values of N_y might lead the system to instability. In fact, the analysis of system's closed-loop eigenvalues shows that the stability is obtained from $N_y = 260$ samples onwards. In practice it means that if the plant is stable, a sufficient increase in UHPC's prediction horizon ensures that the closed-loop system will also be stable, however with a remarkable difference: since the

*For a sampling time $t_s = 10$ ms.

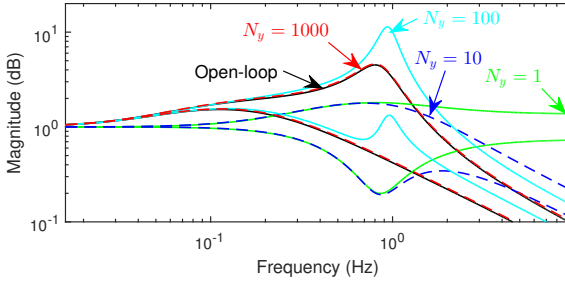


Figure 6.4: Singular values of the open and closed-loop system with the increase of N_y .

UHPC has an intrinsic integrator in its direct loop, the controlled plant will track the reference (for step inputs) and reject perturbations.

Notice that $N_y = 1500$ samples represents exactly system's open-loop settling time, which is 15 seconds. This is in fact a known result from MPC's literature which states that the prediction horizon should be large enough to capture all system's dynamics [72, 75]. Although possible due to UHPC's unique features, an increase over this value for N_y does not bring any relevant benefit for the controlled system, therefore $N_y = 1500$ is the value to be used from now on in the simulations.

Hence, it is possible to affirm that the increase of the prediction horizon *restores* the free response of the plant to a state with unity gain. Another interesting feature is that, if there is no mismatch between the actual system and the model, the UHPC control signal is given in a stepwise shape.

Remarkable at this point is UHPC's prediction horizon. As already cited, for most MPCs the length of the control signal matrices are given by $z N_y$, with z being the order of the controlled system. For this small example, considering the same prediction horizon of the UHPC, the GPC would have a control signal $\mathbf{u}(k)$ composed by matrices of length 12000. On the other hand, the UHPC control signal deals with matrices of length 8. Therefore, UHPC's computation effort is about 0.07% of GPC's one being this the most important justification for its implementation in power systems.

Aiming at a more didactic understanding of UHPC's features, the analysis presented so far has considered that all the states are available for measurement. However, since this assumption does not hold in

practice, the Kalman Filter may also be designed, which is performed through its frequency response in a way that system's main dynamics is maintained. At the same time, eventual nonlinearities and mismatches shall excite the filter aiming at UHPC's state feedback. Besides, the measurement noise should be properly filtered.

The above statements give an overview on the Kalman Filter design. Nevertheless its deeper analysis is also beyond the scope of the thesis and the reader may find several examples in the Control System literature, such as in [63, 69, 70, 81]. Another possibility is to find the state disturbance matrix through System Identification techniques, see, *e.g.*, [67, 78, 83]. For completeness Figure 6.5 shows the distortion on system's closed-loop singular values caused by the selected Kalman Filter (KF) for $N_y = 1500$ samples.

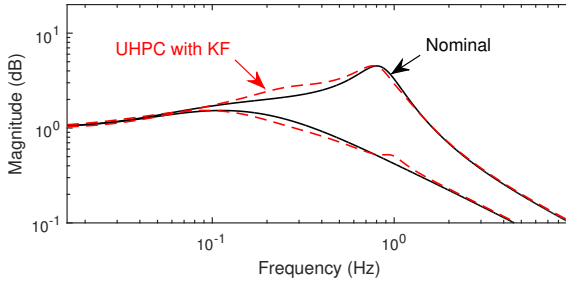


Figure 6.5: Singular values of the open and closed-loop system with Kalman Filter ($N_y = 1500$ samples).

Noise rejection: As stated throughout this chapter, the UHPC has an intrinsic ability on dealing with noisy signals, which is inherited from the Kalman Filter properties. Therefore, a random signal with variance $\sigma^2 = 1e^{-6}$ is applied at model's active power outputs \bar{P}_1, \bar{P}_2 , which represents a variation of nearly $\pm 1\%$ on the variables.

Consider in Figure 6.6 the simulation of the identified model for a 3% step in \bar{P}_1^r at $t = 1$ s, where the noiseless results of \bar{P}_1 and \bar{P}_2 for both the UHPC and PI governors are shown along with their control signals.

Notice the remarkable difference mainly on the control signals. As it is clear, UHPC's ones are smoother due to the Kalman filtering. The calculated variances for UHPC's $\bar{u}_{1,2}$ are nearly 93% lower than for the

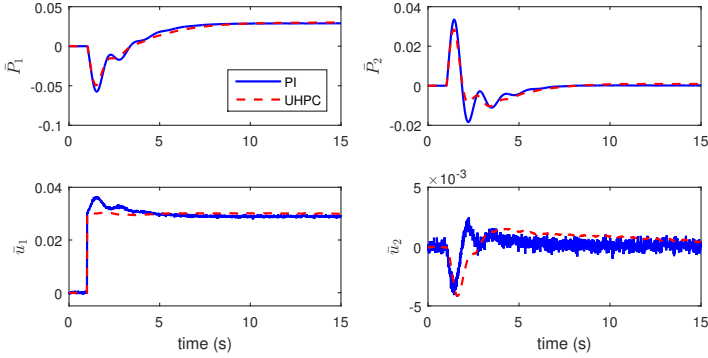


Figure 6.6: Comparison between the UHPC and PI controllers for the noisy case ($N_y = 1500$ samples).

PI ones. This result is particularly important whenever one remarks that the shown control signal is applied directly on a mechanical device – namely the turbine valve – where it is known that the less high frequency excitation it has, the longer its life-time will be, being this one of the fundamental results of the present thesis. Likewise important is that this feature does not harm UHPC’s regulation of the controllable variables.

Observe also UHPC’s stepwised control signal for \bar{u}_1 , which has this shape due to the matrix* \mathbf{R} that is set to zero. The tuning of this matrix weights the control signal effort, *i.e.*, the higher the value for \mathbf{R} the more conservative the system will be, and therefore less energy is utilized by the UHPC.

Next section evaluates the UHPC action as a full turbine governor that might replace the current PI-based one.

6.4.2 UHPC-based governor

Despite the promising results obtained in the previous section w.r.t. reference tracking and disturbance rejection, it is known that in Power Systems a compensation for the speed deviation must be regarded in the governor structure for islanded conditions [1, 2, 4]. However, this compensation makes the closed-loop system to become more oscillatory,

*In this case, \mathbf{R} is scalar since the governor has only one output.

and therefore the PSSSt shall be also inserted. Thus, the analysis to be performed in the following concerns the governor structure shown in Figure 6.3 applied on the actual 2M/1L system.

Notice that $K_\omega \neq 1/\beta$ and hence this gain shall be also tuned with the aim at a small speed deviation. Remark that due to this compensation a steady-state error is to be expected despite the integrator presented in both cited governor types.

The gain K_ω is tuned in order to match the current result given by the PI-based governor. However, it is important to remark that in the present thesis this tuning is realized with the aim at performing a fairer comparison between the two governor approaches, *i.e.*, in practical applications it shall be done only with the intention of reducing the frequency deviation.

With this said, let us consider the results for system's modal analysis, which is presented in Table 6.1.

Table 6.1: Modal analysis -regulated system

	Natural frequency (Hz)	Damping ratio (%)	Eigenvalues
Nominal governor	0.7605	15.7	$-0.75 \pm j4.72$
	0.1339	59.9	$-0.50 \pm j0.67$
	0.0015	100	-0.0096
PI governor with PSSSt ($T_f = 0.05$ s)	0.6645	43.8	$-1.83 \pm j3.75$
	0.1316	52.1	$-0.43 \pm j0.71$
	0.0015	100	-0.0096
UHPC governor with PSSSt ($T_f = 0.05$ s, $K_\omega = 10$)	0.6777	46.5	$-1.98 \pm j3.77$
	0.1407	59.5	$-0.53 \pm j0.71$
	0.0015	100	-0.0096

The cited table shows that there is a slight improvement concerning the UHPC-based governor with PSSSt w.r.t. the PI-based one. Specifically, what is interesting to notice is that the damping percentage of system's secondary oscillation mode (0.1339 Hz, 59.9%) is kept almost unchanged, whilst the damping of the main mode is even higher than for the PI-based governor with PSSSt.

Finally, for completeness consider the dynamic results of the system in Figures 6.7 to 6.9. As well as in Chapter 5, the first simulation regards a 2% step in \bar{V}_1^r , the second a 3% step in \bar{P}_2^r and the third a short-circuit between busbars 3 and 5.

The three figures show explicitly that the UHPC-based governor

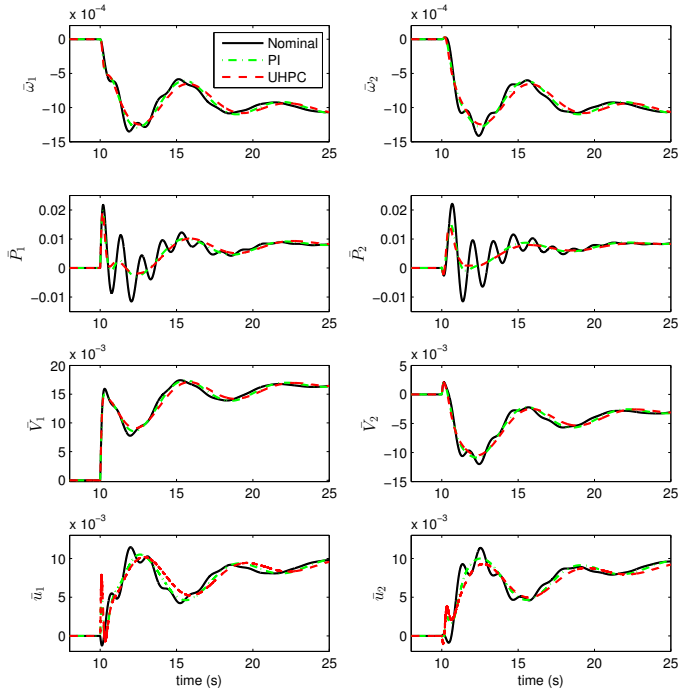


Figure 6.7: Step of 2% in reference voltage \bar{V}_1^r .

is able to damp out system's modes properly in a similar way as the PI-based one does, both with PSS. In fact, there is a slight enhancement in UHPC's results over PI's, which was already expected from the modal analysis performed beforehand.

Chapter conclusion

This chapter has presented the development of a new state-space controller, named here *Unrestricted Horizon Predictive Controller*, short UHPC, due to its unique feature of predicting a very long horizon N_y without overloading controller's memory, what is different from the most common MPCs.

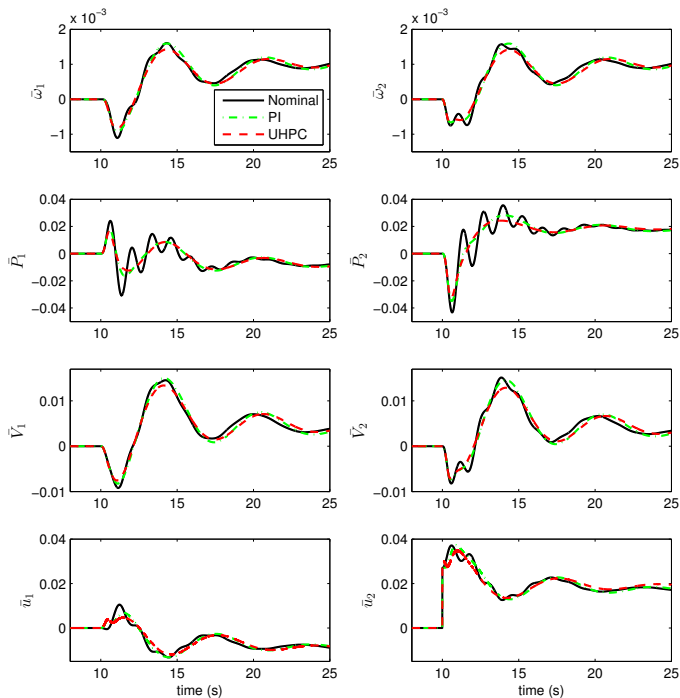


Figure 6.8: Step of 3% in reference power \bar{P}_2^r .

As an important side effect of UHPC's equating, the so-called *N_y-steps ahead Kalman Predictor* is also developed. This predictor is in fact responsible for UHPC's long prediction horizons. Further, it has been shown that the UHPC solves inherently the two Diophantine Equations that arise in the polynomial development of the GPC, which results are given directly by matrices \mathbf{F} and \mathbf{H} .

Making use of the 2M/1L benchmark system, the study has shown that a prediction horizon N_y of nearly system's settling time is enough for restoring plant's free response if $\mathbf{R} = \mathbf{0}$ and $\mathbf{Q} = \mathbf{I}$. Setting the control signal weighting matrix \mathbf{R} to zero means in practice that the designer allows the UHPC to use all energy required to regulate system's output. It is in fact true that for fast systems, the output error

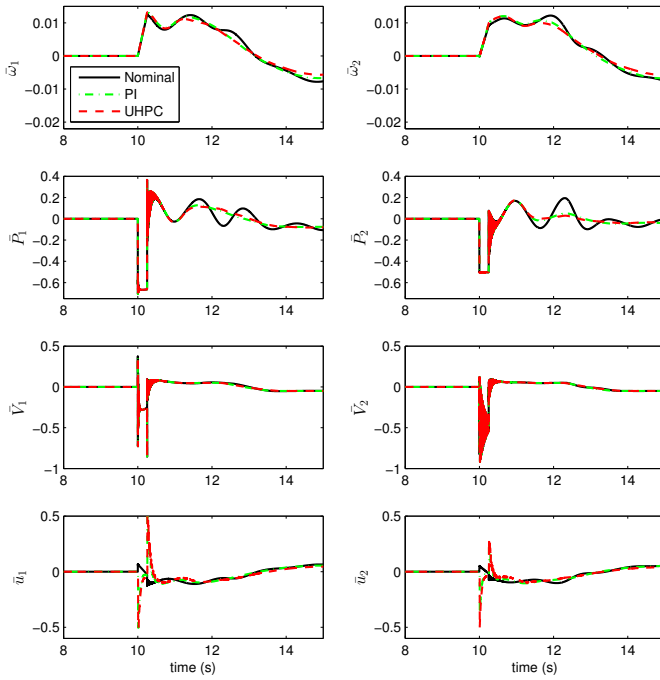


Figure 6.9: Short-circuit between busbars 3 and 5.

weighting matrix \mathbf{Q} might be set to identity, and therefore only matrix \mathbf{R} may be used to tune the controller. On the other hand, the tuning of matrix \mathbf{Q} may be performed whenever the designer needs a faster response in comparison to system's open-loop behavior*.

UHPC's ability in dealing with noise and inherent oscillations in power systems is also highlighted. The study has shown that the UHPC uses much less energy to achieve very similar output and control signal profiles as the actual governor does. This feature is achieved due to the Kalman Filter implementation, remarking that the state disturbance matrix $\mathbf{\Gamma}$ is designed according to the requirements of the project.

Lastly, it is also shown that the UHPC with PSS_t and compensa-

*For this case it is required that $\mathbf{R} \neq 0$.

tion for the speed deviation, called here UHPC-based governor, is able to provide the main result that this thesis is pursuing: the intrinsic damping of system modes through the tuning of the governor gains. Precisely, it is demonstrated that the system oscillation frequency of 0.7605 Hz is easily damped even without being necessary the tuning of the control signal weighting matrix \mathbf{R} .

At this point one could argue about the required effort for the development of the UHPC compared to the relatively small improvement in system's response given by the PI-based governor with PSS_t. However what must be highlighted is that the UHPC delivers interesting results besides the damping of system's modes.

For instance, the UHPC is a stochastic controller that regards a Kalman Filter intrinsically. This feature is very welcome in Power Systems, where, according to practitioners, it is known that the measurement noise level might be high. It has been demonstrated that the UHPC is able to deliver a much smoother control signal to turbine's valve than a common PI.

Furthermore, UHPC's design becomes natural whenever one remarks that system's open-loop response is restored in the closed-loop, however with unity gain due to controller's integrators. Hence, the UHPC enables the designer to choose its weighting matrices with this known starting assumption, which eases the search for their values.

Moreover, the UHPC also enables an ease and light computing implementation of a Model-based Predictive Controller in extended power systems, what has been an issue within the field due to systems' high order and, as a consequence, very large control signal matrices. For the UHPC, the length of these matrices are limited by the order of the system, what reduces dramatically controller's computational cost.

At last, one should also remark the SMIB example presented at the conclusions of Chapter 5. For this case the proposed PI-based governor with PSS_t does not present an acceptable active power regulation. The next chapter of the thesis presents the implementation of the UHPC on it and also on the Two-Area benchmark system in order to prove its feasibility.

7

Benchmark test systems

This chapter presents the simulations of two different benchmark systems in order to evaluate the proposed governor developed throughout the previous chapters.

The systems analyzed here are namely the SMIB (one generating unit) and the Two-Area (four generating units) systems, which are presented in details in the following. All simulation data can be found in Appendix B.

7.1 SMIB system

The Single-Machine Infinite-Bus system shown in Figure 7.1, or simply SMIB, is certainly the most studied benchmark system in the Power Systems field. In spite of being an ideal representation of a generator connected to a huge static power grid with infinite short-circuit power, it in fact depicts relatively well the behavior of several generating units worldwide, and this is the main justification for its study in this work.

According to the proposal of the thesis, the analysis to be performed in this section intends to substitute the current PI-based governor with the developed UHPC-based one. The main idea is to improve system's damping without being required the PSS re-tuning. It is important to notice that the SMIB system does not require a frequency deviation compensation in its governor due to the connection with a static source (infinite bus), and therefore this loop is omitted in the analysis.

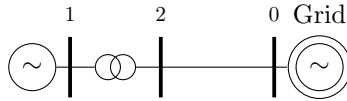


Figure 7.1: Single-Machine Infinite-Bus System.

Thence, remarking Taylor’s seminal paper [23], which indicates that there is a strong suspicion among the power engineers that several actual PSSs are poorly tuned, in this example SMIB system’s PSS is regarded intentionally in a sub-optimum fashion in order to better exploit the intended damping to be introduced by the UHPC.

The section starts firstly with system’s modal analysis and parameter identification in order to obtain a reliable *design model* for implementing the UHPC. Afterwards, UHPC’s gain (matrix \mathbf{R}) is tuned making use of the singular values analysis obtained from the identified model. At last, the work analyzes the dynamical performance of the UHPC-based governor in comparison to the actual PI-based one.

Modal analysis and parameter identification

SMIB’s mathematical model is obtained directly from the Electromechanical Energy Approach presented in Chapter 2, whilst the identified model is gained following the steps given in Chapter 4.

For the identification procedure, two noisy signals with variance of $\sigma^2 = 1e^{-6}$ are applied both in the active power \bar{P} and terminal voltage \bar{V} outputs in order to simulate the uncertainty added by the sensors. This variance represents in practice a relatively small amount of noise with amplitude varying nearly in the range of 2% of the nominal values.

Figure 7.2 shows the comparison between the actual data, the nominal model from Chapter 2 and the identified one. Notice that the latter is able to represent system’s oscillations more precisely than the former. The fitting percentages, calculated with Equation 4.5 gives 85% and 94% of accuracy for the nominal and identified models, respectively.

In Table 7.1 is presented the main oscillation mode of the two cited models in comparison to the actual system after its linearization. Again, it is possible to observe that the identified system depicts system’s mode with a higher accuracy than the nominal one.

It is very important to highlight the quality of the parameter identification result despite the noise introduced by the measurement sensor.

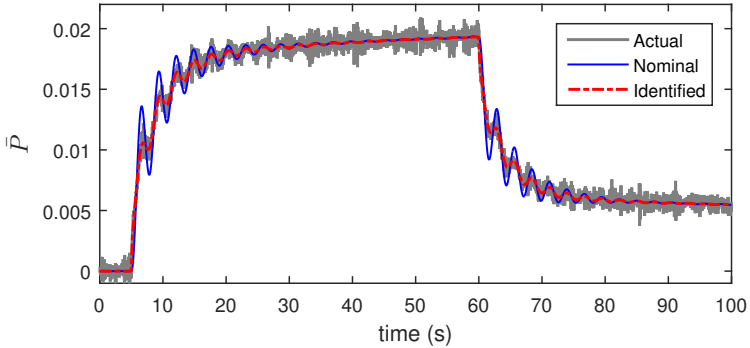


Figure 7.2: Comparison of actual, nominal and identified models – SMIB system.

Table 7.1: Modal analysis of the SMIB system

	Natural frequency (Hz)	Damping ratio (%)	Eigenvalues
Actual system	0.3615	5.46	$-0.12 \pm j2.27$
Nominal system	0.3609	2.40	$-0.05 \pm j2.27$
Identified system	0.3607	5.15	$-0.12 \pm j2.26$

Furthermore, although the nominal system also depicts with a good degree of accuracy the actual one, the identification procedure modifies just slightly the parameters obtained by the former in order to improve its dynamic response. The identified system is used from now on for the PSS_t and UHPC designs.

PSS_t design

The design of the PSS_t is performed using the current PI-based governor structure through its modal analysis, which is shown in Table 7.2.

It is interesting to notice that there is in fact an active damping in system's main mode (0.3621 Hz) with the increase of PSS_t's time constant T_f . However, the price to be paid is high: the increase in damping of this mode reflects on the appearing of another slow mode,

Table 7.2: Modal analysis of regulated SMIB system (with PSSSt)

	Natural frequency (Hz)	Damping ratio (%)	Eigenvalues
Nominal governor	0.3621	4.90	$-0.11 \pm j2.27$
	0.0395	100	-0.2481
Governor with PSSSt ($T_f = 1$ s)	0.3427	5.01	$-0.11 \pm j2.15$
	0.0526	100	-0.3304
Governor with PSSSt ($T_f = 10$ s)	0.3444	7.93	$-0.17 \pm j2.16$
	0.0326	37.7	$-0.08 \pm j0.19$
Governor with PSSSt ($T_f = 100$ s)	0.3452	8.09	$-0.18 \pm j2.16$
	0.0170	21.8	$-0.02 \pm j0.11$

and the further increase of T_f reduces its damping.

An acceptable compromise between the two damping ratios lays around $T_f = 10$ s, which is the value to be used from now on. On the other hand, one should remark that this setting ensures solely an acceptable external disturbance rejection, and not a good reference tracking for \bar{P}^r due to its oscillatory behavior.

Since the SMIB system is the most fundamental power system representation of real generating unit conditions worldwide, another solution for the matter must be properly tackled, which is shown next with the UHPC design.

UHPC's design

For UHPC's design, first of all it is necessary to observe system's settling time, which in this case is nearly 30 s. Hence, UHPC's prediction horizon N_y for the SMIB system here presented is set to 3000 samples*. Notice again the long prediction horizon used in the UHPC algorithm, which would demand heavy computer calculations for other MPCs like the GPC, where its control signal would have to deal with matrices of size 12000. On the other hand, UHPC's control signal matrices have a maximum size of 4 for the present system.

With this said, refer now to Figure 7.3 for the analysis on system's singular values with the increase of the control signal weighting matrix \mathbf{R} , remembering that the UHPC configuration with $\mathbf{Q} = \mathbf{I}$ and $\mathbf{R} = 0$ corresponds nearly to plant's open-loop behavior.

*With sampling time of $t_s = 10$ ms.

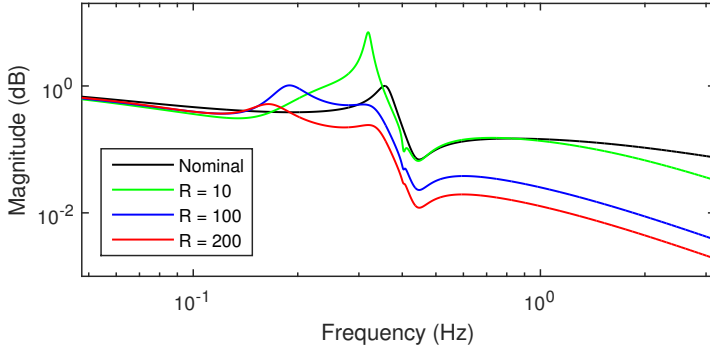


Figure 7.3: Singular values of the closed-loop system with the increase of \mathbf{R} (for $N_y = 3000$ and $T_f = 10$ s) – SMIB system.

The cited figure explicits that the tuning of $\mathbf{R} = 100$ might be dangerous since the damping of system’s risen mode (0.19 Hz) is poorly damped. Therefore, aiming at a steeper damping of this mode, $\mathbf{R} = 200$ is the tuning to be used in the remaining of this section. More important, notice that all system’s mode are well damped with this configuration.

Dynamic simulation

At last, let us evaluate the just designed UHPC-based governor using the actual SMIB system.

As well as for the previous chapters, two simulations for the small-signal stability analysis and one for the transient one are performed, being:

- step of 2% in reference voltage \bar{V}^r ;
- step of 3% in reference power \bar{P}^r .
- short-circuit at the infinite busbar with duration $t_{sc} = 250$ ms.

Step in reference voltage: Figure 7.4 shows the simulation for a 2% step in \bar{V}^r at $t = 5$ s for both the PI- and the UHPC-based governors, evaluated with and without the PSS_t.

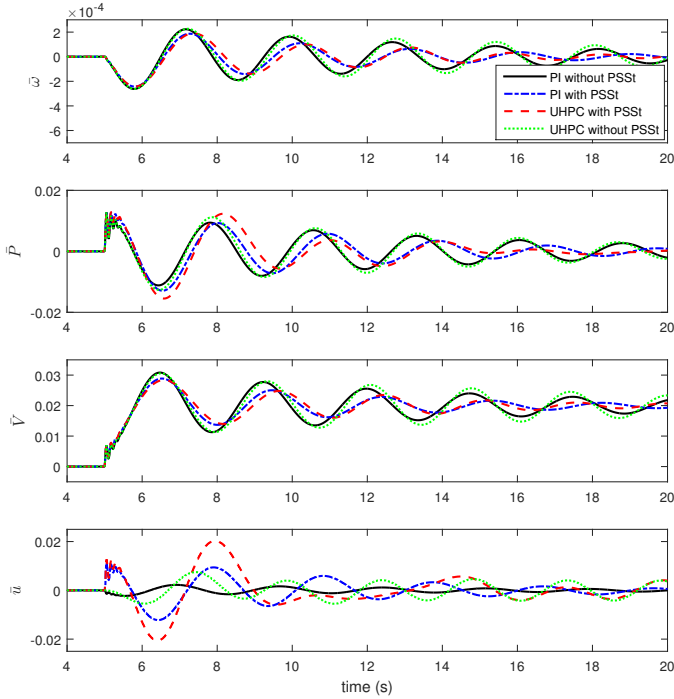


Figure 7.4: Step of 2% in reference voltage \bar{V}^r .

It is possible to observe that both the solutions with PSS present improved results compared to the governors without this device. Notice how similar are the responses for the PI- and UHPC-based governors without PSS.

Interesting is that, despite the higher deviation during the first oscillation, the UHPC-based governor damps faster the power oscillations than the other controllers. Specifically, active power's settling time is reduced in 50% (from 30 s to 15 s) for the cited governor.

Step in reference power: The results for a 3% step in \bar{P}^r at $t = 5$ s are presented in Figure 7.5.

In fact, this result is perhaps the most interesting of the present

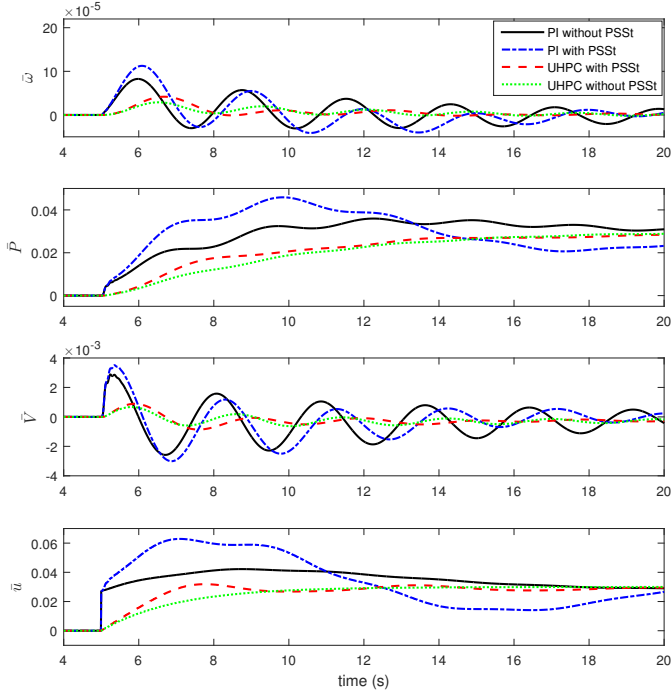


Figure 7.5: Step of 3% in reference power \bar{P}^r .

section, since it highlights the governors' capability in dealing with reference tracking.

The figure shows that the PI-based governor with PSS presents a poorly damped low frequency oscillation that hampers severely the active power response.

In this example the advantage of the UHPC becomes evident. Both UHPC-based governors are capable to damp out system's main mode (0.3621 Hz). At the same time their reference tracking is also ensured. On the other hand, these results are achieved due to a more conservative control signal \bar{u} , which makes the system to reach the reference slower and in a more stable way.

Short-circuit: System's transient behavior is evaluated through the enforcement of a short-circuit at the infinite busbar, with duration of $t_{sc} = 250$ ms and applied at $t = 5$ s, which is shown in Figure 7.6.

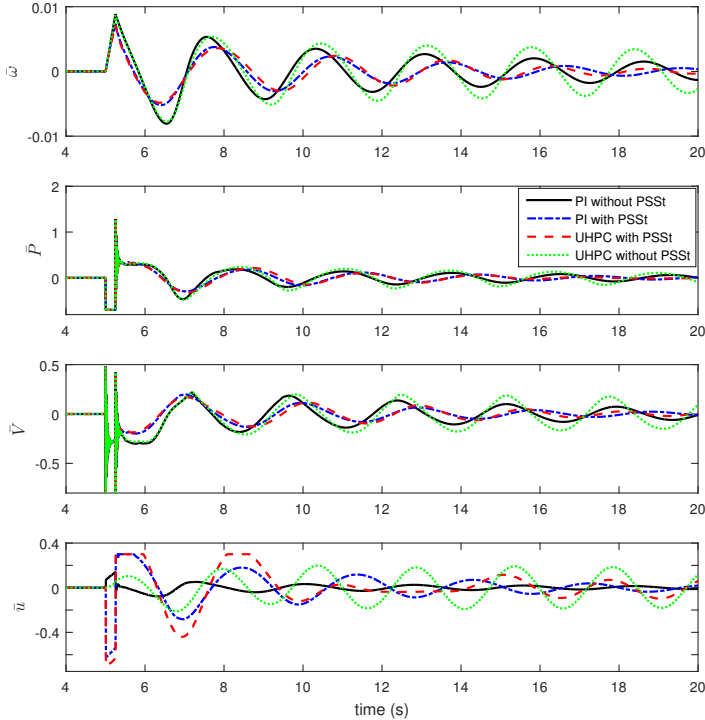


Figure 7.6: Short-circuit at the infinite busbar.

It is interesting to notice that the UHPC-based governor without PSS is not able to damp out properly system's oscillatory mode after the posed short-circuit.

Conversely, both governor structures that implement the PSS present a relatively good result w.r.t. the oscillations settling time, which is reduced in nearly 20 s in comparison to the current governor solution.

Also remarkable is the control signals of the cited governors. Notice

that for both cases the control signal decreases instantaneously in order to avoid a further increase in generator's speed, being later on saturated due to the physical limitations of the valve.

Conclusions of the section: This section has presented the evaluation of the UHPC-based governor with PSS_t for the SMIB system. The system is first modeled using the Electromechanical Energy Approach and then identified for reducing the deviation between the model and the actual data. PSS_t's time constant T_f is set to 10 s after system's closed-loop modal analysis, whilst UHPC's control signal weighting matrix \mathbf{R} is tuned to 200 after the observation of system's singular values. The dynamic simulations have shown that the proposed controller structure delivers more stable results for all the three simulated system conditions in comparison to the current solution with and without PSS_t, and also to the UHPC without PSS_t.

7.2 Two-Area system

The widely-known Two-Area system, also called Kundur's Two-Area system and shown in Figure 7.7, was first presented by Klein *et al.* [10] for the sake of the analysis of the causes of the interarea modes.

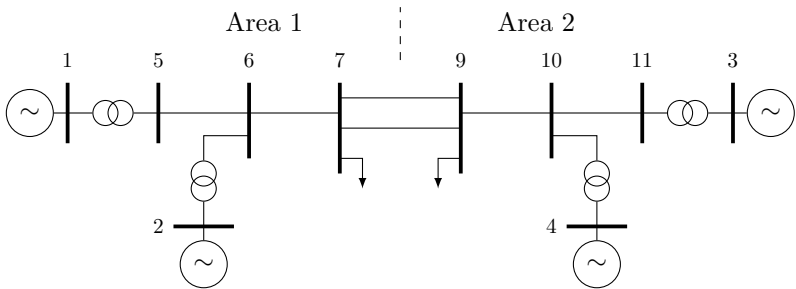


Figure 7.7: Kundur's Two-Area System.

As its name states, the system is composed by two symmetric areas containing two generators each and linked through two relatively long transmission lines. Thanks to its symmetry it is possible to observe easily both local and interarea modes, being this the main justification for its wide use among power system studies.

The Two-Area system has an unstable behavior if its PSSs are out of service. On the other hand, with the PSSs tuned in the way the authors suggest the system presents a very stable performance.

For this reason, in this work the Two-Area system is modified in order to highlight the main contribution of the thesis, *i.e.*, the replacement of the current turbine governors with the new UHPC-based one in order to increase system's damping.

Thence, the idea is to reduce system's stability margin up to the point where the low frequency oscillations are critical, however without losing stability. Here it is proposed to disconnect the PSSs of generators 2 to 4 and insert the PSS_t at generator 1. This choice is justified by the fact that the idea of this example is to show the effectiveness of the PSS_t along with the exciter-based PSS, *i.e.*, with both PSSs working in parallel at the same generating unit, as already highlighted throughout the thesis.

Following the same steps for the SMIB system, this section starts firstly with system's modal analysis and parameter identification in order to obtain the *design model* for the UHPC design. In the sequence, UHPC's gain (matrix \mathbf{R}) is tuned through the analysis of the singular values obtained from the identified model. At last, the dynamical performance of the UHPC-based governor is presented.

Modal analysis and parameter identification

The Electromechanical Energy Approach gives the model structure for the Two-Area system, where its parameter deviation are obtained through the identification procedure developed in Chapter 4.

As well as for the SMIB system, two noisy signals with variance of $\sigma^2 = 1e^{-6}$ are applied both in the active power \bar{P} and terminal voltage \bar{V} outputs of each generating unit.

Figure 7.8 shows the comparison between the actual data, the nominal model from Chapter 2 and the identified one for generator 1. The fitting percentages are 90.7% and 95.1% for the nominal and identified models, respectively.

Table 7.3 presents the main oscillatory modes of the two cited models in comparison to the actual system after its linearization. As already cited, the modified Two-Area system presents mainly one local (1.1608 Hz, 9.12% damping) and one interarea mode (0.6487 Hz, 1.96% damping), along to a fully damped synchronous mode of 0.0016 Hz. In fact, the actual system is depicted by 51 differential equations, whilst the nominal and identified ones require only 20 states.

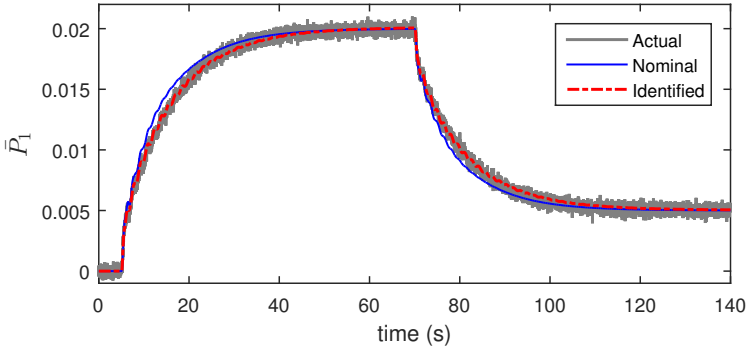


Figure 7.8: Comparison of actual, nominal and identified models (Generator 1) – Two-Area system.

Table 7.3: Modal analysis of the Two-Area system

	Natural frequency (Hz)	Damping ratio (%)	Eigenvalues
Actual system	1.1608	9.12	$-0.67 \pm j7.26$
	0.6487	1.96	$-0.08 \pm j4.08$
	0.0016	100	-0.01
Nominal system	1.1299	9.31	$-0.66 \pm j7.07$
	0.6237	6.48	$-0.25 \pm j3.91$
	0.0016	100	-0.01
Identified system	1.2069	9.36	$-0.71 \pm j7.55$
	0.6488	1.97	$-0.08 \pm j4.08$
	0.0014	100	-0.009

As well as Figure 7.8, the table shows that the identified system represents actual system's mode with a higher accuracy than the nominal one. The identified system is used from now on for the PSS_t and UHPC designs.

PSS_t design

The PSS_t is designed from the modal analysis of the identified model using the PI-based governor, which is shown in Table 7.4.

Table 7.4: Modal analysis of regulated Two-Area system (with PSSSt)

	Natural frequency (Hz)	Damping ratio (%)	Eigenvalues
Nominal governor	1.3089	22.25	$-1.83 \pm j8.02$
	0.6493	0.88	$-0.04 \pm j4.08$
	0.0257	100	-0.16
Governor with PSSSt ($T_f = 1$ s)	1.2991	24.98	$-2.04 \pm j7.90$
	0.6460	1.82	$-0.07 \pm j4.06$
	0.0277	100	-0.17
Governor with PSSSt ($T_f = 10$ s)	1.3034	24.98	$-2.05 \pm j7.93$
	0.6476	1.92	$-0.08 \pm j4.07$
	0.0217	77.5	$-0.10 \pm j0.09$
Governor with PSSSt ($T_f = 100$ s)	1.3038	24.98	$-2.05 \pm j7.93$
	0.6477	1.92	$-0.08 \pm j4.07$
	0.0036	100	-0.02

Notice that for the implemented system the PSSSt has little effect on the damping of both local- and interarea modes (1.3089 Hz and 0.6493 Hz, respectively). In fact, the damping ratio is increased from 0.88% to 1.92% for a long range of T_f .

In spite of representing an increase in damping of nearly twice of the nominal governor, the solution is clearly not sufficient aiming a more reliable operation of the power system, and in practice other solutions should be implemented. However, for the sake of provability of PSSSt's working principle, this result shows that it is possible to add damping to the overall system from the turbine governor through a slight modification on its structure, therefore fulfilling one of thesis' aims.

It is also interesting to observe that the increase of PSSSt's time constant changes the synchronous frequency of the plant. Remark that this frequency is directly responsible for the adequate reference tracking profile, therefore the tuning of T_f must be performed carefully.

An acceptable compromise between a good reference tracking and an increase in system's damping can be obtained for $T_f = 10$ s, which is the value to be used in the remaining of the section.

In the following, the UHPC-based governor is designed in order to effectively damp out the most oscillatory mode of the power grid.

UHPC's design

The first step for the UHPC design is to define its prediction horizon. Since system's settling time is nearly 50 s, N_y is set to 5000 samples*. Remarkable at this point is again UHPC's very long prediction horizon, which reduces the computation effort to a small fraction of GPC's one.

Remembering that $\mathbf{Q} = \mathbf{I}$ and $\mathbf{R} = 0$ gives nearly plant's open-loop response, consider now Figure 7.9 for the analysis on system's singular values with the increase of the control signal weighting matrix \mathbf{R} .

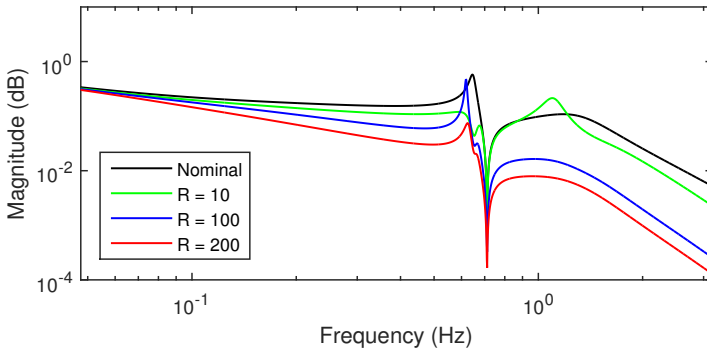


Figure 7.9: Singular values of the closed-loop system with the increase of \mathbf{R} (for $N_y = 5000$ and $T_f = 10$ s) – Two-Area system.

The singular values shows explicitly that UHPC's tuning $\mathbf{R} = 10$ is capable of damping system's interarea mode (0.6493 Hz), however with the decrease in damping of the local-area one (1.3089 Hz). The tuning $\mathbf{R} = 100$ is not a good choice either due to the poor damping ratio for the frequency 0.6177 Hz. Therefore, a fair compromise between reference tracking and damping of system's main modes is the tuning $\mathbf{R} = 200$, which is the configuration to be used in the following of the section.

Dynamic simulation

The evaluation of the just designed UHPC-based governor under the Two-Area system is performed in the following.

*With sampling time of $t_s = 10$ ms.

As well as for the previous simulations, two simulations for the small-signal stability analysis and one for the transient one are performed, being:

- step of 2% in reference voltage \bar{V}_1^r ;
- step of 3% in reference power \bar{P}_1^r .
- short-circuit between busbars 7 and 9 with duration $t_{sc} = 250$ ms.

Step in reference voltage: Figure 7.10 shows the simulation results for generating unit 1 for a 2% step in \bar{V}_1^r for both the PI- and the UHPC-based governors, evaluated with and without the PSS_T.

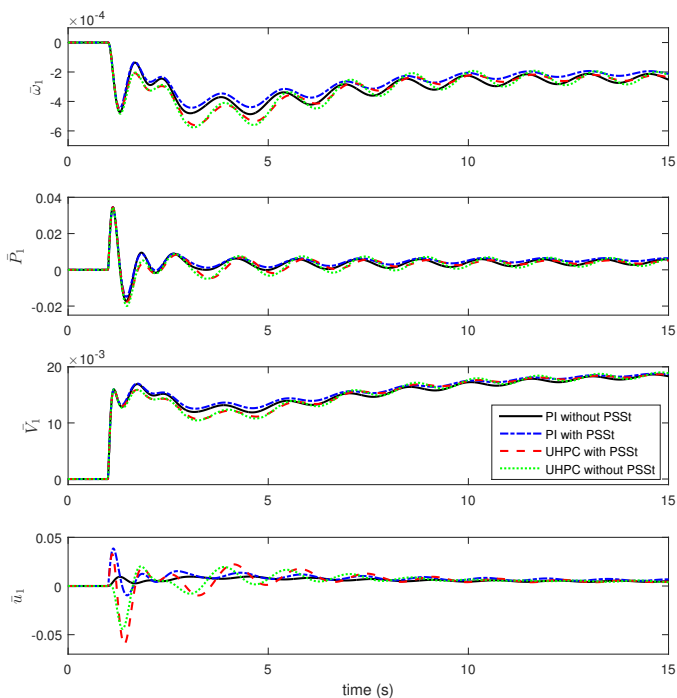


Figure 7.10: Step of 2% in reference voltage \bar{V}_1^r .

As expected, both solutions with PSS_t present less oscillations than the governors without it. In fact, the magnitude of the oscillations for PI- and UHPC-based governors with PSS_t is the same, and both governors damp them out nearly 45% faster than the traditional governor approach.

Step in reference power: The simulation results for generating unit 1 for a 3% step in \bar{P}_1^r are presented in Figure 7.11.

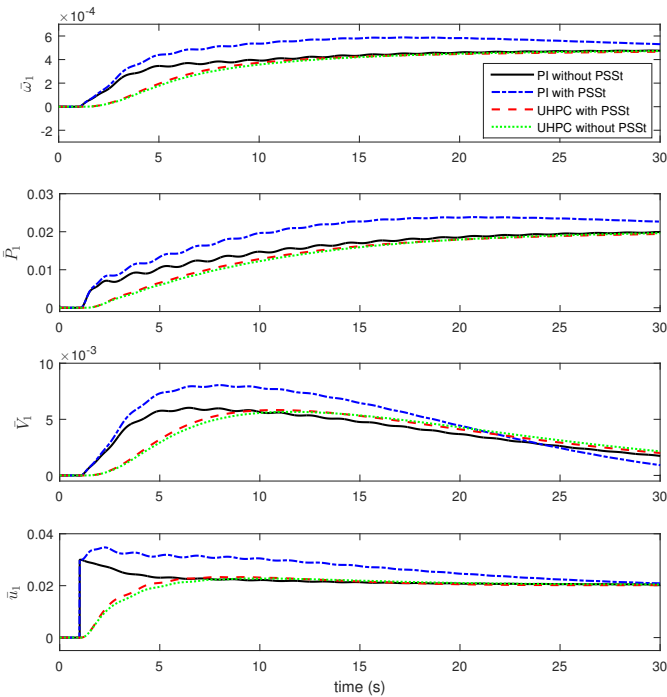


Figure 7.11: Step of 3% in reference power \bar{P}_1^r .

As well as for the SMIB system, notice that the PSS_t harms the reference tracking of the PI-based governor. This result was also expected due to system's modal analysis presented in Table 7.4.

On the other hand, both UHPC-based governors give a non-

oscillatory response with only a slight difference in the settling time (from 18 s to 20 s).

Short-circuit: System's transient behavior is evaluated for generating unit 1 through the enforcement of a short-circuit in half of line's length between busbars 7 and 9 with duration $t_{sc} = 250$ ms, which is shown in Figure 7.12.

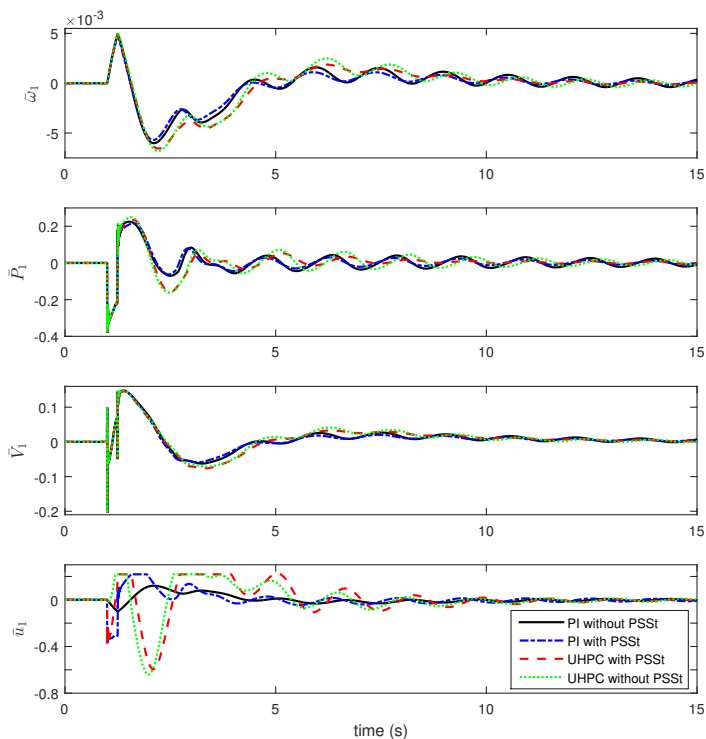


Figure 7.12: Short-circuit between busbars 7 and 9 ($t_{sc} = 250$ ms).

It is possible to observe again that both governor solutions that implement the PSS damp 50% faster system's oscillations.

Notice again the effect of the PSS on the control signals. For these governors, they decrease instantaneously after the outage in order to

avoid the increase in generator's speed, what is a very desired result that is not achieved with the traditional governor approach. Also remarkable is the saturation of the control signal due to the physical limitation of the turbine valve.

Conclusions of the section: The evaluation of the Two-Area system has been presented in this section. The Electromechanical Energy Approach is used for plant's modeling, where the parameter identification procedure is performed in order to reduce the deviation between the model and the actual data. Afterwards the PSS_t time constant T_f is tuned using system's closed-loop modal analysis. UHPC's control signal weighting matrix \mathbf{R} is designed from the observation of system's singular values. Again, the dynamic simulations have shown that the proposed controller structure delivers more stable results for all the three simulated system conditions in comparison to the current solution with and without PSS_t, and also to the UHPC without PSS_t.

This example shows that it is possible to increase further the damping effect on a specific generator from the turbine side, which in fact increases also the overall damping of the entire system, despite the fact that the remaining generators of the grid do not implement any damping device.

8

Conclusions and outlook

8.1 Conclusions

The inherent high complexity of power systems is a natural barrier for the implementation of more sophisticated controller approaches both for excitation systems and turbine governor, such as state feedback and MPC. Model-based control approaches are known to be optimum in the sense of the minimization of a cost function, which in practice usually reflects in a smoother and more effective output profile. These features are very welcome in power systems due to grid's intrinsic oscillatory behavior.

The main issue for this type of designs is grid's modelling. In fact, accurate representations of only one generating unit – with generator, AVR, PSS, prime mover and governor – often leads the order of the models to be greater than fifteen. The expansion to extended power systems increases proportionally model's order and therefore hampers its control through state-space approaches due to the difficulty of dealing with the high-order systems.

This is specially true for MPC implementations, since the length of the matrices that compose its control signal $\mathbf{u}(k)$ increases with system's order z and prediction horizon N_y . For the same one generating unit just cited, regarding a typical prediction horizon of $N_y = 3000^*$ requires the solution of matrices of 45000 in length at each sampling

*With sampling time $t_s = 10$ ms and settling time of 30 s.

period, which is unfeasible in practice.

MPCs are known to be one of the leading controller architectures being implemented nowadays. Wang [82] cites that its intrinsically ability to deal with noise, to perform online process optimization and to work with constraints in a multivariable control framework are very attractive mainly to industries where tight profit margins and limits on the process operation are inevitable present, which is exactly the case for the power system companies.

With this said, it becomes obvious that a MPC approach is desirable aiming at the damping of power system's oscillations. With this information in mind the present thesis was promoted.

The main idea of the work was to develop a novel turbine governor structure that is able to contribute positively to the damping of systems' most problematic oscillatory modes. The justification for the implementation of a governor instead of new excitation system structure lays on the fact that it is known that these oscillations are caused mainly by mechanical interactions of the generators. Therefore a natural choice for the approach is to implement the cited controller at the turbine side, which in fact was already proposed by Machowski *et al.* [4], however has never been implemented in practice.

The proposal here presented is thought to work in parallel to the ongoing PSS solution. In other words, the new governor is implemented as a help on the damping of the modes in which the current approach is not able to damp properly. In fact, this work has started from the principle that, according to Taylor [23], there is a strong suspicion among the power engineers that a considerable amount of the current PSSs are either poorly tuned or even out of service. Further, PSSs' re-tuning is often a very laborious task due to their amount of parameters. Notice that an easy-to-tune approach is also a common advantage of the MPCs, being therefore another good justification for its application.

Thence, aiming at its implementation, the thesis has developed a novel control-based modeling for power system which is based on the Lagrangian Energy Method, named here *Electromechanical Energy Approach* since it converts the system to an electromechanical structure for obtaining its differential equations.

In fact, considering N_g the number of generating units of the power grid, the Electromechanical Energy Approach results in a simplified system of order $3N_g$ for the unregulated case. Additionally, the insertion of simplified versions of prime movers ($2N_g$) and governors (N_g) leads the power grid to be represented by a $5N_g^{\text{th}}$ -order linear system. In comparison to most of the commercial softwares it represents a re-

duction of nearly 70% in system's size.

It is shown that the Electromechanical Energy Approach is able to represent relatively well the main oscillatory modes of power systems for all possible cases: unregulated, with only AVR, with AVR and governor, and with AVR, governor and PSS. In contrast to the Steady-State Approach, the method has the intrinsic ability of fitting also the low frequencies of the system due to its tuning of the damping parameters.

However, a drawback of the presented method is the difficulty in estimating the model's damping coefficients since they do not have real meanings. Therefore a parameter identification methodology was also developed. This procedure accounts for system's uncertainties, namely parametric mismatches and noise.

The parametric identification is fully based on the EKF algorithm for ensuring both state and parameter convergence. The procedure has shown that the identified model is able to depict system's power outputs both for the noiseless and noisy cases in a more accurate fashion than the nominal one.

Afterwards the identified model, which has its structure fully based on the model obtained from the Electromechanical Energy Approach, is used for the tuning of the so-called PSS_t. This device is also one of the main contributions of the thesis, since it represents a slight modification in governor's architecture which enables the current governor to react properly against the system's oscillations that are not well damped through the common exciter-based PSS.

It has been shown that the PSS_t is nothing but a high pass filter which acts as the derivative part of an Output Feedback controller. What the PSS_t in fact does is to add a signal that opposes system's oscillations at governor's output \bar{u} . Its main advantage to the exciter-based PSS relies on the fact that the PSS_t has only one tuning parameter (T_f), which represents its time constant.

Computer simulations have shown that the PSS_t is able to damp very well the main oscillatory mode of the 2M/1L system. Conversely, it was also shown that PSS_t's time constant T_f shall be properly tuned otherwise this device might excite other modes of the system.

It was demonstrated that this is in fact true for the SMIB system and hence, despite being a simple solution, the PSS_t implementation alone in the current governor architecture does not ensure the improvement of system's stability margins for all power system configurations, being this the main reason for the pursue of a more suitable control architecture, such as a MPC, for solving the posed problem.

The development of the *Unrestricted Horizon Predictive Controller*, short UHPC, has started considering that it should be able to cope at the same time with high-order state-space systems and long prediction horizons without overloading controller's memory. Likewise, a stochastic effect is also welcome due to the known measurement noise level presented in power systems.

It is exposed that the UHPC achieves these features through the usage of a cost function that regards solely one point in the future (N_y), instead of all the trajectory from the current sample k until N_y , which is often implemented by the most common MPCs.

As an important side effect of UHPC's equating, the so-called *N_y -steps ahead Kalman Predictor* is also developed. This predictor is in fact responsible for UHPC's long prediction horizons. Further, it has been shown that the UHPC solves inherently the two Diophantine Equations that arise in the polynomial development of the GPC, which results are given directly by matrices \mathbf{F} and \mathbf{H} .

Making use of the 2M/1L benchmark system, the study has shown that a prediction horizon N_y of nearly system's settling time is enough for restoring plant's free response if $\mathbf{R} = \mathbf{0}$ and $\mathbf{Q} = \mathbf{I}$, which makes natural the further tuning of the UHPC since this is a known design starting point.

UHPC's ability in dealing with noise and inherent oscillations in power systems is also highlighted. The study has shown that the UHPC uses much less energy to achieve very similar output and control signal profiles as the actual governor does. This feature is inherited from the Kalman Filter synthesis.

Lastly, it is also shown that the UHPC with PSS_t and compensation for the speed deviation, called here UHPC-based governor, is able to provide the main result that this thesis pursues: the intrinsic damping of system modes through the tuning of the governor gains.

What is eventually achieved is that the UHPC enables an ease and light computing implementation of a Model-based Predictive Controller in extended power systems, what has been an issue within the field due to systems' high order and, as a consequence, very large control signal matrices. For the UHPC, the length of these matrices are limited by the order of the system, what reduces dramatically controller's computational cost.

Finally, three benchmark systems are simulated throughout the thesis in order to evaluate the proposed turbine governor solution. For all systems it is proved the ability of the proposed UHPC-based governor to damp systems' main oscillatory modes.

8.2 Outlook

Some aspects of the present thesis might be deeply investigated in future works. This section splits them into topics concerning the previous chapters.

Electromechanical Energy Approach

Further contributions on the Electromechanical Energy Approach might focus on the representation of node's voltage in the modeling. This assumption would allow the design of a fully state feedback controller for each machine, *i.e.*, a controller that regards inherently both the turbine governor and the excitation system.

The idea would be to damp out system's most problematic oscillatory modes in a more efficient fashion making use of less tuning parameters.

Uncertainties and parameter identification in Power Systems

System's identification might be improved if one regards the so-called *regularization*, which means in practice that weights are posed in each parameter to be identified. The higher the weight, the more confidence the designer has on a certain parameter.

This feature would help on a faster convergence of the parameters, helping on the identification of large power systems.

Power System Stabilizer at the turbine side – PSS_t

Extensive research on the PSS_t might be easily performed. For example, it is possible to investigate an extension on its structure – like in an exciter-based PSS – for the improvement of PSS_t's performance in low frequencies.

Further, aiming at a reduction in governor's control signal variance, a stochastic PSS_t may be also designed based on the Generalized Minimum Variance Controller (GMVC), such as the one developed in [57].

Unrestricted Horizon Predictive Controller – UHPC

At last, an interesting improvement on the UHPC-based governor would be the consideration of the PSS_t and the compensation for the speed deviation inside its cost function.

This modification would ensure the governor to be optimum in a mathematical viewpoint. Further, it would also ensure an even smaller control signal variance.

Bibliography

- [1] C. W. Taylor, *Power system voltage stability*. McGraw-Hill, 1994.
- [2] P. Kundur, N. J. Balu, and M. G. Lauby, *Power system stability and control*. McGraw-Hill New York, 1994, vol. 7.
- [3] P. M. Anderson and A. A. Fouad, *Power system control and stability*. John Wiley & Sons, 2008.
- [4] J. Machowski, J. Bialek, and J. Bumby, *Power system dynamics: Stability and control*. John Wiley & Sons, 2011.
- [5] “Review of on-line dynamic security assessment tools and techniques”, CIGRÉ, Tech. Rep., 2007.
- [6] G. Rogers, *Power system oscillations*. Springer Science & Business Media, 2012.
- [7] “Analysis of the CE inter-area oscillations of 19 and 24 February 2011”, ENTSO-E - European Network of Transmission System Operators for Electricity, Tech. Rep., 2011.
- [8] I. Kamwa, R. Grondin, and G. Trudel, “IEEE PSS2B versus PSS4B: The limits of performance of modern power system stabilizers”, *IEEE Transactions on Power Systems*, vol. 20, no. 2, pp. 903–915, 2005.
- [9] P. Kundur, M. Klein, G. Rogers, and M. Zywno, “Application of power system stabilizers for enhancement of overall system stability”, *Power Systems, IEEE Transactions on*, vol. 4, no. 2, pp. 614–626, May 1989, ISSN: 0885-8950.
- [10] M. Klein, G. Rogers, P. Kundur, *et al.*, “A fundamental study of inter-area oscillations in power systems”, *IEEE Transactions on Power Systems*, vol. 6, no. 3, pp. 914–921, 1991.
- [11] J. J. Grainger and W. D. Stevenson, *Power system analysis*. McGraw-Hill New York, 1994, vol. 621.
- [12] B. Cova, “Progress of the Mediterranean Ring and the Interconnection with Europe”, in *Power Engineering Society General Meeting, 2004. IEEE*, IEEE, 2004, pp. 1229–1234.

- [13] E. Grebe, J. Kabouris, S. L. Barba, W. Sattinger, and W. Winter, “Low frequency oscillations in the interconnected system of continental Europe”, in *IEEE PES General Meeting*, IEEE, 2010, pp. 1–7.
- [14] O. Tor, C. Gencoglu, O. Yilmaz, E. Cebeci, and A. Guven, “Damping measures against prospective oscillations between Turkish grid and ENTSO-E System”, in *Power System Technology (POWERCON), 2010 International Conference on*, IEEE, 2010, pp. 1–7.
- [15] I. Colak, G. Fulli, S. Vitiello, I. Tekin, R. Bayindir, and K. Demirtas, “Developments of Turkish grid system infrastructure for integration with Europe”, in *Power Engineering, Energy and Electrical Drives (POWERENG), 2013 Fourth International Conference on*, IEEE, 2013, pp. 1765–1770.
- [16] C. Gama, “Brazilian North-South Interconnection control application and operating experience with a TCSC”, in *Power Engineering Society Summer Meeting, 1999. IEEE*, IEEE, vol. 2, 1999, pp. 1103–1108.
- [17] M. Xiao-Ming, Z. Yao, G. Lin, and W. Xiao-Chen, “Coordinated control of interarea oscillation in the China Southern power grid”, *IEEE Transactions on Power Systems*, vol. 21, no. 2, pp. 845–852, 2006.
- [18] N. Mithulanathan, C. A. Canizares, J. Reeve, and G. J. Rogers, “Comparison of PSS, SVC, and STATCOM controllers for damping power system oscillations”, *Power Systems, IEEE Transactions on*, vol. 18, no. 2, pp. 786–792, 2003.
- [19] B. Lei, S. Fei, and J. Zhai, “Coordinated control of static synchronous compensator and automatic voltage regulator in multi-machine power systems using pseudo-generalized Hamiltonian theory”, *Proceedings of the Institution of Mechanical Engineers, Part I: Journal of Systems and Control Engineering*, 2013.
- [20] J. Dai and A. Ghandakly, “A decentralized adaptive control algorithm and the application in power system stabilizer (PSS) design”, in *Industry Applications Conference, 1995. Thirtieth IAS Annual Meeting, IAS '95., Conference Record of the 1995 IEEE*, vol. 2, Oct. 1995, 1641–1648 vol.2.
- [21] R. Kutzner, “A robust H_∞ PSS with enlarged damping range”, in *Power Engineering Society Summer Meeting, 1999. IEEE*, IEEE, vol. 1, 1999, pp. 53–57.

- [22] A. A. Ba-Muquabel and M. A. Abido, "Review of conventional PSS design methods", in *GCC Conference IEEE*, 2006.
- [23] C. W. Taylor, "Improving the grid behavior", *IEEE Spectrum*, vol. 36, no. 6, 1999.
- [24] S. Abe and A. Doi, "A new power system stabilizer synthesis in multimachine power systems", *IEEE transactions on power apparatus and systems*, vol. 12, no. PAS-102, pp. 3910–3918, 1983.
- [25] M. Dobrescu and I. Kamwa, "A new fuzzy logic power system stabilizer performances", in *Power Systems Conference and Exposition, 2004. IEEE PES*, IEEE, 2004, pp. 1056–1061.
- [26] E. Daryabeigi, M. Moazzami, A. Khodabakhshian, and M. Mazidi, "A new power system stabilizer design by using Smart Bacteria Foraging Algorithm", in *Electrical and Computer Engineering (CCECE), 2011 24th Canadian Conference on*, IEEE, 2011, pp. 000 713–000 716.
- [27] C. Abdelghani, C. Lakhdar, A. Salem, B. M. Djameledine, and M. Lakhdar, "Robust design of fractional order PID Sliding Mode based Power System Stabilizer in a power system via a new meta-heuristic Bat algorithm", in *Recent Advances in Sliding Modes (RASM), 2015 International Workshop on*, IEEE, 2015, pp. 1–5.
- [28] H. Wang, Y. Hao, B. Hogg, and Y. Yang, "Stabilization of power systems by governor-turbine control", *International Journal of Electrical Power & Energy Systems*, vol. 15, no. 6, pp. 351–361, 1993.
- [29] J. Milanovic, "Damping of the low-frequency oscillations of the generator: Dynamic interactions and the effectiveness of the controllers", *IEE Proceedings-Generation, Transmission and Distribution*, vol. 149, no. 6, pp. 753–760, 2002.
- [30] K. Ogata, *Engenharia de Controle Moderno*. Prentice-Hall Brasil, 2003, ISBN: 9788587918239.
- [31] B. Marinescu and D. Petesch, "Three-level coordination in power system stabilization", *Electric Power Systems Research*, vol. 111, pp. 40–51, 2014.
- [32] N. Kishor, R. Saini, and S. Singh, "LQG/LTR controller for speed governing of hydro-turbine", in *Electrotechnical Conference, 2004. MELECON 2004. Proceedings of the 12th IEEE Mediterranean*, IEEE, vol. 3, 2004, pp. 1125–1128.

- [33] I. Eker, “Governors for hydro-turbine speed control in power generation: A SIMO robust design approach”, *Energy Conversion and Management*, vol. 45, no. 13, pp. 2207–2221, 2004.
- [34] K. J. Åström, *Introduction to Stochastic Control Theory*, ser. Dover Books on Electrical Engineering Series. Dover Publications, 1970, ISBN: 9780486445311.
- [35] A. Silveira, R. Trentini, A. Coelho, R. Kutzner, and L. Hofmann, “Generalized minimum variance control under long-range prediction horizon setups”, *ISA Transactions*, vol. 62, pp. 325–332, 2016.
- [36] E. Camacho and C. Bordons, *Model predictive control*, ser. Advanced Textbooks in Control and Signal Processing Series. Springer London, Limited, 2004, ISBN: 9781852336943.
- [37] M. Zima and G. Andersson, “Model predictive control employing trajectory sensitivities for power systems applications”, in *Proceedings of the 44th IEEE Conference on Decision and Control*, IEEE, 2005, pp. 4452–4456.
- [38] G. A. M. Muoz-Hernandez and D. Jones, “MIMO generalized predictive control for a hydroelectric power station”, *IEEE Transactions on Energy Conversion*, vol. 21, no. 4, pp. 921–929, 2006.
- [39] T. H. Mohamed, J. Morel, H. Bevrani, and T. Hiyama, “Model predictive based load frequency control_design concerning wind turbines”, *International Journal of Electrical Power & Energy Systems*, vol. 43, no. 1, pp. 859–867, 2012.
- [40] H. Bevrani, *Robust Power System Frequency Control*, ser. Power Electronics and Power Systems. Springer International Publishing, 2014, ISBN: 9783319072784.
- [41] D. Powerfactory, “PowerFactory User’s Manual”, *DIgSILENT*, vol. 14, 2011.
- [42] B. Busarello, “Cott+Partner AG”, *NEPLAN User’s Guide*, vol. 5, p. 2012, 2005.
- [43] U. G. SimPowerSystems, “Version 4”, *The MathWorks Inc*, 2006.
- [44] H. Ping, L. Jibin, W. Yunbing, W. Xiaoning, D. Xiaoyong, and Z. Yong, “Analysis of Special Mode Order Reduction of Large Power System”, in *Intelligent System Design and Engineering Application (ISDEA), 2010 International Conference on*, vol. 1, Oct. 2010, pp. 290–294.

- [45] S. Ghosh and N. Senroy, “A comparative study of two model order reduction approaches for application in power systems”, in *Power and Energy Society General Meeting, 2012 IEEE*, Jul. 2012, pp. 1–8.
- [46] P. Li, B. Zhang, J. Shu, Z. Bo, and A. Klimek, “Research on order reduction of power system modeling for dynamic voltage stability analysis”, in *Transmission and Distribution Conference and Exposition, 2010 IEEE PES*, Apr. 2010, pp. 1–5.
- [47] B. R. Oswald, *Berechnung von Drehstromnetzen: Berechnung stationärer und nicht stationärer Vorgänge mit Symmetrischen Komponenten und Raumzeigern*. Springer Vieweg, 2012.
- [48] C. D. Vournas and J. C. Mantzaris, “Quasi-Steady-State modeling of interarea oscillations”, in *PowerTech, 2009 IEEE Bucharest*, IEEE, 2009, pp. 1–7.
- [49] D. Rimorov, I. Kamwa, and G. Joós, “Quasi-Steady-State Approach for Analysis of Frequency Oscillations and Damping Controller Design”, *IEEE Transactions on Power Systems*, vol. 31, no. 4, pp. 3212–3220, Jul. 2016.
- [50] M.-E. Grenier, D. Lefebvre, and T. Van Cutsem, “Quasi steady-state models for long-term voltage and frequency dynamics simulation”, in *Power Tech, 2005 IEEE Russia*, IEEE, 2005, pp. 1–8.
- [51] A. Wenzel, “Beitrag zur lokalen Schwingungsdämpfung in ausgedehnten Hochspannungsnetzen”, PhD thesis, TU Braunschweig, 2009.
- [52] D. Nelles, *Netzdyamik*. VDE-Verlag, 2009.
- [53] R. Trentini, R. Kutzner, L. Hofmann, A. Campos, and C. F. Neto, “Modeling, parameter estimation and state-space control of a steam turbine”, in *Proceedings of the 23rd ABCM International Congress on Mechanical Engineering*, Rio de Janeiro, Dec. 2015.
- [54] R. Trentini, R. Kutzner, and L. Hofmann, “State-space generalized minimum variance controller based PSS for damping of interarea modes”, in *Proceedings of the 18th IEEE Mediterranean Electrotechnical Conference (MELECON 2016)*, Limassol, Apr. 2016.

- [55] R. Trentini, R. Kutzner, and L. Hofmann, “Power grid modeling based on the Electromechanical Energy Approach aiming power systems stability studies”, in *Proceedings of the 24th IEEE Mediterranean Conference on Control and Automation (MED’16)*, Athens, Jun. 2016.
- [56] R. Trentini, A. Silveira, R. Kutzner, and L. Hofmann, “On the Unrestricted Horizon Predictive Control – a fully stochastic model-based predictive approach”, in *Proceedings of the European Control Conference (ECC’16)*, Aalborg, Jun. 2016.
- [57] R. Trentini, A. Silveira, M. Bartsch, R. Kutzner, and L. Hofmann, “On the design of stochastic RST controllers based on the Generalized Minimum Variance”, in *Proceedings of the 11th UKACC International Conference on Control*, Belfast, Aug. 2016.
- [58] R. Trentini, R. Kutzner, and L. Hofmann, “Stochastic speed governor based on the Generalized Minimum Variance Controller”, in *Tagungsband der 43. Kraftwerkstechnisches Kolloquium*, Dresden, Oct. 2016.
- [59] R. Kutzner, “Integrierte Regelung eines Gasturbosatzes unter Berücksichtigung von Nichtlinearitäten und veränderlichen Netzparametern”, PhD thesis, Technische Universität Braunschweig, 1997.
- [60] VDI/VDE, *Guidelines for testing control systems of steam turbines - Dynamic behavior of speed and load control - Sheet 4 VDI/VDE 3521*, 2000.
- [61] W. Leonhard, *Regelung in der elektrischen Energieversorgung: Eine Einführung*. Teubner, 1980.
- [62] R. Hermans, M. Lazar, and A. Jokić, “Distributed predictive control of the 7-machine CIGRÉ power system”, in *Proceedings of the 2011 American Control Conference*, IEEE, 2011, pp. 5225–5230.
- [63] B. D. O. Anderson and J. B. Moore, *Optimal control: Linear quadratic methods*. Prentice-Hall, Inc., 1990.
- [64] P. R. Kumar and P. Varaiya, *Stochastic systems: Estimation, identification, and adaptive control*. P, 1986, vol. 986.
- [65] F. G. Nogueira, J. A. Barreiros, W. Barra, C. T. Costa, and A. M. Ferreira, “Development and field tests of a damping controller to mitigate electromechanical oscillations on large diesel generating units”, *Electric Power Systems Research*, vol. 81, no. 2, pp. 725–732, 2011.

- [66] L. Ljung, *System Identification Toolbox 7 - User's Guide*, MathWorks, 2011.
- [67] L. A. Aguirre, *Introdução à identificação de sistemas: Técnicas lineares e não-lineares aplicadas a sistemas reais*. E, 2007.
- [68] J. Corriou, *Process Control: Theory and Applications*. Springer London, 2013, ISBN: 9781447138488.
- [69] W. Levine, *The Control Handbook*, ser. Electrical Engineering Handbook. Taylor & Francis, 1996, ISBN: 9780849385704.
- [70] M. Green and D. Limebeer, *Linear Robust Control*, ser. Dover Books on Electrical Engineering. Dover Publications, Incorporated, 2012, ISBN: 9780486488363.
- [71] J. Richalet and D. O'Donovan, *Predictive functional control: Principles and industrial applications*. Springer Science & Business Media, 2009.
- [72] J. A. Rossiter, *Model-based predictive control: A practical approach*. CRC press, 2003.
- [73] N. S. Raibman, *Identification and system parameter estimation: Proceedings of the 4th IFAC Symposium, Tbilisi, USSR, 21-27 September 1976*. North-Holland Pub. Co., 1978, vol. 3.
- [74] D. W. Clarke and P. J. Gawthrop, "Self-tuning controller", *Proceedings of the Institution of Electrical Engineers*, vol. 22, pp. 929–934, 1975.
- [75] D. Clarke, C. Mohtadi, and P. Tuffs, "Generalized predictive controller - Part I: The basic algorithm", *Automatica*, vol. 23, no. 2, pp. 137–148, 1987, ISSN: 0005-1098.
- [76] E. F. Camacho and C. Bordons, *Model predictive control in the process industry*. Springer Science & Business Media, 2012.
- [77] D. W. Clarke and C. Mohtadi, "Properties of generalized predictive control", *Automatica*, vol. 25, no. 6, pp. 859–875, 1989.
- [78] E. Ikonen and K. Najim, *Advanced process identification and control*. CRC Press, 2001.
- [79] A. Silveira and A. Coelho, "Generalised minimum variance control state-space design", *Control Theory Applications, IET*, vol. 5, no. 15, pp. 1709–1715, Oct. 2011, ISSN: 1751-8644.
- [80] K. Ogata, *Discrete-time control systems*. P, 1995, vol. 2.

- [81] K. J. Åström and B. Wittenmark, *Computer-Controlled Systems: Theory and Design*, ser. Dover Books on Electrical Engineering Series. Dover Publications, 1996, ISBN: 9780486486130.
- [82] L. Wang, *Model predictive control system design and implementation using MATLAB®*. Springer Science & Business Media, 2009.
- [83] L. Ljung, *System identification: Theory for the user*, ser. Prentice-Hall information and system sciences series. Prentice-Hall, 1987, ISBN: 9780138816407.
- [84] R. R. Bitmead, M. Gevers, and V. Wertz, *Adaptive optimal control: The thinking man's GPC*. Elsevier, 1990.



Matrices of the regulated system

Chapter 3 shows the development of power system's reduced model. The matrices of the regulated system (Equations 3.11) are given by,

$$\mathbf{A}_n = \begin{bmatrix} \mathbf{A}_{11} & \mathbf{A}_{12} \\ \mathbf{A}_{21} & \mathbf{A}_{22} \end{bmatrix},$$

$$\mathbf{B}_n = \begin{bmatrix} \mathbf{B}_1 & \mathbf{B}_2 \end{bmatrix}^T,$$

$$\mathbf{C}_n = \begin{bmatrix} \mathbf{C}_1 & \mathbf{0} \end{bmatrix},$$

$$\mathbf{D}_n = \begin{bmatrix} \mathbf{0} & \mathbf{D}_1 \end{bmatrix},$$

with,

$$\mathbf{A}_{11} = \begin{bmatrix} \mathbf{0} & \omega_0 \mathbf{I} \\ -\mathcal{H}_G^{-1} (\Phi_{\lambda 1} + \Theta_{\lambda}) & -\mathcal{H}_G^{-1} \Upsilon_{\omega} \end{bmatrix}$$

$$\mathbf{A}_{12} = \begin{bmatrix} \mathbf{0} & \mathbf{0} & \mathbf{0} \\ \mathcal{H}_G^{-1} \Theta_{\vartheta 1} & \mathcal{H}_G^{-1} \Theta_{\vartheta 2} & \mathcal{H}_G^{-1} \Theta_{\varepsilon p} \end{bmatrix}$$

$$\mathbf{A}_{21} = \begin{bmatrix} \mathbf{0} & \mathbf{0} \\ -K_p^p \Phi_{\lambda 1} & -\Omega_{\omega} \\ -\Phi_{\lambda 1} & -(\beta^{-1} + \Phi_{\omega 1} + \Phi_{\omega 11}) \end{bmatrix}$$

$$\mathbf{A}_{22} = \begin{bmatrix} \mathbf{0} & \mathbf{I} & \mathbf{0} \\ -\kappa_2 & -\kappa_1 & (\mathbf{T}_n^p)^{-1} \mathbf{K}_p^p \\ \mathbf{0} & \mathbf{0} & \mathbf{0} \end{bmatrix}$$

$$\mathbf{B}_1 = \begin{bmatrix} \mathbf{0} & \mathbf{0} & \mathbf{0} \\ \mathcal{H}_G^{-1} \Theta_{Pr} & \mathcal{H}_G^{-1} \Theta_{\omega^r} & \mathcal{H}_G^{-1} (\Phi_{P^{\dagger 1}} - \Theta_{P^{\dagger 1}}) \end{bmatrix}$$

$$\mathbf{B}_2 = \begin{bmatrix} \mathbf{0} & \mathbf{0} & \mathbf{0} \\ \Omega_{Pr} & \Omega_{\omega^r} & -\mathbf{K}_p^p \Phi_{P^{\dagger 1}} \\ \mathbf{I} & \beta^{-1} & -\Phi_{P^{\dagger 1}} \end{bmatrix}$$

$$\mathbf{C}_1 = \begin{bmatrix} \Phi_{\lambda 1} & \Phi_{\omega 1} + \Phi_{\omega 11} \\ \mathbf{0} & \mathbf{I} \end{bmatrix}$$

$$\mathbf{D}_1 = \begin{bmatrix} \Phi_{P^{\dagger 1}} \\ \mathbf{0} \end{bmatrix}$$

and,

$$\begin{aligned} \Theta_\lambda &= \kappa_3 \mathbf{K}_p^p \Phi_{\lambda 1}, & \Theta_\omega &= (\Phi_{\omega 1} + \Phi_{\omega 11}) (\mathbf{I} + \kappa_3 \mathbf{K}_p^p), \\ \Theta_{\vartheta_1} &= \kappa_5 - \kappa_2 \kappa_3, & \Theta_{\vartheta_2} &= \kappa_4 - \kappa_1 \kappa_3, & \Theta_{\varepsilon^p} &= \kappa_3 (\mathbf{T}_n^p)^{-1} \mathbf{K}_p^p, \\ \Theta_{Pr} &= \kappa_3 (\gamma + \mathbf{K}_p^p), & \Theta_{\omega^r} &= \kappa_3 (\beta^{-1} \mathbf{K}_p^p + \mathbf{K}_p^\omega), \\ \Theta_{P^{\dagger 1}} &= \kappa_3 \mathbf{K}_p^p \Phi_{P^{\dagger 1}}, & \Omega_\omega &= \mathbf{K}_p^p (\beta^{-1} + \Phi_{\omega 1} + \Phi_{\omega 11}) + \mathbf{K}_p^\omega, \\ \Omega_{\omega^r} &= \beta^{-1} \mathbf{K}_p^p + \mathbf{K}_p^\omega, & \Omega_{Pr} &= \gamma + \mathbf{K}_p^p, & \Upsilon_\omega &= \Theta_\omega + \Theta_{\omega^r}. \end{aligned}$$

The gains and time constants for the governors and prime movers are given by,

$$\begin{aligned} \mathbf{K}_p^i &= \text{diag}(K_{p_1}^i \quad \cdots \quad K_{p_{N_g}}^i), \quad i = p, \omega, \\ \mathbf{T}_n^p &= \text{diag}(T_{n_1}^p \quad \cdots \quad T_{n_{N_g}}^p), \\ \kappa_i &= \text{diag}(\kappa_{i_1} \quad \cdots \quad \kappa_{i_{N_g}}), \quad i = 1, \dots, 5, \\ \beta &= \text{diag}(\beta_1 \quad \cdots \quad \beta_{N_g}), \\ \gamma &= \text{diag}(\gamma_1 \quad \cdots \quad \gamma_{N_g}), \end{aligned}$$

with N_g being the number of generating units of the system.

B

Simulation data

2M/1L system

General

$$f = 60 \text{ Hz}$$

Transformers

$$S_T = 700 \text{ MVA} \quad V_T = 20/230 \text{ kV} \quad \bar{X}_T = 0.15$$

Transmission lines

$$X = 0.5 \text{ } \Omega/\text{km} \quad \ell_{43} = \ell_{53} = 52.9 \text{ km}$$

Generators (round rotor)

$$\begin{array}{llll} S_G = 700 \text{ MVA} & \bar{V}_1 = 1.01 & \bar{V}_2 = 1.02 & \lambda_1 = 6.67^\circ \\ \lambda_2 = 0^\circ & \bar{P}_1 = 0.71 & \bar{P}_2 = 0.5 & \bar{X}_d = 1.75 \\ \bar{X}'_d = 0.3 & \bar{X}''_d = 0.25 & \bar{X}'_q = 1.75 & \bar{X}'_q = 0.3 \\ \bar{X}''_q = 0.25 & \bar{X}_l = 0.2 & \tau'_{d0} = 8 \text{ s} & \tau''_{d0} = 0.03 \text{ s} \\ \tau'_{q0} = 0.4 \text{ s} & \tau''_{q0} = 0.05 \text{ s} & H = 6.5 \text{ s} & \end{array}$$

Voltage regulators

$$K_p^e = 100 \quad T_n^e = \infty \quad \tau_{\text{ex}} = 0.01 \text{ s} \quad \text{lim}_{\text{pss}} = \pm 5$$

Power System Stabilizers - PSS2B

$$\tau_{\text{tf}} = 0.01 \text{ s} \quad \tau_w = 10 \text{ s} \quad \tau_1 = \tau_3 = 0.1 \text{ s} \quad \tau_2 = \tau_4 = 0.05 \text{ s}$$

$$K_{\text{pss}} = 10 \quad \text{lim}_{\text{ex}} = \pm 0.15$$

Prime movers - hydro turbine

$$\tau_{\text{valve}} = 0.1 \text{ s} \quad \tau_{wt} = 4 \text{ s} \quad q_0 = 1 \quad h_0 = 1 \quad A_t = 1$$

Governors

$$\gamma = 0.8 \quad \beta = 0.04 \quad K_p^\omega = 1 \quad K_p^p = 0.1 \quad T_n^p = 10 \text{ s}$$

Load - static

$$P_3 = 850 \text{ MW}$$

SMIB system**General**

$$f = 50 \text{ Hz} \quad \bar{V}_0 = 1 \quad \lambda_0 = 0^\circ$$

Transformer

$$S_T = 1000 \text{ MVA} \quad V_T = 24/230 \text{ kV} \quad \bar{X}_T = 0.2$$

Transmission line

$$X_{20} = 0.5 \text{ } \Omega/\text{km} \quad \ell = 52.9 \text{ km}$$

Generator (round rotor)

$$\begin{array}{llll}
S_G = 1000 \text{ MVA} & \bar{V}_1 = 1 & \lambda_1 = 29.25^\circ & \bar{X}_l = 0.16 \\
\bar{P}_1 = 0.7 & \bar{X}_d = 1.81 & \bar{X}'_d = 0.3 & \bar{X}''_d = 0.25 \\
\bar{X}_q = 1.76 & \bar{X}'_q = 0.55 & \bar{X}''_q = 0.25 & \tau'_{d0} = 8 \text{ s} \\
\tau''_{d0} = 0.03 \text{ s} & \tau_{q0} = 0.4 \text{ s} & \tau'_{q0} = 0.05 \text{ s} & H = 10 \text{ s}
\end{array}$$

Voltage regulator

$$K_p^e = 250 \quad T_n^e = \infty \quad \tau_{\text{ex}} = 0.01 \text{ s} \quad \lim_{\text{ex}} = \pm 5$$

Power System Stabilizers - PSS2B

$$\begin{array}{llll}
\tau_{\text{tf}} = 0.01 \text{ s} & \tau_w = 3 \text{ s} & \tau_1 = \tau_3 = 0.5 \text{ s} & \tau_2 = \tau_4 = 0.05 \text{ s} \\
K_{\text{pss}} = 20 & \lim_{\text{ex}} = \pm 0.15 & &
\end{array}$$

Prime mover - steam turbine

$$\begin{array}{llll}
\tau_{\text{valve}} = 0.01 \text{ s} & \tau_{\text{ch}} = 0.1 \text{ s} & \tau_{\text{re}} = 4 \text{ s} & \tau_{\text{cr}} = 0.3 \text{ s} \\
F_{\text{hp}} = 0.3 & F_{\text{ip}} = 0.4 & F_{\text{lp}} = 0.3 &
\end{array}$$

Governor

$$\gamma = 0.8 \quad \beta = \infty \quad K_p^\omega = 0 \quad K_p^p = 0.1 \quad T_n^p = 4 \text{ s}$$

Two-Area system**General**

$$f = 60 \text{ Hz}$$

Transformers

$$S_T = 900 \text{ MVA} \quad V_T = 20/230 \text{ kV} \quad \bar{X}_T = 0.15$$

Transmission lines

$$\begin{array}{lll}
X = 0.5 \ \Omega/\text{km} & R = 0.05 \ \Omega/\text{km} & B = 3.3 \ \mu\text{S}/\text{km} \\
\ell_{56} = \ell_{1011} = 25 \text{ km} & \ell_{67} = \ell_{910} = 10 \text{ km} & \ell_{79} = 220 \text{ km}
\end{array}$$

Generators (round rotor)

$$\begin{array}{llll}
S_G = 900 \text{ MVA} & \bar{V}_{1-4} = 1 & \lambda_1 = 10.22^\circ & \lambda_2 = 0^\circ \\
\lambda_3 = -15.88^\circ & \lambda_4 = -26.53^\circ & \bar{P}_{1,2,4} = 0.778 & \bar{P}_3 = 0.799 \\
\bar{X}_d = 1.8 & \bar{X}'_d = 0.3 & \bar{X}''_d = 0.25 & \bar{X}_q = 1.7 \\
\bar{X}'_q = 0.55 & \bar{X}''_q = 0.25 & \bar{X}_l = 0.2 & \tau'_{d0} = 8 \text{ s} \\
\tau_{d0} = 0.03 \text{ s} & \tau_{q0} = 0.4 \text{ s} & \tau''_{q0} = 0.05 \text{ s} & \bar{R}_s = 0.0025 \\
H = 6.175 \text{ s} & & &
\end{array}$$

Voltage regulators

$$K_p^e = 200 \quad T_n^e = \infty \quad \tau_{\text{ex}} = 0.02 \text{ s} \quad \text{lim}_{\text{ex}} = \pm 6.5$$

Power System Stabilizers - PSS1A

$$\begin{array}{llll}
\tau_{\text{tf}} = 0.015 \text{ s} & \tau_w = 10 \text{ s} & \tau_1 = 0.05 \text{ s} & \tau_2 = 0.02 \text{ s} \\
\tau_3 = 3 \text{ s} & \tau_4 = 5.4 \text{ s} & K_{\text{pss}} = 30 & \text{lim}_{\text{ex}} = \pm 0.15
\end{array}$$

Prime movers - steam turbine

$$\begin{array}{llll}
\tau_{\text{valve}} = 0.01 \text{ s} & \tau_{\text{ch}} = 0.5 \text{ s} & \tau_{\text{re}} = 10 \text{ s} & \tau_{\text{cr}} = 3.3 \text{ s} \\
F_{\text{hp}} = 0.28 & F_{\text{ip}} = 0.36 & F_{\text{ip}} = 0.36 &
\end{array}$$

Governors

$$\gamma = 1 \quad \beta = \infty \quad K_p^\omega = 20 \quad K_p^p = 0 \quad T_n^p = \infty$$

Loads - static

$$\begin{array}{lll}
L_7: & P = 967 \text{ MW} & Q_L = 100 \text{ MVAr} \quad Q_C = 387 \text{ MVAr} \\
L_9: & P = 1767 \text{ MW} & Q_L = 100 \text{ MVAr} \quad Q_C = 537 \text{ MVAr}
\end{array}$$

C

The N_y -steps ahead Kalman Predictor

Chapter 6 highlights a valuable contribution of the thesis: the so-called *N_y -steps ahead Kalman Predictor*, given by Equation 6.4.

The present Appendix demonstrates how the cited predictor may be regarded as a generalization of the Kalman Filter. To start with, Equation 6.4 is rewritten for completeness,

$$\hat{\mathbf{x}}(k + N_y) = (\mathbf{A}^{N_y} - \mathbf{F}\mathbf{C}) \hat{\mathbf{x}}(k) + \mathbf{H}\mathbf{u}(k) + \mathbf{\Upsilon}_1 \mathbf{u}(k) + \mathbf{F}\mathbf{y}(k), \quad (\text{C.1})$$

with $\mathbf{\Upsilon}_1 = [\mathbf{A}^{N_y-d+1}\mathbf{B} \quad \dots \quad \mathbf{A}^{N_y-1}\mathbf{B}]$, $\mathbf{F} = \mathbf{A}^{N_y-1}\mathbf{\Gamma}$ and $\mathbf{H} = \mathbf{A}^{N_y-d}\mathbf{B}$.

Equation C.1 refers clearly to a predictor, since no future information is required to build the state vector $\hat{\mathbf{x}}(k + N_y)$.

The Kalman Filter* is directly obtained from Equation C.1 if $N_y = d = 1$, such that,

$$\hat{\mathbf{x}}(k + 1) = \mathbf{A}\hat{\mathbf{x}}(k) + \mathbf{B}\mathbf{u}(k) + \mathbf{\Gamma}[\mathbf{y}(k) - \mathbf{C}\hat{\mathbf{x}}(k)].$$

*In fact the correct term to be employed here is *Kalman Predictor*, since the filter assumes intrinsically a propagation and a correction steps. However, as well as several specialized literature, in this work it was decided to stick on the term Kalman Filter since it represents a more general and known term within the Engineering field.

D

The intrinsic solution of the Diophantine Equations

As already cited in Chapter 6, the UHPC solves intrinsically two Diophantine Equations that arise for the SISO case when the polynomial approach is used, being one for the noise and other for the control signal, which are the same that arise in the GPC solution. This Appendix exploits this specific case for proving the cited statement.

Let the general polynomial ARMAX* model be plant's representation,

$$A(q^{-1})y(k) = B(q^{-1})u(k-d) + C(q^{-1})\xi(k), \quad (\text{D.1})$$

with $y(k)$, $u(k)$ and $\xi(k)$ are system's output, input and noise signals. Also,

$$\begin{aligned} A(q^{-1}) &= 1 + a_1q^{-1} + \dots + a_{n_a}q^{-n_a}, \\ B(q^{-1}) &= b_0 + b_1q^{-1} + \dots + b_{n_b}q^{-n_b}, \\ C(q^{-1}) &= 1 + c_1q^{-1} + \dots + c_{n_c}q^{-n_c}, \end{aligned}$$

with q^{-1} being the backward shift operator.

Shifting Equation D.1 N_y -steps forward,

$$A(q^{-1})y(k + N_y) = B(q^{-1})u(k-d + N_y) + C(q^{-1})\xi(k + N_y),$$

*ARMAX: AutoRegressive Moving Average with eXogenous input.

it is clear that in order to obtain $y(k + N_y)$, the future of the noise and control signal must be known. Hence, one might represent both signals in terms of present and future parts such that,

$$\begin{aligned} \frac{C(q^{-1})}{A(q^{-1})}\xi(k + N_y) &= \underbrace{F(q^{-1})\xi(k)}_{\text{present}} + \underbrace{E(q^{-1})\xi(k + N_y)}_{\text{future}}, \\ &\vdots \\ C(q^{-1}) &= A(q^{-1})E(q^{-1}) + q^{-N_y}F(q^{-1}), \end{aligned} \quad (\text{D.2})$$

where Equation D.2 is called *Noise's Diophantine Equation*, and,

$$\begin{aligned} E(q^{-1}) &= 1 + e_1q^{-1} + \cdots + e_{N_y-1}q^{-N_y+1}, \\ F(q^{-1}) &= f_0 + f_1q^{-1} + \cdots + f_{n_a-1}q^{-n_a+1}, \end{aligned}$$

The same analysis holds for the control signal, thus,

$$\begin{aligned} \frac{B(q^{-1})}{A(q^{-1})}u(k - d + N_y) &= \underbrace{H(q^{-1})u(k)}_{\text{present}} + \underbrace{J(q^{-1})u(k - d + N_y)}_{\text{future}}, \\ &\vdots \\ B(q^{-1}) &= A(q^{-1})J(q^{-1}) + q^{-N_y+d}H(q^{-1}), \end{aligned} \quad (\text{D.3})$$

and Equation D.3 is called *Control Signal's Diophantine Equation*, with,

$$\begin{aligned} H(q^{-1}) &= h_0 + h_1q^{-1} + \cdots + h_{n_a-1}q^{-n_a+1}, \\ J(q^{-1}) &= j_0 + j_1q^{-1} + \cdots + j_{N_y-d-1}q^{-N_y+d+1}. \end{aligned}$$

The biggest issue in predicting a long ahead horizon is clearly the solution of both unknown polynomials of the Diophantine Equations for large d and mainly N_y . Important to highlight that the problem extends to the determination of the control law (see, *e.g.*, [36, 84]).

Silveira and Coelho [79] present the intrinsic solution for Noise's Diophantine Equation using the state-space representation of an AR-MAX model such as,

$$\begin{aligned} \mathbf{x}(k) &= \mathbf{A} \mathbf{x}(k - 1) + \mathbf{B} u(k - d) + \mathbf{\Gamma} \xi(k - 1) \\ y(k) &= \mathbf{C} \mathbf{x}(k) + \xi(k), \end{aligned} \quad (\text{D.4})$$

with,

$$\begin{aligned}\mathbf{A} &= \begin{bmatrix} -\mathbf{a} & \mathbf{I} \\ & \mathbf{0} \end{bmatrix}, \\ \mathbf{B} &= [\mathbf{b} \quad \mathbf{0}]^T, \\ \mathbf{C} &= [1 \quad \mathbf{0}], \\ \mathbf{\Gamma} &= [(c_1 - a_1) \quad \cdots \quad (c_{n_a} - a_{n_a})]^T,\end{aligned}$$

and $\mathbf{a} = [a_1 \quad \cdots \quad a_{n_a}]^T$, $\mathbf{b} = [b_0 \quad \cdots \quad b_{n_b}]^T$.

In their paper, the authors prove that the unknown polynomials of the Diophantine Equation D.2 are given directly by the coefficients of the following vectors,

$$\begin{aligned}\mathbf{F} &= \mathbf{A}^{N_y-1} \mathbf{\Gamma} = [f_0 \quad \cdots \quad f_{n_a-1}]^T, \\ \mathbf{E} &= \mathbf{1} + \sum_{i=1}^{N_y-1} \mathbf{C} \mathbf{A}^{i-1} \mathbf{B} q^{-i} = [1 \quad e_1 \quad \cdots \quad e_{N_y-1}]^T.\end{aligned}$$

The present thesis introduces also the solution for Control Signal's Diophantine Equation D.3 using the same principle as in [79] such that,

$$\mathbf{H} = \mathbf{A}^{N_y-d} \mathbf{B} = [h_0 \quad \cdots \quad h_{n_a-1}]^T, \quad (\text{D.5})$$

$$\mathbf{J} = \sum_{i=1}^{N_y-d} \mathbf{C} \mathbf{A}^{i-1} \mathbf{B} q^{-i+1} = [j_0 \quad \cdots \quad j_{N_y-d-1}]^T. \quad (\text{D.6})$$

For proving this statement, let us consider the following example. However, it is important to highlight that the analysis holds also for general representations.

Example: Consider the plant represented by the following polynomials,

$$\begin{aligned}A(q^{-1}) &= 1 + a_1 q^{-1} + a_2 q^{-2}, \\ B(q^{-1}) &= b_0 + b_1 q^{-1},\end{aligned}$$

with $d = 3$ and $N_y = 5$. The polynomials $H(q^{-1})$ and $J(q^{-1})$, solved using Equations D.2 and D.3, are then,

$$\begin{aligned}H(q^{-1}) &= b_0 (a_1^2 - a_2) - a_1 b_1 + a_2 (a_1 b_0 - b_1) q^{-1}, \\ J(q^{-1}) &= b_0 + (b_1 - a_1 b_0) q^{-1}.\end{aligned}$$

Finally, using Equations D.5 and D.6, the Control Signal's Diophantine polynomials are,

$$\mathbf{H} = \left[(b_0 (a_1^2 - a_2) - a_1 b_1) \quad (a_2 (a_1 b_0 - b_1)) \right]^T,$$
$$\mathbf{J} = [b_0 \quad (b_1 - a_1 b_0)]^T,$$

which is exactly the same result as obtained from the solution of Equations D.2 and D.3.

Curriculum Vitae

Personal information	
Name	Rodrigo Trentini Preuss
Date of birth	03.04.1985
Place of birth	Joinville, Brazil

Professional experience	
09.2014 – 04.2017	Lecturer Hochschule Hannover, Germany
03.2011 – 12.2012	Lecturer Universidade do Estado de Santa Catarina, Brazil
05.2006 – 01.2013	Technical representative Veeder-Root do Brasil, Brazil
05.2005 – 03.2006	Electronic designer KaVo do Brasil Indústria e Comércio, Brazil
06.2003 – 03.2005	Electronic designer Sintex Industrial de Plásticos, Brazil

Academic background	
04.2013 – 04.2017	PhD student in Electrical Engineering Leibniz Universität Hannover, Germany
03.2010 – 12.2012	M.Sc. in Electrical Engineering Universidade do Estado de Santa Catarina, Brazil
02.2005 – 12.2009	B.Sc. in Control and Automation Instituto Superior Tupy, Brazil
02.2002 – 12.2003	A.Sc. in Industrial Automation Escola Técnica Tupy, Brazil
